Strengthening of Steel Bridge Components with Externally Bonded Ultra-High Modulus CFRP

by

Mohamadreza DELZENDEH MOGHADAM

MANUSCRIPT-BASED THESIS PRESENTED TO ÉCOLE DE TECHNOLOGIE SUPÉRIEURE IN PARTIAL FULFILLMENT FOR THE DEGREE OF DOCTOR OF PHILOSOPHY
Ph.D.

MONTREAL, NOVEMBER 21, 2024

ÉCOLE DE TECHNOLOGIE SUPÉRIEURE
UNIVERSITÉ DU QUÉBEC

BOARD OF EXAMINERS

THIS THESIS HAS BEEN EVALUATED

BY THE FOLLOWING BOARD OF EXAMINERS

Mr. Omar Chaallal, Thesis Supervisor
Department of Construction Engineering at École de Technologie Supérieure

Mr. Hakim A. Bouzid, President of the Board of Examiners
Department of Mechanical Engineering at École de Technologie Supérieure

Mr. Amar Khaled, Member of the jury
Department of Construction Engineering at École de Technologie Supérieure

Mr. Georges El-Saikaly, Member of the jury
Department of Construction Engineering at École de Technologie Supérieure

Mr. Hassan Aoude, External Evaluator
Department of Engineering, Faculty of Engineering, University of Ottawa

THIS THESIS WAS PRESENTED AND DEFENDED

IN THE PRESENCE OF A BOARD OF EXAMINERS AND PUBLIC

ON OCTOBER 28, 2024

AT ÉCOLE DE TECHNOLOGIE SUPÉRIEURE

ACKNOWLEDGMENTS

I would like to express my deepest gratitude to Professor Omar Chaallal, my research director, for his invaluable mentorship and unconditional support throughout my PhD studies. His encouragement and guidance have been prominent factors in the successful completion of this thesis. I am also profoundly grateful to Professor Brahim Benmokrane for his generous collaboration and expertise, which significantly enriched my research.

Additionally, I extend my appreciation to the technicians at École de technologie supérieure: Mr. Jonathan Auger, Mr. Sylvain Bibeau, Mr. Juan Mauricio Rios, and Ms. Marielle Jacques. I am sincerely grateful for their assistance in carrying out the experimental tests.

I would also like to acknowledge the financial support of our esteemed industrial partner, the Jacques-Cartier and Champlain Bridges Incorporated (PJCCI, Longueuil, QC, Canada). Many thanks also go to Fyfe FRP, Sika-Canada, and MAPEI-Canada for contributing to the cost of the materials used in this research experimental program.

Finally, I express my deepest gratitude to my parents, who have always been a source of endless love, and energy. Their unwavering support has been the foundation of my success, and I dedicate this work to them with all my heart.

Renforcement des éléments de ponts en acier avec du PRFC à ultra-haut module collé en surface

Mohamadreza DELZENDEH MOGHADAM

RÉSUMÉ

L'application de la technique de polymère renforcé de fibres de carbone (PRFC) collé en surface (CS) pour le renforcement des infrastructures civiles a gagné de plus en plus de popularité et de parts de marché. Cependant, les investigations sur la performance des composants en acier renforcés ou réhabilités avec du PRFC CS sont plutôt limitées, et la majorité des études ont été consacrées aux structures en béton renforcées avec du PRFC. Ces dernières années, de nouvelles opportunités de recherche se sont ouvertes avec l'émergence du PRFC à ultra-haut module (UHM) pour évaluer la performance de la technique de réhabilitation des éléments structuraux en acier avec du PRFC UHM. La performance des éléments en acier réhabilités est fortement influencée par le lien entre le PRFC et l'interface acier. En effet, le décollement peut entraîner une défaillance prématurée de la technique de réhabilitation avec du PRFC. À cet égard, l'étude du comportement de l'adhérence des joints PRFC/acier est d'une importance capitale.

Cette étude vise à comprendre au profondeur le comportement des composants en acier réhabilités avec du PRFC en mettant en évidence les paramètres influents. À cet égard, dans la première phase, une revue de la littérature exhaustive est menée pour identifier les paramètres influents affectant le comportement de l'adhérence de l'interface PRFC/acier, et par conséquent, le comportement en flexion des éléments réhabilités. Dans la seconde phase, une investigation expérimentale approfondie est menée pour combler les lacunes existantes dans la littérature. Tout d'abord, une série de joints doubles PRFC/acier sont testés sous charge statique pour évaluer divers paramètres, y compris le type d'adhésif, la longueur du PRFC et la préparation de la surface. De plus, l'effet du module d'élasticité du PRFC sur la technique de réhabilitation est examiné en comparant le PRFC à module normal (MN) et à ultra-haut module (UHM) tout en gardant une capacité de traction approximativement égale. Ensuite, le comportement en flexion des poutres en acier entaillées réhabilitées avec du PRFC est examiné sous charge statique. Les paramètres considérés dans cette phase incluent le type de PRFC, la configuration du PRFC, la profondeur de l'entaille, le système d'ancrage et le type d'adhésif.

Les résultats révèlent que le type d'adhésif joue un rôle crucial dans le comportement de l'adhérence des joints PRFC/acier. Cependant, en ce qui concerne les poutres réhabilitées avec ancrage, l'impact de l'adhésif est négligeable sur la performance en flexion des poutres en raison des mécanismes d'ancrage. L'effet du type de préparation de surface s'est également révélé trivial sur le comportement de l'adhérence des joints PRFC/acier. De plus, il est constaté que le PRFC UHM tout en exposant une longueur d'adhérence efficace plus courte comparée à celle associée au PRFC MN a une capacité de charge plus élevée.

Mots-clés: étude expérimentale, comportement de l'adhérence, comportement en flexion, technique de réhabilitation avec PRFC, PRFC collé en surface, vieux éléments de pont en acier, poutres entaillées, structures en acier

Strengthening of steel bridge components with externally bonded ultra-high modulus CFRP

Mohamadreza DELZENDEH MOGHADAM

ABSTRACT

The application of the externally bonded (EB) carbon fiber reinforced polymer (CFRP) technique for retrofitting civil infrastructure has been increasingly gaining acceptance and market share. However, investigations on the performance of steel components strengthened or rehabilitated with EB CFRP are rather limited and most of the studies have been dedicated to concrete structures retrofitted with EB CFRP. In recent years, new research opportunities have opened with the emergence of ultra-high modulus (UHM) CFRP to evaluate the performance of UHM CFRP retrofitting technique in steel structural elements. The performance of the retrofitted steel elements is highly influenced by the bond between CFRP and steel interface. Indeed, debonding failure can lead to premature failure of the CFRP retrofitting technique. In this regard, the study of the bond behavior of the CFRP/steel joints is of paramount importance.

This study aims to fully understand the behavior of steel components rehabilitated with CFRP and thereby highlighting the influential parameters. To that end, a comprehensive literature review is initially carried out to identify the key parameters that influence the bond behavior of the CFRP/steel interface, and thereby the flexural behavior of the retrofitted elements. In the second phase, a thorough experimental investigation is conducted to fill the existing gaps in the literature. Firstly, a series of double strap CFRP/steel joints are tested under static loading to evaluate various parameters, including the adhesive type, CFRP length, and surface preparation. Additionally, the effect of CFRP elastic modulus on the rehabilitation technique is examined by comparing Normal Modulus (NM) and Ultra-High Modulus (UHM) CFRP with approximately the same tensile capacity. Secondly, the flexural behavior of the CFRP rehabilitated notched steel beams are examined under static loading. The parameters considered in this phase include CFRP type, CFRP configuration, notch depth, anchorage system, and adhesive type.

The results reveal that the effect of adhesive type plays a crucial role on the bond behavior of CFRP/steel joints. However, when it comes to the anchored rehabilitated beams, the adhesive impact is negligible on the flexural performance of the beams due to the anchorage mechanisms. The effect of surface preparation type has also been found trivial on the bond behavior of the CFRP/steel joints. Moreover, it is found that UHM CFRP has a shorter effective bond length compared to its NM CFRP counterpart and it generally outperforms NM CFRP in terms of load-carrying capacity.

Keywords: experimental study, bond behavior, flexural behavior, CFRP rehabilitation technique, externally bonded CFRP, old steel bridge elements, notched beams, steel structures

TABLE OF CONTENTS

LIST OF TABLES

LIST OF FIGURES

LIST OF ABREVIATIONS

AFRP	Aramid Fiber-Reinforced Polymer
ASTM	American Society for Testing and Materials
BFRP	Basalt Fiber-Reinforced Polymer
CFRP	Carbon Fiber-Reinforced Polymer
CMOD	Crack Mouth Opening Displacement
CZM	Cohesive Zone Model
DOF	Degree of Freedom
EB	Externally Bonded
FRP	Fiber-Reinforced Polymer
GFRP	Glass Fiber-Reinforced Polymer
HM	High Modulus
IM	Intermediate Modulus
LM	Low Modulus
LVDT	Linear Variable Differential Transducers
NM	Normal Modulus
RC	Reinforced Concrete
UHM	Ultra-High Modulus

LIST OF SYMBOLS

b_p	Width of CFRP plate
b_s	Width of steel plate
E_a	Young's modulus of adhesive
E_p	Young's modulus of CFRP plate
E_s	Young's modulus of steel plate
h_b	Height of beam
f_a	Tensile strength of adhesive
f_p	CFRP tensile strength
f_y	Steel yield stress
f_u	Steel ultimate stress
G_a	Shear modulus of adhesive
G_f	Interfacial fracture energy
L_e	Effective bond length of CFRP plate
$L_{span,b}$	Span length of steel beam
N	Number of interfaces working in parallel
P_u	Ultimate load (bond strength)
t_a	Thickness of adhesive layer
t_p	Thickness of CFRP plate
t_s	Thickness of steel plate
W_b	Width of beam
W_s	Steel plate width

τ_f	Peak interfacial shear stress
τ^*	Interlaminar shear strength of the CFRP plate
δ_1	Relative slip corresponding to the peak interfacial stress
δ_2	Relative slip when the shear stress begins to decrease in the tri-linear model
δ_f	Maximum slip

INTRODUCTION

In recent years, the use of advanced composite materials has become one of the most popular methods for retrofitting civil infrastructures. Among these materials, carbon fiber-reinforced polymer (CFRP) laminate is well established. The high strength-to-weight ratio as well as corrosion resistance play an important role in choosing CFRP materials for retrofitting exiting structures (Chataigner, Benzarti et al., 2018; Hu, Li et al., 2020; Oudah & El-Hacha, 2013). Although extensive research studies have been carried out on the application of CFRP materials, most of them have been dedicated to concrete structures. However, the emergence of the UHM CFRP in the last years opened new research opportunities to investigate the performance of this material in retrofitting steel structures.

Many steel structures worldwide, particularly bridges, are prone to deterioration during their service life span. The strength and stiffness of the steel members tend to decrease due to cracks and corrosion that stem from fatigue loading and extreme weather conditions, respectively. Furthermore, deficiencies may also occur during the design and construction processes. Therefore, there is a considerable demand for rehabilitation of steel structures. The conventional approach for retrofitting steel structures is by welding or bolting additional steel plates to the deficient element (Dexter & Ocel, 2013). The steel plates are still susceptible to corrosion and are typically heavy, which makes installation challenging. Therefore, the use of externally bonded CFRP, in particular ultra-high modulus (UHM) CFRP, can offer a promising and speedy alternative method to meet this demand. However, debonding failure is a significant challenge in CFRP retrofitted materials, as it can lead to premature failure and prevent this technique from reaching its full potential capacity. The present research aims to integrate the up-to-date findings regarding the application of CFRP in retrofitting steel structural elements and further explore to fill the gaps in the literature through an extensive experimental program. The contents of this research study are provided through the following chapters:

- Chapter 1 presents the research description including problem statement, research objectives and methodology for the current PhD studies.

- Chapter 2 presents the first paper entitled “Retrofitting of steel structures with CFRP: literature review and research needs” which focuses on the influential parameters on the bond behavior between CFRP and steel substrate. Furthermore, the existing bond slip models, and effective bond length relationships are documented in this paper. Further discussion on the flexural performance of the retrofitted steel elements as well as numerical modeling of the bond behavior are provided in this chapter.

- Chapter 3 presents the second paper entitled “Bond Behavior of CFRP/Steel Double Strap Joints: An Experimental Study”. This chapter delves into the results of an experimental program on the bond behavior of CFRP/steel interface considering various influencing parameters such as CFRP elastic modulus, adhesive type, CFRP bond length, and surface preparation. Moreover, the existing bond slip models as well as effective bond length relationships are evaluated based on the obtained experimental results.

- Chapter 4 presents the third paper entitled “Flexural behavior of the retrofitted notched steel beams using CFRP: Experimental study”. In this paper, the influential parameters such as CFRP elastic modulus, adhesive type, anchorage mechanism, CFRP configuration on the flexural behavior of the rehabilitated notched beams are investigated. Furthermore, two types of beams are used in this study. The W200×22 beams that were received directly from a factory, and the W14" wide flange beams were extracted from the Old Champlain Bridge.

- Finally, the conclusions of the present research, along with research recommendations for future studies, are summarized at the end.

CHAPTER 1

RESEARCH DESCRIPTION

1.1 Context

Steel bridges play a key role in the transportation infrastructure. Many of the existing steel bridge structures have been designed according to the old design codes. On the other hand, the evolved design codes urge the old structures to meet the updated requirements of the current provisions. In most cases, it is not economically feasible to replace the components of the structures to satisfy the new codes. Furthermore, retrofitting takes less construction time, resulting in less service interruption (Shaat, Schnerch et al., 2004). Moreover, many steel bridges around the world are prone to deterioration during their service life period. The strength and stiffness, and hence the capacity of steel bridge components decrease with time as a result of fatigue loadings and extreme weather conditions. Therefore, a large number of steel bridges worldwide need retrofitting due to corrosion, cracks, and lack of proper maintenance. The federal highway administration of the US Department of Transportation estimated that around 40% of the metallic highway bridges are either structurally deficient or functionally obsolete (Kamruzzaman, Jumaat et al., 2014). In 2011, part of the Mercier Bridge, located in Montreal, was closed for a couple of months as a result of dangerously deteriorated steel plates (CBC News Staff, 2011). As another example, in 2021, a significant crack was found on the I-40 interstate bridge in the United States. The crack occurred in an element pivotal to the integrity of the bridge structure, as shown in Figure 1.2 (CBC News Staff, 2021).

These examples reveal the importance of inspecting existing structures and implementing cost-effective and speedy rehabilitation techniques. Improper inspection and rehabilitation can lead to catastrophic consequences. The steel I-35W Bridge over the Mississippi River collapsed in August 2007, resulting in 13 dead and 145 injuries, and damaging 111 vehicles (Figure 1.3) (Hao, 2010). According to the National Transportation Safety Board, the collapse was attributed to a design fault, improper maintenance, and increasing traffic volume, which resulted in fatigue failure (Hao, 2010).

Figure 1.1 Corroded elements of Mercier Bridge
Taken from CBC News Staff (2011)

Figure 1.2 Cracked element of I-40 bridge
Taken from CBC News Staff (2021)

Figure 1.3 I-35W Bridge over the Mississippi River after the collapse
Taken from MinnPost staff (2007)

1.2 CFRP retrofitting system

FRP materials are made of a reinforcement material provided by the fiber, and a matrix material provided by the base material, such as resin. The matrix transfers the stresses to fibers and protects them, while the fibers are the main stress bearing (Jagtap, Pore et al., 2015). Fibers in the FRP laminate can be unidirectional, bidirectional, or randomly distributed (Reddy, 2003). The well-known FRP composites are carbon fiber-reinforced polymer (CFRP), glass fiber-reinforced polymer (GFRP), aramid fiber-reinforced polymer (AFRP), and basalt fiber-reinforced polymer (BFRP). Among the mentioned composite materials, CFRP is well established in civil engineering as it has superior stiffness, which is desirable in retrofitting structures. Although it has a higher price compared to GFRP, it may become more economical over time (Borrie, Al-Saadi et al., 2021). CFRP was produced by the Royal Aircraft Establishment in the United Kingdom to fulfill the need for stiff and light advanced materials in the aircraft industry (Cheng, Qiu et al., 2016). The reinforcement of the CFRP is carbon, and the matrix is usually a polymer resin, namely epoxy. It is usually produced as a unidirectional lamina or interwoven fabric (Figure 1.4). CFRP laminates are also categorized

based on their elastic modulus into low modulus (LM), normal modulus (NM) or Intermediate Modulus (IM), high modulus (HM), and ultra-high-modulus (UHM). There is no unanimous approach to characterize the elastic modulus range of each category. However, Ghafoori and Motavalli (2015) suggested a range relative to the steel elastic modulus, as presented in Table 1.1. The stress-strain curves of the CFRPs, GFRP, and steel are also illustrated in Figure 1.5.

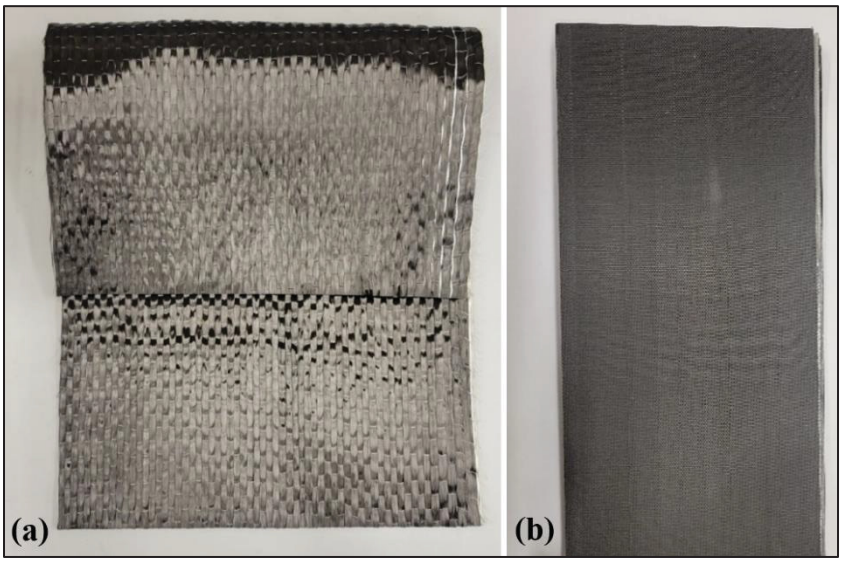

Figure 1.4 (a) CFRP fabric (SikaWrap 1400C); (b) CFRP plate (UHM MAPEI)

Table 1.1 CFRP laminate classification in terms of elastic modulus
Taken from Ghafoori and Motavalli (2015, p. 2)

Laminate Type	Laminate Modulus	Laminate Modulus Relative to Steel
Low Modulus (LM)	< 100 GPa	($E_{CFRP} < 0.5\ E_{steel}$)
Normal Modulus (NM)	100-200 GPa	($0.5\ E_{steel} \leq E_{CFRP} < E_{steel}$)
High Modulus (HM)	200-400 GPa	($E_{steel} \leq E_{CFRP} < 2\ E_{steel}$)
Ultra-High Modulus (UHM)	≥ 400 GPa	($E_{CFRP} \geq 2\ E_{steel}$)

The application of the FRP has become popular for retrofitting existing reinforced concrete (RC) structures (Huo, Liu et al., 2016). The deficient element of a concrete structure can be retrofitted in shear and flexure as shown in Figure 1.6. The possible failure modes of RC element retrofitted with EB FRP are shown in Figure 1.7. The dominant failure mode is

debonding at the interface between the adhesive and the concrete substrate (Fathi, El-Saikaly et al., 2023). In this case, concrete is also bonded on the FRP surface as shown in Figure 1.8, indicating that the concrete is the weakest link. In this regard, many studies have been conducted to investigate the bond behavior between FRP and concrete (Daud, Cunningham et al., 2015; Fathi, El-Saikaly et al., 2023; Lu, Teng et al., 2005; Pellegrino, Tinazzi et al., 2008; Yuan, Chen et al., 2019; Zhou, Fernando et al., 2021). Figure 1.9 shows the debonding failure for the CFRP/concrete double lap joint. However, when it comes to steel structures, the application of these materials is relatively rare due to the lack of documenting research data in the literature (Figure 1.10). Furthermore, the elastic modulus of the early generations of these materials was lower than steel, which make the use of FRP impractical.

The conventional approach for the rehabilitation of steel structures is by using steel plates (Dexter & Ocel, 2013). However, this retrofitting technique presents some disadvantages, namely, steel plates are heavy and bulky, which makes the installation difficult. Furthermore, new damages might raise from using welds or bolts on a structure (Fisher, 1997; Schnerch, Dawood et al., 2007). For instance, the local strength of high-strength steels can be reduced in the heat-affected zone that welding applies (Jiao & Zhao, 2004). In addition, the steel plates are susceptible to corrosion. Hence, this method is not reliable in the long term.

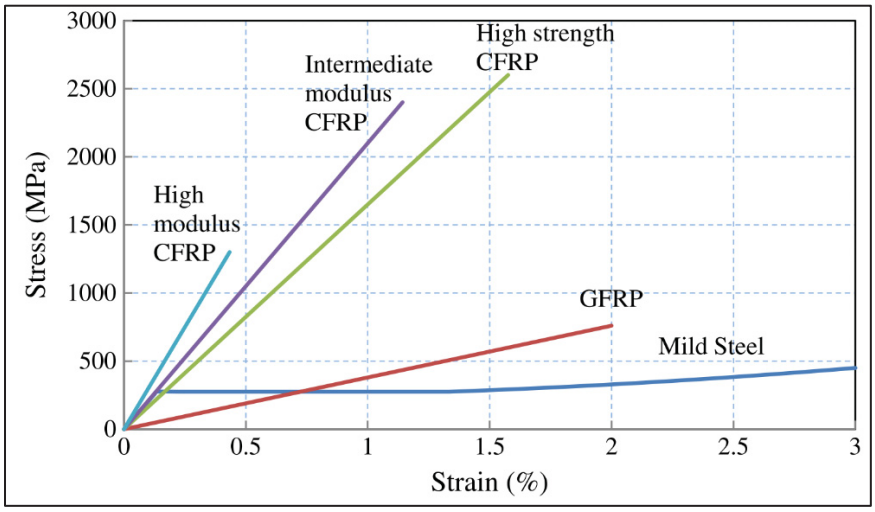

Figure 1.5 Stress-strain curves of steel, GFRP, and CFRPs
Taken from Teng, Yu et al. (2012, p. 2)

On the other hand, the emergence of CFRP with higher elastic modulus has opened new opportunities to use this material for retrofitting purposes. The CFRP retrofitting system has several advantages over the conventional approach. This innovative rehabilitation system offers a durable alternative, and its low weight can facilitate transportation and installation. Furthermore, FRP systems are attractive for structures where welding can increase the fire risk (Teng, Yu et al., 2012).

Figure 1.6 Retrofitting of a concrete bridge using the EB FRP technique
Taken from Siddika, Mamun et al. (2020, p. 2)

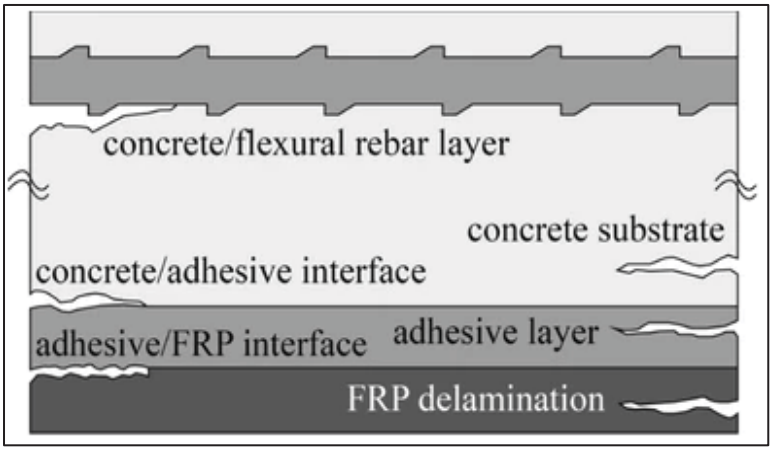

Figure 1.7 Possible failure modes of FRP retrofitted concrete element
Taken from Buyukozturk, Gunes et al. (2004, p. 11)

Figure 1.8 Debonding failure in RC beam retrofitted with FRP
Taken from El-Saikaly and Chaallal (2015, p. 7)

Figure 1.9 Concrete substrate failure of Concrete/CFRP joint
Taken from (Fathi, El-Saikaly et al., 2023, p. 6)

Figure 1.10 Retrofitting steel bridge elements - Pottawattamie County, Iowa
Taken from Phares, Wipf et al. (2003, p. 10)

1.3 Problem statement

A review of studies regarding the application of CFRP materials, especially UHM CFRP, for retrofitting steel members suggests that research in this area is rather limited. This study aims to address the following gaps related to retrofitting steel components using EB UHM CFRP:

- UHM CFRP has been developed very recently and therefore, current investigations are not sufficient to fully understand the behavior of steel components retrofitted with UHM CFRP. Moreover, the effect of CFRP elastic modulus on the bond behavior as well as retrofitted elements is not clear.

- Further research should be conducted to investigate the effect of interrelated parameters on the bond behavior of the CFRP/steel interface to propose an optimal retrofitting system encompassing epoxy type, surface preparation, and bond length.

- The current literature does not provide a thorough state-of-the-art review including the latest findings on the bond behavior of CFRP/steel interface, the flexural behavior of the retrofitted steel elements, and the proposed numerical modelling to simulate the bond between CFRP and steel substrate.

- The evaluation of CFRP flexural retrofitting needs further investigation to present an effective retrofitting solution that ensures that the CFRP fails by rupture, hence reaching its maximum capacity.

- There is a need for conducting research on real structural elements that were subjected to prolonged periods of loading and unloading. This ultimately leads to more accurate and reliable predictions of structural behavior of the retrofitted elements.

1.4 Research objectives

Considering the aforementioned research gaps, this study aims to address the following main and specific objectives:

1.4.1 Main objective

The main objective is to investigate the bond behavior between the CFRP/steel interface and evaluate the flexural performance of steel elements, especially existing steel bridge components, retrofitted with EB UHM CFRP composites subjected to static loading.

1.4.2 Specific objectives

- To determine the key parameters that influence the bond behavior of the CFRP/steel interface.

- To assess the bond behavior between CFRP and steel substrate with respect to the influencing parameters through double strap bonded joints under static load.

- To examine the feasibility and efficiency of using UHM CFRP to retrofit steel bridges.

1.5 Methodology

Figure 1.11 provides an outline of the methodology for the present PhD research project. To achieve the research objectives, a literature review is initially carried out to determine the influential parameters impacting the bond behavior and the flexural performance of the retrofitted steel elements, as well as to identify the research gaps in the existing research. Afterward, an extensive experimental study is performed. The experimental program consists of bond tests and flexure tests. In the bond test, the mechanism of failure is investigated, and the bond-slip curves and the effective bond lengths are determined. These tests are aimed to evaluate the effect of CFRP elastic modulus, adhesive type, surface preparation, and bond length on the bond behavior of CFRP/steel double strap bonded joints under static loading. As for flexure test, the four-point tests under static loading are conducted on W200×22 beams as well as on 14" wide flange beams extracted from the old Champlain bridge. In this case, CFRP elastic modulus, adhesive type, anchorage system, CFRP configuration, and notch depth are thoroughly examined. Figure 1.12 illustrates the details of the experimental program of the present study.

As illustrated, the bond behavior of two CFRPs with different elastic moduli is evaluated by conducting 25 double strap joint tests. In this regard, MAPEI® Carboplate UHM Laminate and Sika® CarboDur® S512 are utilized, representing UHM CFRP and NM CFRP, respectively. To achieve a rational comparison of the impact of CFRP elastic modulus on the behavior of retrofitted elements, both NM and UHM are selected to have approximately same tensile capacity. Furthermore, the effect of adhesive type is considered by using linear (MapeWrap12) and nonlinear adhesive (TYFO TC/S). In addition, different bond lengths are considered to achieve the effective bond length. The effect of surface preparation is also investigated by applying sandpaper machine, needle scaler and sandblasting method to treat the steel surface and remove the rust and contaminants. All the specimens are tested using an MTS machine, and the data are obtained by the strain gauges installed along the CFRPs. The results of these tests are mainly presented in terms of failure modes, bond strength, strain distribution curves along the CFRPs, effective bond length, and bond-slip curves.

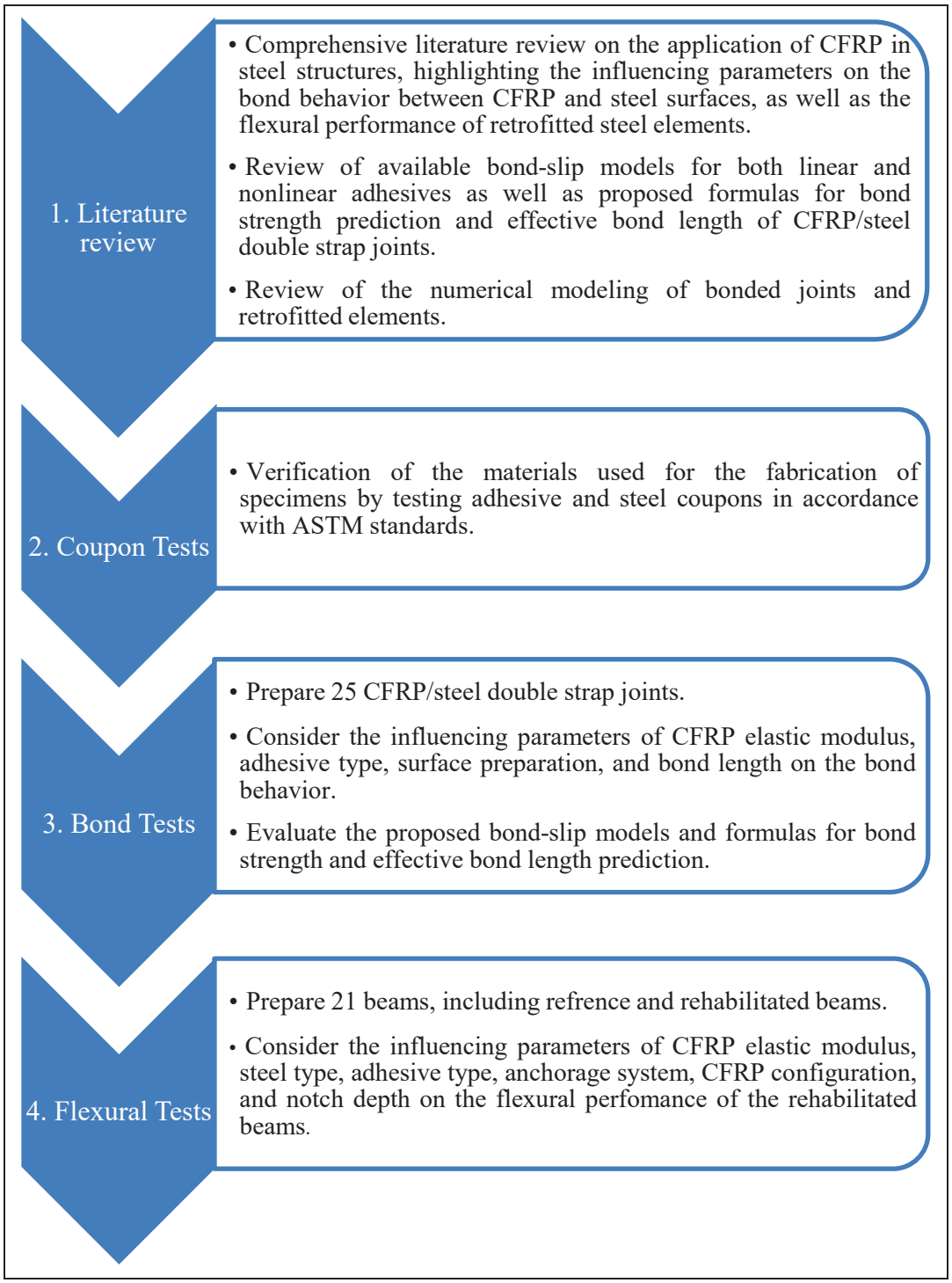

Figure 1.11 Methodology of the present PhD project

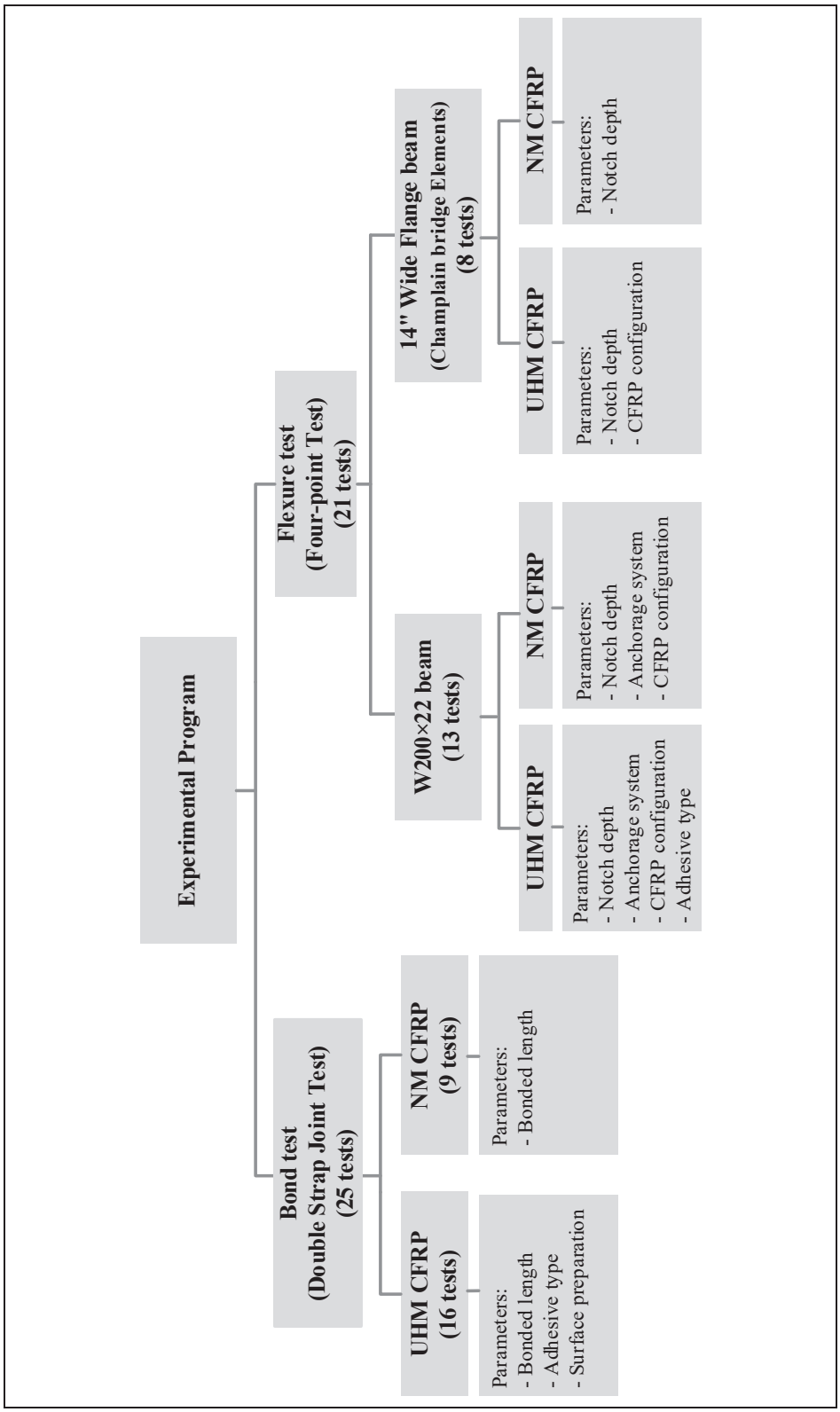

Figure 1.12 Experimental program of the present PhD project

After revealing the bond behavior between CFRP and steel substrates, the flexural behavior of the rehabilitated steel notched beams is evaluated experimentally by testing 21 beams. In this regard, two series of tests are considered: the W200×22 beams, which were received directly from a factory, and the W14" wide flange beams that were extracted from the Old Champlain Bridge located in Montreal. For both series of tests, two different notch depths are considered to evaluate different levels of damage: (i) the notch extends to the beam's flange; (ii) the notch extends to the web of the beam. To rehabilitate these notched beams, NM and UHM CFRP with roughly the same tensile capacity are used. It should be noted that for the first series, the effect of the anchorage system is studied by using SikaWrap 1400C (cured with Sikadur-300 Epoxy). Moreover, the effect of adhesive type is studied by using linear (MapeWrap12) and nonlinear adhesive (TYFO TC/S).

The beams are tested under four-point bending using an MTS machine. The ultimate load-carrying capacity of each beam is obtained and failure modes are observed. All the data are gathered from the linear variable differential transducers (LVDTs), crack gauges, and strain gauges. In these series of tests, the results are evaluated in terms of failure modes, load-deflection behavior, strain distributions along the CFRPs, and Crack Mouth Opening Displacement (CMOD).

It should be mentioned that four steel coupons extracted from each type of beam and five coupons of each adhesive type are tested under tensile tests to verify the mechanical properties of materials. The coupon tests are performed in accordance with ASTM standards (ASTM-A370, 2020; ASTM-D638, 2014). The details of each coupon are presented in Figure 1.13 and Figure 1.14 where the dimensions are expressed in mm.

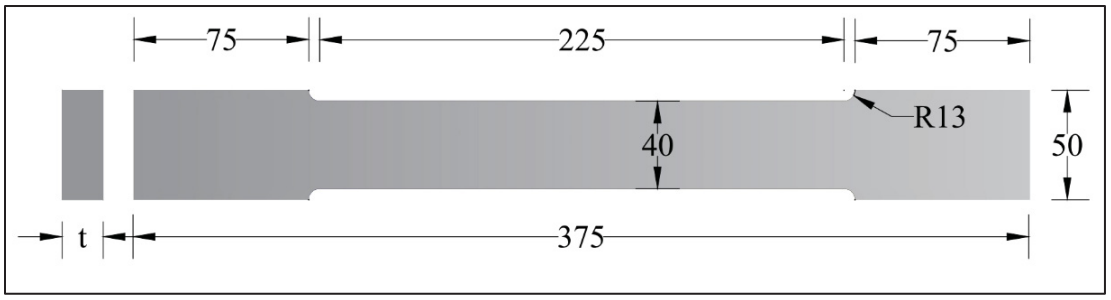

Figure 1.13 Schematic of steel coupon specimen
Taken from ASTM-A370 (2020, p. 6)

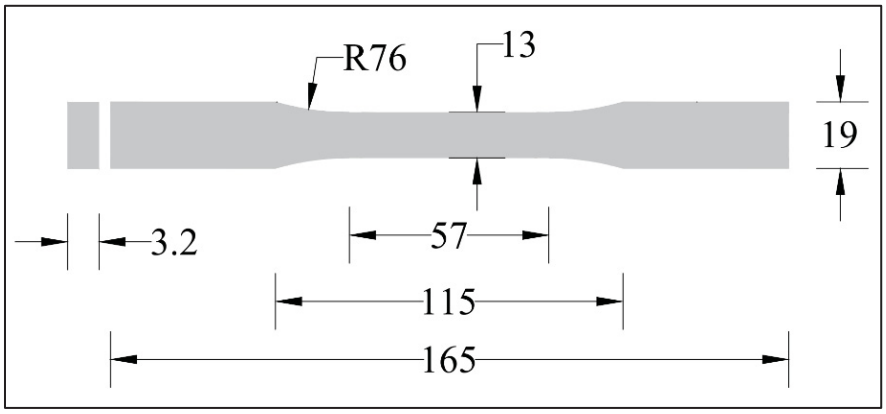

Figure 1.14 Schematic of adhesive coupon specimen
Taken from ASTM-D638 (2014, p. 4)

CHAPTER 2

RETROFITING OF STEEL STRUCTURES WITH CFRP: LITERATURE REVIEW AND RESEARCH NEEDS

Mohamadreza Delzendeh Moghadam [1], Abbas Fathi [2], Omar Chaallal [3]

[1,2,3] Department of Construction Engineering, École de Technologie Supérieure
1100 Notre-Dame St. West, Montreal, Quebec, Canada H3C 1K3

Article published in *Journal of Applied Sciences*, Volume 14, Issue 13, July 2024.

2.1 Abstract

The application of the externally bonded (EB) carbon fiber-reinforced polymer (CFRP) technique for retrofitting steel elements offers significant advantages over the conventional method. The high strength-to-weight ratio and corrosion resistance of CFRP materials have made them a viable alternative for retrofitting steel structures. This paper covers a wide range of aspects discussed in the research investigations to date on CFRP bonded steel elements and provides a critical review of the topic under both static and fatigue loading conditions. In the end, research needs and recommendations are presented in this respect.

Keywords: Steel structures; Retrofitting technique; Carbon fiber-reinforced polymer (CFRP); Bond–slip relationship; Static loading; Fatigue loading; Finite element analysis; Research progress.

2.2 Introduction

Steel structures around the world are susceptible to deterioration over their service life period. This deterioration can reduce the potential strength and stiffness of the steel members due to cracks and corrosion induced by fatigue loading and extreme weather conditions, respectively. Additionally, defects may arise during the design and construction phases. The conventional approach for retrofitting steel structures is by using steel plates that are attached to the structure

by weld or bolt (Dexter & Ocel, 2013). However, this approach presents disadvantages, including the residual stress imposed by welding, which can lead to new damage to the structure (Fisher, 1997; Schnerch, Dawood et al., 2007). Furthermore, the steel plates are susceptible to corrosion and their heavy weight poses challenges during installation (Tavakkolizadeh & Saadatmanesh, 2003; Zhao & Zhang, 2007). Alternatively, the application of externally bonded carbon fiber-reinforced polymer (CFRP) can offer a durable solution to address these challenges (Hollaway & Cadei, 2002; Kamruzzaman, Jumaat et al., 2014). The high strength-to-weight ratio and corrosion resistance of CFRP materials have an important role in their selection for retrofitting steel components (Chataigner, Benzarti et al., 2018; Hu, Li et al., 2020; Oudah & El-Hacha, 2013).

In recent years, the application of advanced composite materials has been gaining acceptance in retrofitting civil infrastructures. Among these types of materials, CFRP and graphite fiber-reinforced polymer (GFRP) are well established (Jagtap, Pore et al., 2015). However, CFRP exhibits superiority over GFRP due to its higher strength. Studies show that CFRP retrofitting systems can effectively enhance the flexural capacity of steel members and prolong their fatigue life (Aljabar, Zhao et al., 2017; Aljabar, Zhao et al., 2016; Colombi & Fava, 2015, 2016; Elkhabeery, Safar et al., 2018; Emdad & Al-Mahaidi, 2015; Fam, MacDougall et al., 2009; Ghafoori, 2015; Hmidan, Kim et al., 2011; Hu, Zhao et al., 2016; Ke, Li et al., 2020; Linghoff, Al-Emrani et al., 2010; Liu, 2003; Schnerch & Rizkalla, 2008; Shaat & Fam, 2008; Sweedan, Alhadid et al., 2016; Tafsirojjaman, Fawzia et al., 2021; Tavakkolizadeh & Saadatmanesh, 2003; Tong, Xu et al., 2021; Wang, Wu et al., 2019; Wu, Zhao et al., 2013; Yu & Wu, 2018). CFRPs are classified based on their elastic modulus into Low Modulus (LM), Normal Modulus (NM) or Intermediate Modulus (IM), High Modulus (HM), and Ultra-High Modulus (UHM). There is not a unanimous approach to characterize the elastic modulus range of each category. However, it can be expressed relative to the steel elastic modulus as presented in Table 2.1 (Ghafoori & Motavalli, 2015).

The significance of this review lies in its comprehensive and up-to-date examination of the current state of knowledge on steel elements retrofitted with CFRP. This paper integrates

findings from multiple dimensions and examines key parameters affecting the performance of CFRP retrofitted components and the bond behavior between CFRP and steel interfaces, including adhesive types, surface preparation, bond length, etc. By synthesizing findings from various investigations, this review aims to guide future research efforts and enhance the application of CFRP in retrofitting steel structures.

Table 2.1 CFRP laminate classification in terms of elastic modulus
Taken from Ghafoori and Motavalli (2015, p. 2)

Laminate Type	Laminate Modulus	Laminate Modulus Relative to Steel
Low Modulus (LM)	< 100 GPa	($E_{CFRP} < 0.5\ E_{steel}$)
Normal Modulus (NM)	100-200 GPa	($0.5\ E_{steel} \leq E_{CFRP} < E_{steel}$)
High Modulus (HM)	200-400 GPa	($E_{steel} \leq E_{CFRP} < 2\ E_{steel}$)
Ultra-High Modulus (UHM)	≥ 400 GPa	($E_{CFRP} \geq 2\ E_{steel}$)

This paper is presented in the following sections: (i) a review of studies on the bond behavior between CFRP and steel; (ii) research findings regarding the flexural behavior of the retrofitted steel beams; and (iii) a review of numerical simulations of CFRP/steel retro-fitted elements and their bond behavior. Finally, gaps in previous research are identified, and suggestions for further investigations are provided.

2.3 Bond behavior between CFRP and steel

The bond between CFRP and steel plays a major role in the performance of steel components retrofitted with CFRP. The role of the adhesive layer is to carry the tensile forces of the steel substrates and transfer them to the CFRP composites. A comparison between the CFRP/steel and CFRP/concrete bonded interfaces reveals the main contrast in terms of the bond behavior. Indeed, adhesives in the CFRP/steel joints are regarded as the weakest link, whereas the bond behavior of the CFRP/concrete shows that concrete acts as the weakest link (Yu, Fernando et al., 2012). Therefore, to achieve the maximum capacity of the CFRP retrofitting system that follows up with the CFRP rupture, the selection of the most effective adhesives is crucial (Stanford, 2009). Furthermore, many other parameters have been found influential on the bond behavior of the retrofitted elements. These parameters include the CFRP elastic modulus,

CFRP bond length, CFRP configuration, adhesive type, adhesive thickness, anchorage system, and surface preparation of the steel substrate. It should be noted that temperature is also considered as one of these influential parameters. There are some comprehensive literature reviews that focus on the thermal and environmental effects (Borrie, Al-Saadi et al., 2021; Gholami, Sam et al., 2013).

2.3.1 Bond test configuration and failure modes

To study the bond behavior between the CFRP and steel substrate, two test setups have been mainly adapted, as shown in Figure 2.1. In the single strap joint configuration (a), two steel plates are attached by CFRP only on one side, while in the double strap joints configuration (b), CFRPs are attached to both sides of steel plates. In both configurations, the loading is applied to the steel plates. It should be noted that in the single strap joint test setup, the adherends are subjected to bending during loading due to load eccentricity. This asymmetrical configuration can lead to rotation of the bond plane, resulting in significant peel stresses at the adhesive layer ends, which may cause premature adhesive failure and consequently lead to an underestimation of the capacity of the CFRP/steel joint (Duncan, 2010). In contrast, the double strap joint is symmetrical about the mid-plane of the specimen. Therefore, given the adherends, the amount of peel stress due to bond rotation is considerably less than a single strap joint configuration (Duncan, 2010).

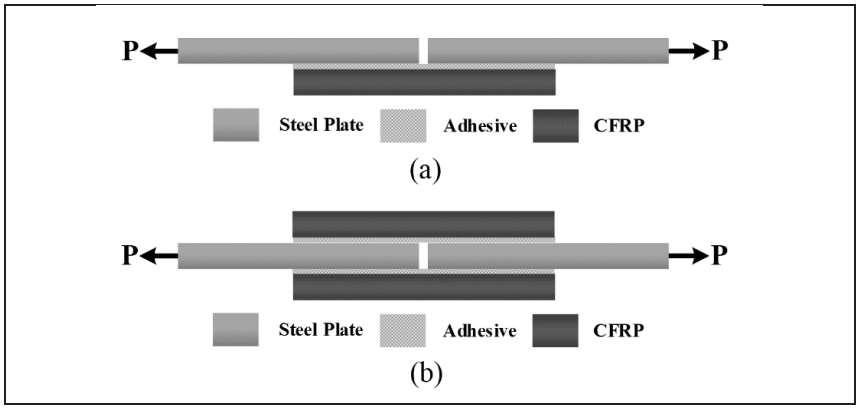

Figure 2.1 Schematic view of the (a) single strap joint; (b) double strap joint test setups

Possible failure modes of the CFRP/steel joints under tensile loading include the following (Zhao & Zhang, 2007): (a) adhesion failure at CFRP/adhesive interface; (b) adhesive layer failure; (c) adhesion failure at steel/adhesive interface; (d) CFRP delamination; (e) CFRP rupture; (f) steel yielding. Figure 2.2 presents a schematic view of these failure modes.

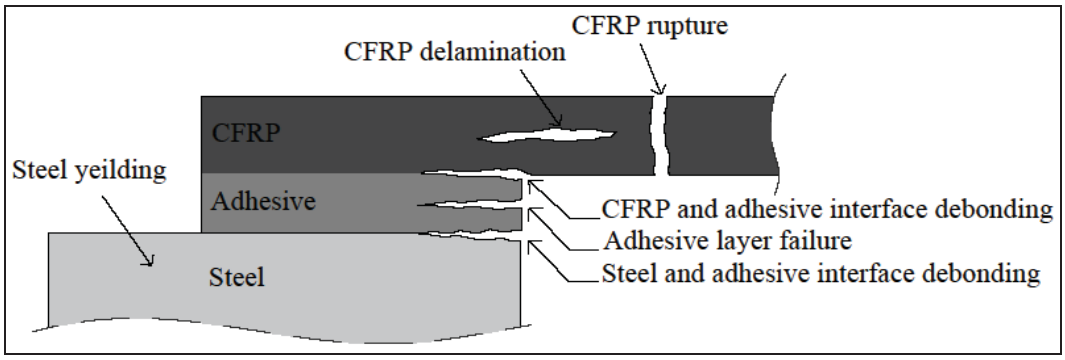

Figure 2.2 Possible failure modes of CFRP/steel joints under tensile loading
Adapted from Zhao and Zhang (2007, p. 1812)

Table 2.2 presents details of the previous studies on the bond behavior of CFRP/steel joints. It should be noted that in some research studies, the applied CFRP was claimed to be UHM. However, based on the classification presented in Table 2.1, they should be considered HM or NM CFRP. The elastic modulus of the applied CFRPs in these studies varied from 270 GPa to 640 GPa. However, investigations involving UHM CFRP have not been adequately documented. Based on these studies, it can be inferred that using CFRP with a higher elastic modulus can lead to an improvement in the load-carrying capacity of CFRP/steel joints (Peiris, 2011). Moreover, it has been found that the failure mode is altered as the elastic modulus and type of CFRP change (Fawzia, Zhao et al., 2005; Jiao & Zhao, 2004). Nevertheless, the influence of fatigue loading on bond behavior was reported to be insignificant, as only a limited bond region adjacent to the joint, known as the fatigue damage zone, was prone to fatigue damage (Wu, Zhao et al., 2013). It was also found that the failure mode changed as the temperature increased (He, Xian et al., 2020). The dominated failure mode at elevated temperatures is cohesion failure within the adhesive layer (Zhou, Fernando et al., 2020). In addition, the debonding loads of the CFRP/steel joints are notably decreased at both low and high service temperatures (Guo, Wu et al., 2022).

Table 2.2 Experimental details of studies regarding the bond behavior of CFRP/steel joints. Note: (a) Adhesive Thickness, (b) Adhesive Type, (c) Adhesive Elastic Modulus, (d) Steel Stiffeners, (e) CFRP Configurations, (f) CFRP Thickness, (g) CFRP to Steel Width Ratio, (h) CFRP Bond Length, (i) CFRP Axial Rigidity, (j) Loading Amplitude

Ref.	fy (MPa)	Es (GPa)	fa (MPa)	Ea (GPa)	ta (mm)	fp (MPa)	Ep (GPa)	tp (mm)	Type of FRP	Test set-up	Steel plate (mm) ($L_s \times w_s \times t_s$)	Influencing parameters								
												a	b	c	d	e	f	g	h	i	j
Photiou (2005)	375	205	14.8 43 32	6.8-7.3 2.1 3.5	0.1 0.5 1	2109.3 1120.8	135.3 270.1	1.2	NM HM	*S *D	225×25×1.5 225×25×3 225×25×6	✓	✓	✓		✓				✓
Xia and Teng (2005)	–	–	22.53 20.48 13.89	4.01 10.79 5.43	1 2 3 4	–	165	1.2	NM	S	305×118×12	✓	✓	✓						
Schnerch, Dawood et al. (2006)	–	–	37.1	3	1	–	338 460	4 8	HM UHM	D	L_s =200, 400					✓	✓			
Colombi and Poggi (2006)	317.8	–	24.8 30	4.5 3.8	0.8 1	>2800	197	1.4	NM	D	460×60×6 600×60×6 1200×60×60		✓			✓				
Stanford (2009)	–	200	76	3.1	-	2448 1190	640 340	0.19 1.42	UHM HM	D	128.2×25.4×3.3 258.3×25.4×3.3	✓				✓	✓	✓		✓
Peiris (2011)	409	200	34.6	3	0.6-0.7	2979 1923	187 514	1.2	NM UHM	D	250×50×4.8 300×50×4.8 610×50×4.8							✓		
Wu, Zhao et al. (2012)	300	200	28.6 24	1.9 9.2	var	1500	460	1.45	UHM	D	300×50×30		✓						✓	
Yu, Fernando et al. (2012)	–	200	22.34 31.28 14.73 21.46	11.25 4.82 1.75 1.83	0.5 2 3	– –	150 235 340	1.2 1.4	NM MM HM	S	L_s =450 t_s =30	✓	✓						✓	
Nguyen, Bai et al. (2013)	359	200	32	1.9	-	2300	256	-	HM	D	180×50×5									✓
Wu, Zhao et al. (2013)	487	200.6	28.6	1.90	0.66	1607	478.73	1.45	UHM	D	300×50×10									✓
He and Xian (2017)	300	–	33.16	11.3	1	1970	185	1.44	NM	S	**100 × 100 L_s = 250 t_s = 5									
Chataigner, Benzarti et al. (2018)	235	210	35	–	var	–	460	-	UHM	D	450×60×15 450×60×10		✓							
Peiris and Harik (2018)	410	–	34.6	3.01	-	1200 2800	450 165	1.2	UHM NM	D	610×50×5 610×50×4.8 610×50×9.5					✓		✓		
Wang and Wu (2018)	414	198	27.6 15.1	12.2- 1.75	var	2760	164	1.4	NM	S	t_s =20		✓	✓						
Elkhabeery, Safar et al. (2018)	235	-	26–31	11.2	1-2	3100	170	1.2	NM	D	w_s=75 t_s=12								✓	
Yang, Zhao et al. (2021)	400	210	21.76	8.4	-	1820 1840	180.5 163.3	1.46 1.26	NM	D	w_s=55 t_s=5					✓				

* S = single strap joints/D = double strap joints; ** square steel tubes.

2.3.2 Adhesive

The mechanical properties of adhesive have a notable effect on the bond behavior of steel members retrofitted with CFRP (Al-Mosawe & Al-Mahaidi, 2019; Al-Mosawe, Al-Mahaidi et al., 2016; He & Xian, 2016; Li, Li et al., 2020). As the adhesive is the weakest link in the CFRP and steel joint, selecting a proper adhesive can ensure the maximum capacity of the retrofitting system. In most research studies, commercial adhesives are utilized for retrofitting structures (Li, Ke et al., 2019; Wang & Wu, 2018; Yu, Fernando et al., 2012). Figure 2.3 shows the stress–strain curves for these adhesives. It should be noted that the mechanical properties of the adhesive may decrease with increasing temperature (Zhou, Fernando et al., 2020). Commercial adhesives have been found to possess insufficient strength, often resulting in brittle failure. Consequently, research efforts have been directed towards enhancing adhesive performance, particularly in terms of mechanical properties (Ferreira, Brito et al., 2018; Li, Li et al., 2020; Sousa, Correia et al., 2018; Wan, Gong et al., 2014; Xie, You et al., 2023; Zhou, Liu et al., 2016). Utilizing enhanced adhesive can change the failure mode of the CFRP/steel joints (Razavi, Ayatollahi et al., 2018; Saraç, Adin et al., 2018).

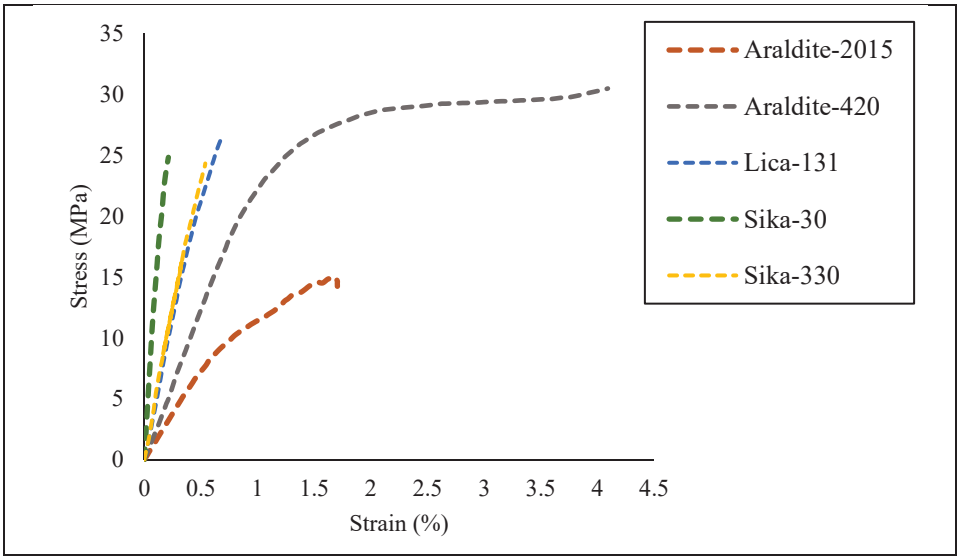

Figure 2.3 Tensile stress–strain curve of commercial adhesives used in bonding CFRP to steel substrate
Taken from Wang and Wu (2018, p. 1205) and Li, Li et al. (2020, p. 6)

Among the commercial adhesives, Sikadur and Araldite have been commonly utilized. It was shown that specimens with Araldite 2015 adhesive exhibited a much higher interfacial fracture energy compared to the specimens with Sikadur 30 adhesive (Wang & Wu, 2018). Indeed, specimens retrofitted with nonlinear adhesives having higher strain capacity but lower elastic modulus exhibit higher interfacial fracture energy and thereby a higher bond strength compared to the ones with linear adhesives having similar or even higher elastic modulus (Mohabeddine, Malik et al., 2023; Yu, Fernando et al., 2012). The type of adhesive can also significantly influence the bond–slip relationship. Bond–slip can be estimated as a triangular shape for linear adhesive and a trapezoidal shape for nonlinear adhesive (Fernando, 2010). The average effective bond length of specimens bonded with nonlinear adhesive was also found to be greater than that of specimens with linear adhesive, which could be attributable to the higher ductile behavior of nonlinear adhesive compared to the linear one (Wu, Zhao et al., 2012). It is also found that the effective bond length, interfacial fracture energy, and ultimate load increase with the increase in adhesive thickness (Wang & Wu, 2018; Wang, Wu et al., 2016b). In addition, increasing the adhesive thickness can change the failure mode from cohesive failure to CFRP delamination (Wang, Wu et al., 2016a; Xia & Teng, 2005; Yu, Fernando et al., 2012). However, specimens with lower adhesive thickness exhibited better performance in terms of the average peel stresses and failure load (Photiou, 2005). It is worth mentioning that assessing the effect of adhesive thickness on the failure mode is difficult due to the non-uniform thickness of the bond-line (Fawzia, 2007). It is suggested to increase the adhesive thickness up to 2 mm to avoid cohesive failure (The Institution of Structural Engineers (ISE), 1999; Xia & Teng, 2005). Non-cohesive failure in the bond test has been reported in the literature (Fawzia, 2013; Fawzia, Zhao et al., 2010; He & Xian, 2016; Heshmati, Haghani et al., 2018; Wu, Zhao et al., 2012; Yu, Fernando et al., 2012). Increasing the adhesive thickness to 3 mm may result in lower bond strength compared to a thickness of 2 mm (Yu, Fernando et al., 2012). Consequently, it can be concluded that the adhesive's mechanical properties and thickness are the key factors in the bond behavior of CFRP retrofitted steel components (Wang & Wu, 2018; Xie, You et al., 2023). Furthermore, the adhesive layer, regardless of the type of adhesive, can help prevent potential galvanic corrosion if the bond quality is strictly controlled (Wu, Yu et al., 2021). Furthermore, investigations on the impact of bond-line defects on the

bond behavior of CFRP steel joints suggest that the size of the defect plays a more significant role in determining the failure mode than the number of defects (Wu, Yu et al., 2023).

2.3.3 Surface preparation

Surface preparation is one of the most crucial parameters of the bond behavior of the CFRP retrofitted elements. The bond capacity can be determined by the cohesion strength of the adhesive as well as the adhesion strength of the interface between the adhesive and the substrate (Fernando, Teng et al., 2013). Adhesion failure can occur at the CFRP/adhesive or the steel/adhesive interface. However, debonding at the steel/adhesive interface is more likely to occur (Hollaway & Cadei, 2002; Schnerch, 2005). Therefore, the preparation of the steel substrate has received more attention. The adhesion is mainly provided by mechanical interlocking and chemical bonding between the adhesive and the adherend (Lorenzo, 1997). It is debatable regarding the agent that is responsible for strong bonds. However, it seems that chemical bonding is more important than mechanical bonding (Hollaway & Cadei, 2002). To improve the mechanical bonding, the steel substrate is roughened before the CFRP bonding process. However, applying an improper roughening technique may cause tiny crevices in which the trapped air bubbles or solvent can induce failure in a rigid adhesive by increasing the stress concentrations (Baldan, 2004). It can also reduce the contact between the adhesive and the adherent, which is so-called wetting (Ebnesajjad & Ebnesajjad, 2013). Indeed, increasing the contact surface area leads to enhanced wetting and more extensive chemical bonding (Ebnesajjad & Landrock, 2014). The most commonly used mechanical treatments are grit blasting, needle scaler, and sandpaper. In these abrasive techniques, the surface geometry of the substrate is modified and the oxide layer is removed. It is generally accepted that using the grit blasting method is effective (Fernando, Teng et al., 2013; Hollaway & Cadei, 2002; Schnerch, Dawood et al., 2007). It also can lead to modifying the surface chemical composition by removing the contaminants such as oil and grease. However, it can introduce grit residues or other contaminants onto the steel substrate (Islam, Tong et al., 2014). Furthermore, the grit type should be carefully chosen to ensure chemical compatibility with the applied adhesive

(Fernando, Teng et al., 2013). Improper surface preparation can lead to premature failure, thereby hindering the achievement of the full capacity of the CFRP retrofitting technique.

2.3.4 Bond length

Research findings show that the bond strength, as well as the failure modes of CFRP bonded steel elements, can be affected by the bond length (Narmashiri, Jumaat et al., 2012). The bond strength of the CFRP/steel interface tends to increase at greater bond lengths. The strain level experienced by the applied adhesive was seen to drop significantly when a longer bond length was used (Narmashiri, Jumaat et al., 2012). Therefore, it is more likely for specimens with shorter bond lengths to undergo debonding failure, whereas steel components retrofitted with greater CFRP bond lengths are more likely to fail due to CFRP rupture. However, increasing the bond length from a certain threshold, the so-called effective bond length, does not yield a further increase in the bond strength (Al-Zubaidy, Al-Mahaidi et al., 2012; Bocciarelli, Colombi et al., 2009; Chiew, Yu et al., 2011; Fawzia, Al-Mahaidi et al., 2006; Fernando, 2010; Yang, Biscaia et al., 2017). Moreover, increasing either the CFRP elastic modulus or CFRP thickness results in an increase in CFRP/steel bond strength, although applying CFRP with higher axial stiffness seems to require a greater bond length (Al-Zubaidy, Al-Mahaidi et al., 2012, 2013). Furthermore, the type of adhesive has a significant effect on the effective bond length (Korayem, Li et al., 2015). Applying the nonlinear adhesive can increase the bond strength and the effective bond length compared to the linear adhesive as a result of its ductile behavior and larger elongation at break (Wu, Zhao et al., 2012). It was also found that the rate of impact loading has a trivial effect on the effective bond length; however, it has a notable effect on the bond strength and failure modes (Al-Mosawe, Al-Mahaidi et al., 2016; Al-Zubaidy, Al-Mahaidi et al., 2012; Al-Zubaidy, Zhao et al., 2012, 2013; Huo, Zhang et al., 2019). Although the effect of bond length on the stiffness of the retrofitted elements is negligible, it can increase the load-carrying capacity of the components (Shaat & Fam, 2008). The proposed formulas to calculate the effective bond length are provided in Table 2.3.

Table 2.3 Bond strength and effective bond length for CFRP/steel interface

Ref.	Effective bond Length	Maximum Shear Stress	Ultimate Load	Remarks
Xia and Teng (2005)	$\frac{\pi}{2\sqrt{\tau_f/E_p t_p \delta_f}}$	$0.8\, f_a$	$b_p\sqrt{2G_f E_p t_p}$	-
Bocciarelli, Colombi et al. (2007)	$2.77\sqrt{\frac{\beta}{\beta+1}} \times \frac{\sqrt{2G_f E_p t_p}}{\tau_f}$	$\sqrt{\frac{G_a G_f}{2.72 t_a}}$	$N\sqrt{\frac{\beta+1}{\beta}} \times b_p\sqrt{2G_f E_p t_p}$	$\beta = \frac{b_s t_s E_s}{2 b_p t_p E_p}$
Dehghani, Daneshjoo et al. (2012)	$3.5\sqrt{\frac{E_p t_p t_a}{G_a}}$	$0.8\, f_a$	$b_p\sqrt{2G_f E_p t_p}$	-
Fernando, Yu et al. (2014)	$a_d + b_e + \frac{1}{\lambda_1}\ln\left(\frac{1+C}{1-C}\right)$	$0.9\, f_a$	$b_p\sqrt{2G_f E_p t_p}$	$a_d = \frac{1}{\lambda_1}\left[\sqrt{\left(2\frac{\delta_2}{\delta_1} - 1\right)} - 1\right)\right]$ $b_e = \frac{1}{\lambda_2} arcsin\left[\frac{\lambda_2 \lambda}{0.97\delta_1 {\lambda_1}^2}(\delta_f - \delta_2)\right]$ $C = \frac{\lambda_2}{\lambda_1 \delta_1}(\delta_f - \delta_2)\cot(\lambda_2 b_e) - \lambda_1 a_d$ $\lambda^2 = \frac{\tau_f}{2G_f}\left(\frac{1}{E_p t_p} + \frac{b_p}{E_s t_s b_s}\right)$ $\lambda_1^2 = \frac{2G_f}{\tau_f \delta_1}\lambda^2$ $\lambda_2^2 = \frac{2G_f}{\tau_f(\delta_f - \delta_2)}\lambda^2$
Yang, Biscaia et al. (2017)	$\delta_1\sqrt{\frac{2E_p t_p}{G_f(1+2\beta)}}$	-	$b_p\sqrt{2G_f E_p t_p(1+2\alpha)}$	$\alpha = \frac{b_p E_p t_p}{b_s E_s t_s}$

As observed, the ultimate load is not influenced by the adhesive thickness. This issue is also the same for calculating the ultimate load in CFRP/concrete joints (Chen and Teng 2001).

2.3.5 Bond–slip models

The bond–slip model presents a formula that predicts the interfacial fracture energy based on the adhesive properties (Fernando, 2010). The effective bond length and bond strength can be achieved by the bond–slip relationship. This relationship can be experimentally determined from strain gauges along the bond length through bonded joint tests (Wang, Wu et al., 2016a). The bond–slip curve for linear adhesive is different from that of nonlinear adhesive. Linear adhesives have an approximately bi-linear shape. However, nonlinear adhesives exhibit an approximately trapezoidal shape, as presented in Table 2.4. As for the CFRP/concrete joints, the bond–slip curve always has a roughly bi-linear shape due to the brittle behavior of concrete (Yu, Fernando et al., 2012). Therefore, the bond–slip models for CFRP/steel joints are different and should be developed based on the adhesive behavior. A number of bond–slip models have been proposed for CFRP/steel bonded joints, as shown in Table 2.5.

The bond–slip models are categorized as bi-linear, tri-linear, and simplified models. Bi-linear and simplified models were proposed for FRP/concrete and FRP/steel interfaces. The parameters of the bond–slip models for FRP/concrete bonded joints are expressed based on the tensile strength of the concrete, as the concrete is commonly the weakest link of the joint (Fernando, 2010). However, for CFRP/steel joints, these parameters are defined based on the tensile strength of adhesive since the weakest link of the joint is usually adhesive. In addition, the tri-linear model was presented for only CFRP/steel interfaces and utilized for nonlinear adhesive. It should be noted that the area under the curve is representative of the interfacial fracture energy in these models (Pang, Wu et al., 2019; Wang, Liu et al., 2021).

Table 2.4 Type of bond–slip models

Ref.	Type of Model	Bond–Slip Model	Bond–Slip Curves
Monti, Renzelli et al. (2003)	Bi-linear	$\begin{cases} \tau = \tau_f \dfrac{\delta}{\delta_1} & \delta \le \delta_1 \\ \tau = \tau_f \dfrac{\delta_f - \delta}{\delta_f - \delta_1} & \delta_1 < \delta \le \delta_f \\ \tau = 0 & \delta > \delta_f \end{cases}$	
Lu, Teng et al. (2005)	Simplified	$\begin{cases} \tau = \tau_f \sqrt{\dfrac{\delta}{\delta_1}} & \delta \le \delta_1 \\ \tau = \tau_f \exp\left[-\alpha\left(\dfrac{\delta}{\delta_1} - 1\right)\right] & \delta > \delta_1 \end{cases}$ $\alpha = \dfrac{3\tau_f \delta_1}{3G_f - 2\tau_f \delta_1}$	
Dehghani, Daneshjoo et al. (2012)	Tri-linear	$\begin{cases} \tau = \tau_f \dfrac{\delta}{\delta_1} & \delta \le \delta_1 \\ \tau = \tau_f & \delta_1 < \delta \le \delta_2 \\ \tau = \tau_f \dfrac{\delta_f - \delta}{\delta_f - \delta_2} & \delta_2 < \delta \le \delta_f \\ \tau = 0 & \delta > \delta_f \end{cases}$	

Table 2.5 Bond–slip models proposed for CFRP/steel interface

Ref.	Type of Model	τ_f	δ_1	δ_2	δ_f
Xia and Teng (2005)	Bi-linear	$0.8\,f_a$	$0.8\frac{t_a}{G_a}f_a$	N/A	$\frac{2G_f}{\tau_f}$
Fawzia, Zhao et al. (2010)	Bi-linear	f_a	$\frac{t_a}{10}$	N/A	$\begin{cases}\frac{t_a}{4} & if\ t_a = a \\ 0.125 + \frac{t_a - 0.5}{10} & if\ t_a = b\end{cases}$
Fernando (2010)	Bi-linear	$0.9\,f_a$	$0.3(\frac{t_a}{G_a})^{0.65}f_a$	N/A	$\frac{2G_f}{\tau_f}$
Fernando (2010)	Simplified	$0.8\,f_a$	$0.3(\frac{t_a}{G_a})^{0.65}f_a$	N/A	-
Dehghani, Daneshjoo et al. (2012)	Tri-linear	$0.8\,f_a$	$0.8\frac{t_a}{G_a}f_a$	$\frac{\delta_f}{3}$	$\frac{3G_f}{2\tau_f} + \frac{3}{4}\delta_1$
Wang and Wu (2018)	Bi-linear	$0.9\,f_a$	$2.61\frac{t_a^{0.34}}{G_a}f_a$	N/A	$166.2\frac{t_a^{0.4}}{E_a^{1.7}}f_a^{2.4}$
Wang and Wu (2018)	Tri-linear	$0.9\,f_a$	$2.61\frac{t_a^{0.34}}{G_a}f_a$	$55.4\frac{t_a^{0.4}f_a^{2.4}}{E_a^{1.7}} + 0.85\frac{t_a^{0.34}f_a}{G_a}$	$\frac{2}{3}(\frac{2G_f}{\tau_f} + \delta_1)$
Pang, Wu et al. (2021)	Bi-linear	$0.544\,\tau^{*1.21}$	$1.51\frac{t_a^{0.378}}{G_a}\tau^{*1.21}$	N/A	$\frac{2G_f}{\tau_f}$

* a = 0.1 - 0.5 mm/ **b = 0.5 - 1 mm

2.4 Flexural retrofitting of steel beams

This section reviews the studies related to the flexural behavior of the steel structures retrofitted with CFRP. Various modes of failure in CFRP retrofitted beams were reported, as shown in Figure 2.4, such as (a) CFRP end-debonding and intermediate-debonding; (b) CFRP delamination or rupture; (c) bending failure in which yielding occurs in beam flanges and web (d) local bucking, which occurs in compression flange or web; (e) lateral-torsional buckling (Elkhabeery, Safar et al., 2018).

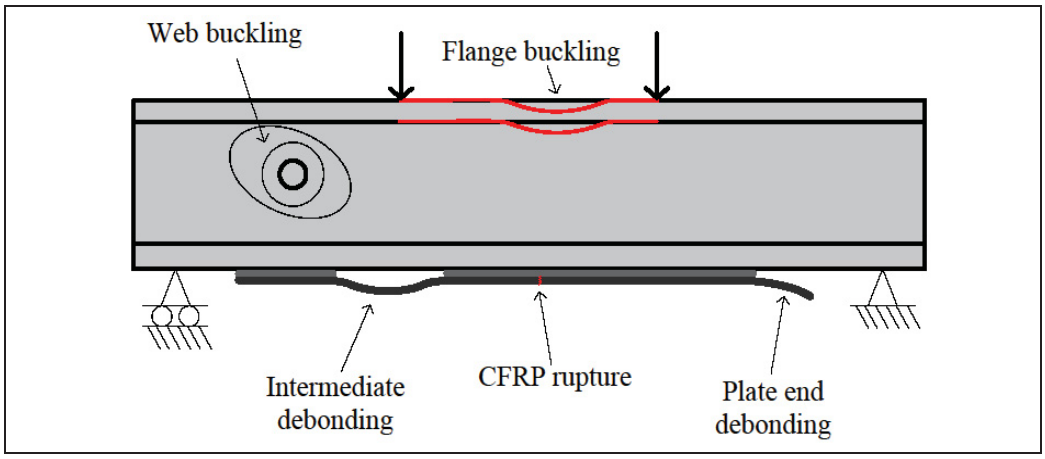

Figure 2.4 Some of the failure modes of steel beams strengthened with FRP plate
Adapted from Teng, Yu et al. (2012, p. 136)

To investigate CFRP retrofitting technique efficiency, the lateral and local buckling of steel beams should be controlled or eliminated (Zeng, Gao et al., 2018). Among the aforementioned failure modes, the debonding of the CFRP has been found as the dominant failure mode for the specimens retrofitted with NM CFRP (Colombi & Poggi, 2006a; Deng & Lee, 2007; Elkhabeery, Safar et al., 2018; Sallam, Ahmad et al., 2006; Teng, Fernando et al., 2015). CFRP end-debonding is the common failure mode for beams that are retrofitted in flexural yielding (Elkhabeery, Safar et al., 2018). It should be noted that if a longer CFRP plate is applied, the failure mode could turn into a different failure mode, in particular, intermediate-debonding (Teng, Fernando et al., 2015). On the other hand, the CFRP rupture was reported as the common failure mode for HM and UHM CFRP (Schnerch & Rizkalla, 2008; Zhao & Zhang,

2007). This phenomenon occurs due to the lower rupture strain of CFRP featuring a higher elastic modulus and the reduced stresses of the adhesives at the ends (Peiris, 2011). However, strengthened steel beams using UHM CFRP strips showed debonding failure at strip panel finger joints due to high shear stresses (Peiris & Harik, 2021). The most studied parameters in existing research investigations of CFRP retrofitted structures in flexure include adhesive thickness, adhesive type, CFRP configurations, CFRP thickness, and CFRP bond length. Details of previous studies on the flexural behavior of the CFRP-strengthened and rehabilitated steel beams are presented in Table 2.6.

Experimental observations on the effect of CFRP retrofitting systems on steel–concrete composite beams indicated a significant strength increase in specimens retrofitted with CFRP (Al-Saidy, 2001; Schnerch & Rizkalla, 2008). In these cases, concrete crushing and CFRP rupture were reported as the main failure modes. In addition, it was suggested to attach CFRP laminates to beam webs which can lead to a decrease in the interfacial shear stress of the adhesive between the bottom CFRP plate and the steel due to shifting the neutral axis to a lower level (Al-Saidy, 2001). The application of small-diameter strands of CFRP was also found effective in flexural strengthening of steel bridge girder, especially for NM CFRP (Tabrizi, Kazem et al., 2015).

The flexural capacity of the steel beams can also be enhanced by using CFRP laminates with higher tensile strength or increased thickness (Linghoff, Al-Emrani et al., 2010). Furthermore, the CFRP laminates with higher elastic modulus have a better performance in enhancing the ductility of the strengthened beams (Al-Saidy, 2001). Failure analysis and structural behavior of CFRP-strengthened steel beams show that the load-carrying capacity with thicker and longer CFRP plates increases, though excessive thickness could cause premature debonding (Narmashiri, Ramli Sulong et al., 2012).

Table 2.6 Experimental flexural tests on CFRP retrofitted steel specimens

Ref.	Loading condition	Test setup	L_{span} (mm)	Steel section (mm)	E_s (GPa)	f_y (MPa)	f_u (MPa)	CFRP Type	t_p (mm)	E_p (GPa)	F_p (MPa)	Adhesive Type	t_a (mm)	E_a (GPa)	f_a (MPa)	τ_a (MPa)
Al-Saidy (2001)	Static	*F	3048	**W8×15	-	363.4	496.4	NM HM	1.4	152 200	2482 >2482	-	-	-	68.9	-
Tavakkolizadeh and Saadatmanesh (2003)	Fatigue	F	1300	S127×4.5	194.4 (flange) 199.9 (web)	336.4 (flange) 330.9 (web)	-	NM	-	144	2137	-	-	-	-	-
Liu (2003)	Static	*T	2743.2	W12×14	-	-	-	HM	1.4	>200	>2300	-	-	-	-	-
Nozaka, Shield et al. (2005)	Fatigue	F	-	W14×68	-	340	-	NM	-	157 114	2600 790	Sikadur 330 Sikadur 30 PLUS 25 DP-460 NS Tyfo TC	- -	4.6 - - 1.8 -	41 25 17 35 47	-
Lenwari, Thepchatri et al. (2006)	Static Fatigue	F	1800	W100×17.5	200	-	-	HM	1.4	300	1800	Sikadur 30	-	2.75	-	-
Colombi and Poggi (2006)	Static	T	2500	HEA140	-	331	469	NM	1.4	197	>2800	Sikadur 30 Sikadur-330	-	4.5 3.8	24.8 30	24.8 -
Dawood, Rizkalla et al. (2007)	Fatigue	F	-	W200×19	200	380	-	UHM	-	460	-	-	-	-	-	-
Schnerch and Rizkalla (2008)	Static	F	6550	**W310×45	-	369-408	-	NM UHM	3.2 2.9 4	229 457	1224 1534	Spabond-345	-	-	-	-
Deng and Lee (2007)	Static	T&F	1200	127×76UB13	205	-	-	HM	3 6	212	-	Sikadur 30	1	8	29.7	-
Linghoff, Al-Emrani et al. (2010)	Static	F	2000	HEA180	212	330	-	NM HM	1.4 1.8 2.4	200 330 165	3300 1500 3100	-	2	7 4.5	25 30	-
Vatandoost (2010)	Fatigue	F	-	W310×74	200	350	450	NM HM	-	165 210	2520 2805	Sikadur-30	-	-	-	-
Peiris (2011)	Static	F	2743	**W10 × 22 C7 × 9.8	200	407 414	510 531	UHM	1.2	514	1923	Spabond-345	2.5	3	34.6	-
Narmashiri, Jumaat et al. (2012)	Static	F	2000	I-section beam: w_b= 100 h_b= 150 t_f= 10 t_w= 6.6	-	250	370	NM	1.2	165	3100	Sikadur-30	1	11.2	24–31	14–19

*Test setup: T = Three-point bending/F = Four-point bending; ** Steel/concrete composite beam

Table 2.6 Experimental flexural tests on CFRP retrofitted steel specimens (continued)

Ref.	Loading condition	Test setup	L_{span} (mm)	Steel section (mm)	E_s (GPa)	f_y (MPa)	f_u (MPa)	CFRP Type	t_p (mm)	E_p (GPa)	F_p (MPa)	Adhesive Type	t_a (mm)	E_a (GPa)	f_a (MPa)	τ_a (MPa)
Wu, Wang et al. (2012)	Fatigue	F	-	H350×175	-	-	-	UHM NM SW-BFRP	-	436.4 145 108.3	1500 2500 1789	Sikadur-30	-	2.627	31.7	14.4
Karam (2015)	Static	F	2000	**UC203×203×46	200	318.75	459	LM	-	65.364	736.6	Sikadur-330	-	4.5	30	-
Tabrizi, Kazem et al. (2015)	Static fatigue	F	3350	W8×13	-	-	-	NM HM	-	134.6 226.3	2288 2218	-	-	-	-	-
Colombi and Fava (2015)	Fatigue	F	1000	IPE120	208	330	444	NM	2.8	195	>2800	Sikadur 30 Sikadur 330	-	>4.5 >3.8	>28.4 >30	-
Ghafoori (2015)	Fatigue	F	-	IPE120	199.3	383	462	NM HM UHM	1.4	159 220 440	2800 2800 1200	Araldite AW106	-	-	-	-
Colombi and Fava (2016)	Fatigue	F	1000	IPE120	208	330	444	HM	1.4	205	3200	Sikadur 30 Sikadur 330	-	>4.5 >3.8	>28.4 >30	-
Sweedan, Alhadid et al. (2016)	Static	T	3000	UB203×102×23	190	335	429	Hybrid CFRP-GFRP	3.175 6.35	62.19	852	-	-	-	-	-
Yu and Wu (2017)	Fatigue	F	-	I-shaped	192.8	378.2	519	NM	-	200.4	3022.4	-	-	-	-	-
Yu and Wu (2017)	Fatigue	F	-	I-shaped	192.8	378.2	519	HM	-	200.4	3022.4	Araldite 420 Sikadur 30	-	1.495 11.2	29 30	-
Zeng, Gao et al. (2018)	Static	F	2000	H-section	185	210.4	332.1	NM	1.2	167.3	2398.3	Sikadur-30	-	11.3	22.3	-
Yu and Wu (2018)	Fatigue	F	-	I-shaped	192.8	378.2	519	HM	-	200.4	3022.4	Araldite 420 Sikadur 30	-	1.495 11.2	29 30	-
Li, Zhu et al. (2022)	Fatigue	F	1300	H-section	197.3	158.8	-	NM	2	183.2	2239.5	Lica-131	-	5.7	39.2	-

*Test setup: T = Three-point bending/F = Four-point bending; ** Steel/concrete composite beam

In order to prevent debonding failure and use the full capacity of the CFRP, mechanical anchorage systems have been utilized. It was shown that the mechanically fastened CFRP technique outperformed CFRP sheets in flexural strength and ductility (Karam, 2015). Moreover, the application of the anchorage system to hybrid FRP also resulted in the same results (Sweedan, Alhadid et al., 2016). Furthermore, in this case, prestressing CFRP increases the efficiency of the retrofitting method (Wang, Bian et al., 2023). In addition, this technique can delay crack propagation and also results in an increase in the fatigue life of specimens (Yu & Wu, 2017b).

A comparison between the performance of different FRP techniques as well as using steel plates for retrofitting reveal that HM CFRP is superior to the other rehabilitation methods in terms of fatigue behavior (Wu, Wang et al., 2012). CFRP can significantly extend the fatigue life of the steel specimens and increase the average number of load cycles to failure (Tavakkolizadeh & Saadatmanesh, 2003). Furthermore, CFRP materials can enhance the flexural fatigue behavior of the steel beams in terms of elastic stiffness, yield load, and nominal capacity (Dawood, Rizkalla et al., 2007). The CFRP retrofitting method can also contribute to a reduction in fatigue crack growth in damaged steel beams (Colombi & Fava, 2015). In this regard, the elastic modulus of the CFRP is also found an important parameter in enhancing the fatigue life of specimens. Specimens retrofitted with higher elastic modulus outperform those retrofitted with CFRP with lower elastic modulus (Vatandoost, 2010). Furthermore, the stress intensity factor can be affected by the number of CFRP layers. It was shown that the stress intensity factor in specimens with a double CFRP configuration is significantly less than of the specimens strengthened with a single CFRP layer (Colombi & Fava, 2016).

As for the type of adhesives, it was found that adhesives with relatively high ductility can effectively redistribute stress within the adhesive layer during increased loading. (Nozaka, Shield et al., 2005). Consequently, it is suggested to use nonlinear adhesives for retrofitting steel structures as the specimens bonded with linear adhesives are more susceptible to interfacial debonding (Yu & Wu, 2017a).

Prestressing CFRP sheets can effectively increase the fatigue life of cracked steel elements as compressive forces are applied to the crack edges, thereby hindering crack growth in steel structures (Emdad & Al-Mahaidi, 2015). It was also shown that the prestressed CFRP can decrease the interfacial stress at the notch location and delay interfacial debonding (Li, Zhu et al., 2022). Also, the level of the prestressing of the CFRP has a significant effect on extending the fatigue life of strengthened specimens (Vatandoost, 2010). The minimum level for prestressing the CFRP needed to increase the fatigue life of steel beams was determined in the literature (Ghafoori, Motavalli et al., 2015).

2.5 Numerical analysis

Computational methods present a cost-effective tool for a better understanding of the performance of the retrofitted components. In this regard, many numerical studies have been proposed to investigate the bond behavior of the retrofitted elements with CFRP.

Peiris (2011) investigated a numerical study on the bond behavior of CFRP/steel joints using ANSYS (2009) software for NM and UHM CFRP by analyzing double-strap joint and doubly reinforced steel plates. An eight-node element of SOLID45 was used due to its large deflection and strain capabilities. The CFRP layer and adhesive were modeled as a single layer of elements. The results showed that the numerical element strains are in good agreement with experimental results except at the gap of the joints. Furthermore, the tensile stress obtained from finite element (FE) analysis is less than the experimental ones for ultra-high modulus CFRP. In this study, steel beams strengthened with UHM CFRP were also modeled. Contrary to CFRP/steel joint models, 4-node SHELL181 elements were utilized to simulate beams to reduce the computational costs. However, the proposed model could not predict the failure of the beam or the laminate for strip panel configuration as a result of the simplified assumptions of the SHELL181 element.

Wu and Zhao (2012) modeled CFRP/steel joints using ABAQUS software, utilizing CPE4R elements for the CFRP and steel adherents and COH2D4 elements for the adhesive layer. The

tie constraint, used in ABAQUS to establish perfect interface connection, was applied to the CFRP/adhesive and steel/adhesive surfaces. The numerical findings aligned well with experimental results in terms of the ultimate load, and bond–slip relationships. Al-Mosawe et al. (2016) presented a numerical investigation of the effect of high load rates on the bond behavior of CFRP/steel double strap joints using ABAQUS for LM and NM CFRP. The C3D8R, SC8R, and COH3D8 elements were utilized to model steel plates, CFRP laminate, and the adhesive layer, respectively. The tie constraint was also applied to the adhesive layer with steel and CFRP. It was found that the effective bond length for specimens subjected to high loading rates was shorter compared to the specimens tested under quasi-static loading.

The flexural behavior of steel beams strengthened with CFRP sheets using ANSYS was studied by Elkhabeery et al. (2018). SOLID186 elements were selected to model steel and CFRP sheets. To model the epoxy layer, the INTER204 element was used. The adhesive layer was defined as linear elastic material and the mixed-mode bi-linear cohesive zone model (CZM) was selected to model the bond between steel and CFRP. The parametric study showed that the CFRP system is very efficient in strengthening compact mono-symmetric sections, whereas its effect is very negligible for non-compact sections. The CFRP/steel double overlapped bonded joints were simulated by Yang et al. (2021). It was revealed that the initial stiffness of the load versus slip relationship increases with the elastic modulus of CFRP laminate. Colombi et al. (2006a) carried out a numerical study on the static behavior of the steel beams strengthened with CFRP strips. A standard two nodes beam element was applied to model the beam and a standard eight-node plane stress element was selected to model CFRP strips as well as the adhesive layer. To ensure the compatibility of the deformations of the beams and strips, multipoint constraints were imposed between the beam nodes and the corresponding adhesive nodes. The adhesive stresses estimated by the FE model were in good agreement with their counterparts obtained from the analytical approach. A 2D FE model was proposed by Lenwari (2006) to investigate the debonding strength of steel beams strengthened with CFRP. To this end, the eight-node element with two degrees of freedom at each node was utilized. Furthermore, it was assumed that the CFRP material is isotropic. The results indicated that the adhesive modulus, the CFRP thickness, and the CFRP modulus significantly affect the

debonding strength. Fernando (2010) studied the prediction of the debonding failure in RHS steel tubes strengthened with CFRP using a bond–slip model under an end-bearing load. C3D8, S4R, and COH3D8 elements were used to model the bearing plate, CFRP plate, and adhesive layer. The tie constraint was applied to adhesive surfaces connected to the CFRP plate and tub web. The results indicated that the debonding process in the FE model is much more gradual which can lead to higher stiffness in the load–displacement curve prior to reaching the ultimate load. A numerical investigation on the interfacial behavior of the bond between CFRP laminate and steel beam was presented by Linghoff et al. (2010). In this study, all parts were modeled using C3D20R solid elements and the common nodes at the interfaces were merged. It is found that interfacial shear stress as well as peel stress are not uniformly distributed over the width of the adhesive layer. Furthermore, the distribution of the peeling stresses along the width of the bond-line is not the same for different strengthened beams. This variation is attributed to the higher axial stiffness of the CFRP laminate as a major parameter. Hmidan et al. (2011) investigated the flexural behavior of the steel beams repaired with CFRP sheets with various initial crack configurations by simulating a three-dimensional model in ANSYS. SOLID45 and LINK8 elements were utilized to model steel beams and CFRP sheets, respectively. These elements can be connected using interface elements as they have the same degree of freedom. The COMIN39 interface element was used to predefine crack propagation at the midspan of the beam. Results showed that the influence of the initial damage level on the failure mode of the repaired beam is negligible, whereas the damage level can have an effect on the web fracture rate of the beams. Moreover, the level of the initial damage determines the initiation of CFRP debonding. Deng (2018) studied the rehabilitation of notched steel beams using CFRP plates. In this regard, a mixed-mode cohesive law was used to model notched retrofitted steel beams. The findings show that increasing the CFRP elastic modulus and thickness can enhance the bearing capacity while reducing the ductility and leading to premature debonding failure. Wang et al. (2023) explored the effectiveness of using externally bonded CFRP using ductile adhesive. A trapezoidal mixed-mode CZM was used to simulate the debonding behavior of the CFRP-strengthened steel beam. The findings revealed that thicker or shorter CFRP laminates resulted in higher interfacial stresses, leading to earlier debonding, whereas longer CFRP laminates delayed debonding by changing the stress transfer path.

Table 2.7 provides a summary of the numerical studies presented in the literature. The realistic representation of stress distribution and failure modes in the rehabilitated elements with CFRP demands high computational costs. However, simplifications of the assumptions may not capture all real-world behaviors. Therefore, finding a middle ground that takes these factors into account is really important.

Table 2.7 Summary of numerical studies

Study	Software	Steel Element Type	CFRP Element Type	Adhesive Element Type	Interactions
Peiris (2011)	ANSYS (2009)	8-node SOLID45	8-node SOLID45	8-node SOLID45	Perfect interface
Wu, Zhao et al. (2012)	ABAQUS (V6.8)	CPE4R	CPE4R	COH2D4	Quadratic traction damage initiation criterion
Al-Mosawe, Al-Mahaidi et al. (2016)	ABAQUS (V6.13)	C3D8R	SC8R	COH3D8	Tie constraint
Elkhabeery, Safar et al. (2018)	ANSYS (V17)	SOLID186	SOLID186	INTER204	Mixed-mode bi-linear CZM
Yang, Zhao et al. (2021)	ABAQUS	T2D2	T2D2	COH2D4	Bi-linear bond–slip derived from experimental data
Colombi and Poggi (2006a)	ABAQUS	2-node beam element	8-node plane stress element	8-node plane stress element	Multipoint constraints
Lenwari, Thepchatri et al. (2006)	Not specified	8-node element with 2 DOF per node	8-node element with 2 DOF per node	Not specified	Reciprocal work contour integral method
Fernando (2010)	ABAQUS (2004)	C3D8	S4R	COH3D8	Tie constraint
Linghoff and Al-Emrani (2010)	ABAQUS (V6.4.1)	C3D20R	C3D20R	C3D20R	Common nodes merged
Hmidan, Kim et al. (2011)	ANSYS	SOLID45	LINK8	COMBIN39	Bi-linear bond–slip model
Deng, Li et al. (2018)	ABAQUS	C3D8I	COH3D8	COH3D8	Mixed-mode cohesive law
Wang, Xian et al. (2023)	ABAQUS	C3D8I	C3D8R	COH3D8	Trapezoidal mixed-mode CZM

2.6 Research needs and recommendations

A review of all the investigations regarding the application of CFRP materials for the retrofitting of steel members suggests that research in this area is rather limited. The number of parameters affecting the behavior of CFRP retrofitted steel members increases the complexity of their behavior. Accordingly, many experimental programs are needed to investigate the effect of these parameters. Furthermore, there are limited numerical investigations that can accurately predict the behavior of CFRP retrofitted steel components. Hence, special attention needs to be devoted to developing reliable numerical modeling. Although the applied CFRP in the literature includes various elastic moduli, investigations involving UHM CFRP have not been adequately documented. Therefore, further research is needed in this regard. Further investigations on the behavior of steel components retrofitted with CFRP could be conducted in the following recommended research areas:

- Further investigation is needed to develop adhesives with enhanced mechanical properties to improve bond strength and durability.

- Further research should be conducted to investigate the effect of interrelated parameters on the bond behavior of the CFRP/steel interface to propose an optimal retrofitting system. The finite element modeling can be considered a cost-effective solution in this regard.

- To better analyze the impact of the CFRP elastic modulus on the performance of the retrofitted steel elements, it is advisable to use CFRPs with approximately the same tensile capacity but varying elastic modulus.

- More investigation is required to develop bond–slip models at the CFRP/steel interface under fatigue loading by considering the influencing variables that are representative of conditions in practice.

- More research is needed to investigate the effect of fatigue loading on the effective bond length. Also, the effect of shear combined with flexure on the bond length is to be clarified.

- More research could be conducted to investigate the effect of galvanic corrosion, especially in the CFRP retrofitting method utilizing a steel anchorage system. The long-term effect of galvanic corrosion has not been properly investigated.

2.7 Conclusions

A state of knowledge on the application of the CFRP in retrofitting steel elements as well as the influencing parameters is presented. Based on the findings obtained from the available literature, the following conclusions can be drawn:

- Using CFRP with higher elastic modulus results in an increase in CFRP/steel bond strength and contributes to an improvement of the performance of retrofitted steel components by increasing structural load-carrying capacity and flexural strength.

- Applying adhesives with higher tensile modulus generally results in enhanced bond strength of the steel/CFRP interface. Nevertheless, adhesives with nonlinear proper-ties can yield higher failure loads than linear adhesives with an even higher tensile modulus.

- As for bond–slip models, studies have shown that in linear adhesive materials, tri-angular bond–slip curves are obtained, whereas in nonlinear adhesives, the bond–slip relationship tends to follow a trapezoidal curve.

- Proper surface preparation of steel substrates is crucial for achieving a strong bond strength. Mechanical treatments like grit blasting improve surface roughness and chemical bonding.

- Increasing the elastic modulus of CFRP reinforcement could lead to an improvement in the fatigue life of specimens. Indeed, it has been found that the fatigue life of a steel structure can

be enhanced by either applying prestressing to the steel details or by in-creasing beam stiffness by using UHM CFRP or adding CFRP layers.

- Regarding the performance of prestressed CFRP, experimental results indicate that prestressing can reduce the stress intensity factor and confine crack growth by ap-plying compressive forces to the edges of cracks in notched steel elements. Therefore, the use of prestressed CFRP patches could enhance the effectiveness of CFRP rehabilitation systems.

- Finally, experimental studies of anchorage systems have shown that using anchorage techniques can help delay crack propagation and thereby prolong fatigue life in strengthened steel specimens. The crack mouth opening displacement could also be reduced as a result of using anchorage systems.

CHAPTER 3

BOND BEHAVIOR OF CFRP/STEEL DOUBLE STRAP JOINTS: AN EXPERIMENTAL STUDY

M. Delzendeh [1], O. Chaallal [2]

[1,2] Department of Construction Engineering, École de Technologie Supérieure
1100 Notre-Dame St. West, Montreal, Quebec, Canada H3C 1K3

Article submitted to *Journal of Composites for Construction*, American Society of Civil Engineers (ASCE)

3.1 Abstract

In recent years, the application of carbon fiber reinforced polymer (CFRP) composites for retrofitting steel structures has gained increasing attention and popularity. The performance of steel elements retrofitted with CFRP relies on the bond behavior of the interface between CFRP and steel substrate, as the adhesive is typically the weakest link of the retrofitting system. Therefore, understanding the bond behavior between CFRP and steel substrate is crucial for retrofitting design of steel structures. This necessity has been the main impetus for conducting the present experimental study on the bond behavior of CFRP/steel double strap joints under static loadings. To that end, the adhesive type, CFRP length, and surface preparation are the parameters considered in this research. Additionally, the effect of CFRP elastic modulus on the rehabilitation technique is examined by using Normal Modulus (NM) and Ultra-High Modulus (UHM) CFRP with approximately the same tensile capacity. Failure modes, bond strength, effective bond length, and bond-slip curves are some of the key issues that will be thoroughly discussed in this study.

Keywords: Experimental study, Bond behavior, Double strap joints, Bond-slip relationship, CFRP rehabilitation technique, Steel structures.

3.2 Introduction

The use of advanced composite materials has emerged as one of the most popular methods for retrofitting civil infrastructures. Among these materials, carbon fiber-reinforced polymer (CFRP) laminate is well-established. The high strength-to-weight ratio, corrosion resistance, and ease of application play crucial roles in choosing CFRP for retrofitting steel components (Chataigner, Benzarti et al., 2018; Hu, Li et al., 2020; Oudah & El-Hacha, 2013; Wang, Liu et al., 2021). Compared to reinforced concrete (RC) structures, which have benefited from extensive research (Afifi, Mohamed et al., 2015; Chaallal, Mofidi et al., 2011; Godat, Chaallal et al., 2013; Godat, Hammad et al., 2020; Honarparast & Chaallal, 2022; Mofidi & Chaallal, 2011, 2014), investigations into the application of CFRP retrofitting technique for steel structures are relatively limited.

The performance of CFRP retrofitted steel structures is significantly influenced by the bond between CFRP and steel. A comparison between the bond behavior of CFRP/concrete and CFRP/steel interfaces reveals that concrete is mainly identified as the weakest link in CFRP retrofitted concrete structures, whereas in CFRP retrofitted steel components, the adhesive acts as the weakest link (Yu, Fernando et al., 2012). The function of the adhesive layer is to carry the tensile forces acting on the steel substrates and transfer them to the CFRP composites. Therefore, to achieve the desired failure mode, which is the CFRP rupture, it is essential that the force is efficiently transmitted to the CFRP without any failure within the adhesive interface. This specific failure mode will allow the bonded joints to reach their maximum capacity (Stanford, 2009). In addition, parameters such as effective bond length, CFRP type, and surface preparation have been found to impact on the bond behavior of CFRP/steel joints (Al-Zubaidy, Al-Mahaidi et al., 2012; Narmashiri, Jumaat et al., 2012).

To investigate the influencing parameters on the bond behavior of the CFRP/steel joint, several studies were conducted. Fernando et al. (2013) investigated the effect of surface preparation to identify an effective surface treatment that avoids adhesion failure at the steel adhesive interface. It was demonstrated that the application of the grit-blasting method for treating steel

surface is an effective method to prevent the adhesion failure. Li et al. (2019) studied the effects of various types of adhesives and CFRPs on the bond characteristics of the CFRP/steel single lap joints. The results show that using different types of adhesives or CFRPs, in terms of mechanical characteristics, may result in different failure modes in CFRP/steel joints. Li et al. (2020) investigated the effects of incorporating functionalized nano-sized silica (Nano-SiO2) into the adhesive. The results showed that adding Nano-SiO2 can improve the mechanical behavior of the adhesive and, consequently, the bond behavior of CFRP/steel joints. The effect of mechanical anchorage devices on the CFRP to steel bonded joints was investigated through experimental and numerical studies by Yang et al. (2021). The results reveal that the mechanical anchorage installation near the CFRP end increases the load capacity of the bonded joints. The impact of the loading rate on the bond characteristics of the CFRP/steel single-shear joints was experimentally studied by Pang et al. (2021b). It was found that the mechanical properties of the CFRP plates and adhesives may increase with the loading rate. Additionally, it was observed that the failure mode shifted from a cohesive failure to CFRP delamination as the loading rate increased.

Russian et al. (2021) investigated the influencing parameters on the interfacial bond behavior of the CFRP/steel double lap shear joints. Based on the experimental results, the surface preparation technique can have a significant impact on the specimen strength. In another study, the effectiveness of glass fiber sheet (GFS) on galvanic corrosion and bond characteristics between CFRP and steel was studied by Wu et al. (2021). The results reveal that the adhesive layer significantly contributes to suppressing potential galvanic corrosion in CFRP/steel joints. The adhesive layer can be effective in preventing corrosion if the bond quality is strictly controlled and there is no direct contact between CFRP and steel.

Guo et al. (2023) investigated the effect of different service temperatures on the bond behavior of CFRP/steel joints. It was experimentally shown that service temperature affects the local bond-slip behavior and interfacial fracture energy. Additionally, it was found that the failure mode changes as the temperature increase (He, Xian et al., 2020). Moreover, at elevated temperatures, cohesion failure within the adhesive layer is found to be the dominated failure

mode (Zhou, Fernando et al., 2020). Wang et al. (2024) evaluated the effect of freezing-thawing cycles on the mechanical behavior of CFRP/steel bonded joints. The findings show that freezing-thawing cycles do not impact the failure mode. However, the ultimate capacity was significantly affected.

Research studies on the interfacial behavior between CFRP and steel, particularly for UHM CFRP, are limited. Moreover, the type of adhesive commonly used in the literature has been linear, with a lower elongation compared to nonlinear adhesives. Therefore, this study aims to fill this gap and provide insight into the influential parameters that should be considered when designing CFRP retrofitting system. In this paper, an experimental study is carried out to investigate the bond behavior of CFRP/steel double strap joints. It should be noted that the double strap joint is considered in this study for its symmetrical configuration, where the amount of peel stress due to bond rotation is considerably less than that of a single strap joint (Duncan, 2010). Consequently, the tensile capacity of the CFRP/steel joint would not be underestimated due to premature failure of the adhesive. The adhesive type (linear versus nonlinear), CFRP bonded length, and surface preparation are the parameters considered in this study. Furthermore, the effect of CFRP elastic modulus is examined by considering NM and UHM CFRP with roughly the same tensile capacity (1500 MPa × 2.2 mm × 50 mm versus 2800 MPa × 1.2 mm × 50 mm). The results are evaluated in terms of failure modes, strain distribution, bond length, load displacement, and bond-slip behavior.

3.3 Experimental program

3.3.1 Material properties

In this experimental program, G40.21 44W steel plates with a thickness of 10 mm and a width of 60 mm are used, with a yield strength of 300 MPa and a minimum tensile strength of 400 MPa. To fabricate the double strap joints, MAPEI® Carboplate UHM Laminate and Sika® CarboDur® S512 are utilized, representing UHM CFRP and NM CFRP, respectively. The nominal width and thickness of the UHM CFRP laminate are 50 mm and 2.2 mm, respectively.

The UHM CFRP plate has an elastic modulus of 460 GPa, a tensile strength of 1500 MPa, and an elongation at break of 0.34%. As for the NM CFRP plate, its nominal width and thickness are 50 mm and 1.2 mm, respectively. The NM CFRP has an elastic modulus of 165 GPa, a tensile strength of 2800 MPa, and an elongation at break of 1.7%.

To bond the CFRP plate to the steel substrate, combined epoxies of TYFO S (Saturant epoxy) and TYFO TC (Tack Coat) which is a ductile adhesive are used. TYFO S has a tensile strength of 72.4 MPa and a tensile modulus of 3.18 GPa. TYFO TC possesses a tensile strength of 22.7 MPa, a tensile modulus of 1.2 GPa, and a shear strength of 19.3 MPa. MapeWrap12 epoxy, which exhibits linear behavior in terms of stress-strain relationship, is also used to bond CFRP to steel substrate. Table 3.1 presents the mechanical properties of the steel, CFRPs, and adhesives used to fabricate the specimens.

Table 3.1 Mechanical properties of materials

Material	Tensile Strength (MPa)	Tensile Modulus (GPa)	Yield Strength (MPa)
UHM CFRP (MAPEI)	1500	460	NA
NM CFRP (Sika)	2800	165	NA
Tyfo S (FYFE)	72.4	3.18	-
Tyfo TC (FYFE)	22.7	1.2	-
MapeWrap12	23.2	-	NA
Steel (G40.21 44W)	400-600	~ 200	300

3.3.2 Specimens preparation

In this study, 25 CFRP/steel double strap joints with different bonded lengths, CFRP types, adhesive types and surface preparations are prepared and tested. Prior to the bonding process, the steel surface is treated to remove the rust and contaminants using sandblasting machines, as suggested in the literature (Wang, Wu et al., 2016a). The applied sandblasting method is in accordance with SSPC SP-10 standard. Furthermore, a needle scaler and a sandpaper machine are used separately to investigate the effect of surface preparation. The treated surfaces are shown in Figure 3.1. In addition, both CFRP and steel surfaces are cleaned with acetone.

To fabricate the specimens, two 400 mm long steel plates, are attached by CFRPs. The gap between the two steel plates is 10 mm. In the case of using TYFO TC&S, TYFO TC is first applied to the steel surface, which is placed on a wooden mold covered with tape. Afterward, TYFO S is applied on the CFRP plate, and placed on the steel plate. Once the CFRP plate is placed on the steel substrate, the CFRP is slightly moved to ensure the adhesive spreads and any entrapped air is removed. For specimens using MapeWrap12 epoxy, this later is applied to both the steel and CFRP surfaces. It should be noted that this epoxy is only used to bond UHM CFRP. After 48 hours, the same process is applied to the other side of the double strap configuration. After the bonding process, the specimens are cured at room temperature for approximately 14 days before testing (Wang, Wu et al., 2016a; Yang, Zhao et al., 2021; Yu, Fernando et al., 2012). It should be mentioned that the thickness of the adhesive is roughly 1 mm –2 mm, as suggested in the literature (The Institution of Structural Engineers (ISE), 1999; Xia & Teng, 2005).

Figure 3.1 Steel plate surface; (a) Before surface treatment; (b) After applying needle scaler; (c) After applying sandpaper machine; (d) After sandblasting

The schematic view of the specimens is shown Figure 3.2. As can be seen, the CFRP's bond length is intentionally made longer on one side to ensure that failure occurs on the side with the shorter bond length. Accordingly, 5 mm strain gauges are installed along the shorter side to measure the strain distribution along the CFRP. The test matrix and specimens labeling are presented in Table 3.2.

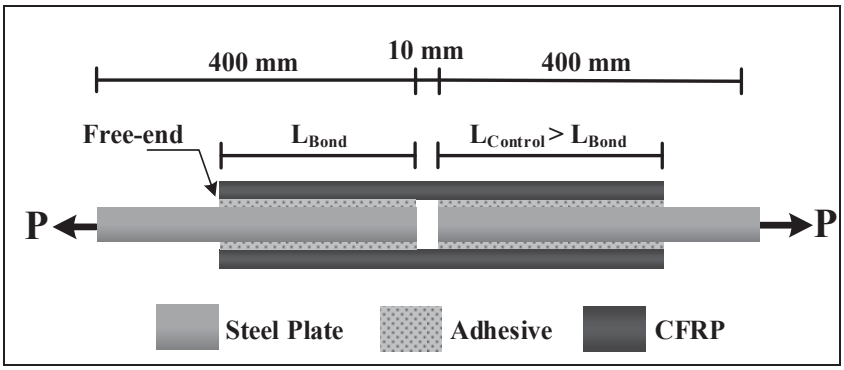

Figure 3.2 Schematic view of the specimen

Table 3.2 Test matrix for bond test

No	Specimen	CFRP type	Adhesive type	Surface preparation	Bond length (mm)
1	U-T-40-S1	UHM	TYFO	Sandblasting	40
2	U-T-80-S1	UHM	TYFO	Sandblasting	80
3	U-T-100-S1	UHM	TYFO	Sandblasting	100
4	U-T-120-S1	UHM	TYFO	Sandblasting	120
5	U-T-150-S1	UHM	TYFO	Sandblasting	150
6	U-T-170-S1	UHM	TYFO	Sandblasting	170
7	U-T-170-S2	UHM	TYFO	Needle scaler	170
8	U-T-170-S3	UHM	TYFO	Sandpaper machine	170
9	U-T-195-S1	UHM	TYFO	Sandblasting	195
10	U-T-210-S1(1)	UHM	TYFO	Sandblasting	210
11	U-T-210-S1(2)	UHM	TYFO	Sandblasting	210
12	U-T -250-S1	UHM	TYFO	Sandblasting	250
13	U-M-100-S1	UHM	MapeWrap12	Sandblasting	100
14	U-M-170-S1	UHM	MapeWrap12	Sandblasting	170
15	U-M-210-S1	UHM	MapeWrap12	Sandblasting	210
16	U-M-250-S1	UHM	MapeWrap12	Sandblasting	250
17	N-T-40-S1	NM	TYFO	Sandblasting	40
18	N-T-60-S1	NM	TYFO	Sandblasting	60
19	N-T-80-S1	NM	TYFO	Sandblasting	80
20	N-T-110-S1	NM	TYFO	Sandblasting	110
21	N-T-170-S1	NM	TYFO	Sandblasting	170
22	N-T-210-S1	NM	TYFO	Sandblasting	210
23	N-T-250-S1	NM	TYFO	Sandblasting	250
24	N-T-270-S1	NM	TYFO	Sandblasting	270
25	N-T-300-S1	NM	TYFO	Sandblasting	300

3.4 Test setup

The double strap joints are tested using an MTS machine with a capacity of 500 kN, as shown in Figure 3.3. The specimens are carefully placed in the machine's jaws, and the wires of the strain gauges are connected to the gauge reader of the machine. The gripping lengths of the specimens are 80 mm. All specimens are loaded in tension under displacement control and at a constant displacement rate of 0.1 mm/min until failure. The applied load, machine displacement, and strain gauges along the bond length are measured as the load increased for each test.

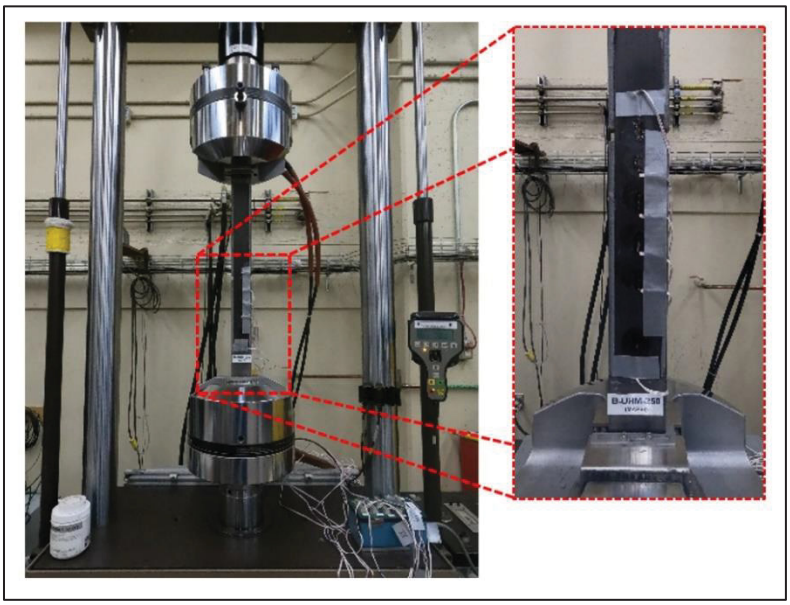

Figure 3.3 MTS testing machine

3.5 Results

3.5.1 Failure modes

The failure modes of the CFRP/steel joints are presented in Figure 3.4 to Figure 3.6. Observations from the bond test revealed that cracking sounds were emitted, particularly at higher applied loads. Furthermore, in some cases, the initial debonding in specimens did not

occur simultaneously on both sides, even though the joints were symmetric. Similar observation were reached in another experimental investigation (Zhao, Liu et al., 2024). For the UHM CFRP joints bonded with nonlinear adhesive, the CFRP did not attain its highest capacity for specimens with bond lengths varying from 40 to 150 mm. However, CFRP rupture occurred for bond lengths exceeding 170 mm, indicating that the CFRP has reached its maximum capacity. In other words, the results indicate that as the bond length of the joints increases, the failure mode of the CFRP/steel joint shifts from CFRP debonding to CFRP rupture, suggesting that the effective bond length has been attained. Moreover, CFRP rupture occurred in the UHM CFRP joints with the same bonded length of 170 mm but different surface preparations, as shown in Figure 3.4. In this regard, the type of surface preparation does not seem to affect the failure mode of specimens with bonded length equal to or greater than the effective bond length. Contrary to the joints bonded with nonlinear adhesive, debonding occurred in all the specimens with UHM CFRP bonded with linear adhesive, with bonded length varying from 100 mm to 250 mm. This reveals that the failure mode of the CFRP/steel joint does not change when the bond length of the joints bonded with linear adhesive increases.

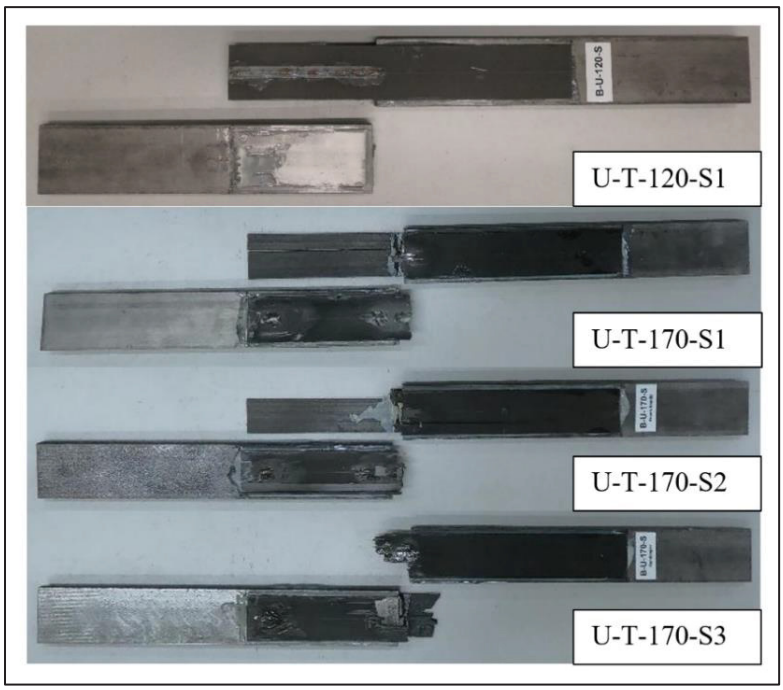

Figure 3.4 Failure modes of specimens with UHM CFRP laminate bonded with nonlinear adhesive

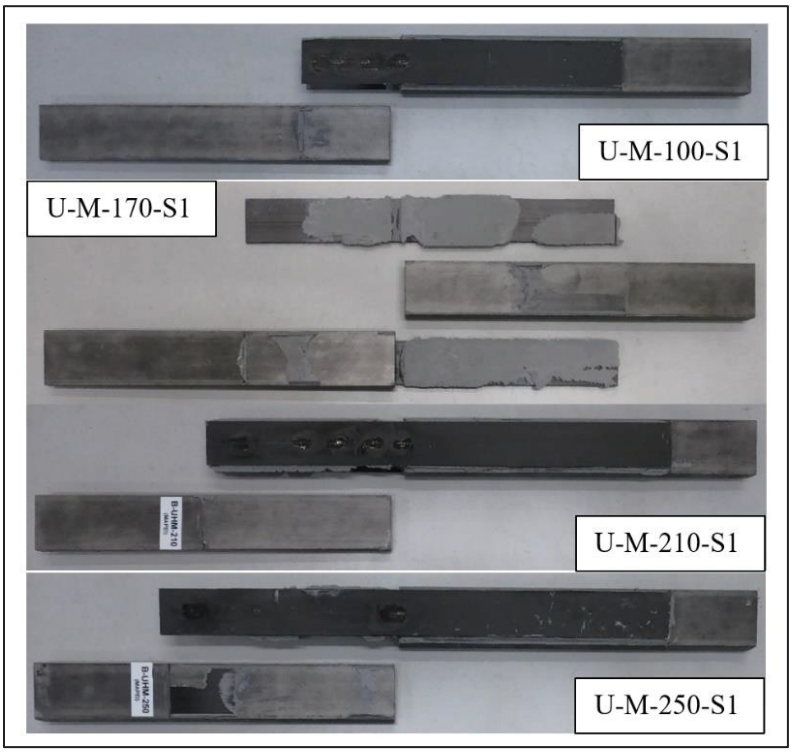

Figure 3.5 Failure modes of specimens with UHM CFRP laminate bonded with linear adhesive

Regarding the NM CFRP/steel joints, the failure modes of the specimens with bond lengths varying from 40 to 250 mm changed from CFRP debonding to CFRP delamination. In these specimens, CFRPs also broke apart in the longitudinal direction for longer bond lengths. The results indicate that increasing the bond length can change the failure mode for NM CFRP joints bonded with nonlinear adhesive. Contrary to UHM CFRP/steel joints, NM CFRP/steel joints did not exhibit CFRP rupture, which can be attributed to the brittle behavior of UHM CFRP. However, in both cases, the nonlinear adhesive successfully transferred the load from steel to CFRP plates.

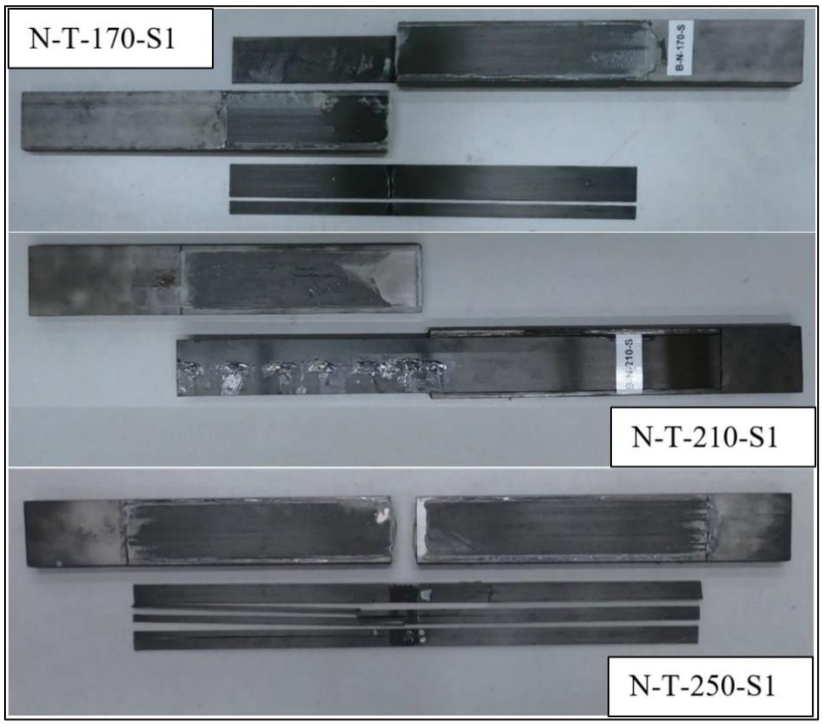

Figure 3.6 Failure modes of specimens with NM CFRP laminate bonded with nonlinear adhesive

3.5.2 Strain distributions along the bonded CFRP

Figure 3.7 presents the strain distribution along the CFRP for the tested specimens at different ratios of ultimate load. Examination of the strain distributions along the bonded length shows that the strains captured at locations closer to the loaded-end featured higher strain values compared to those near the free-end. This clearly shows that, upon the application of monotonic loading, the bond shear resistance mostly occurs in the portion of the bonded length near the loaded-end, while the shear contribution of intervals farther from the loaded-end is relatively lower. This is particularly evident at load levels near the ultimate bond strength (0.9 P_{ult} - 0.99 P_{ult}).

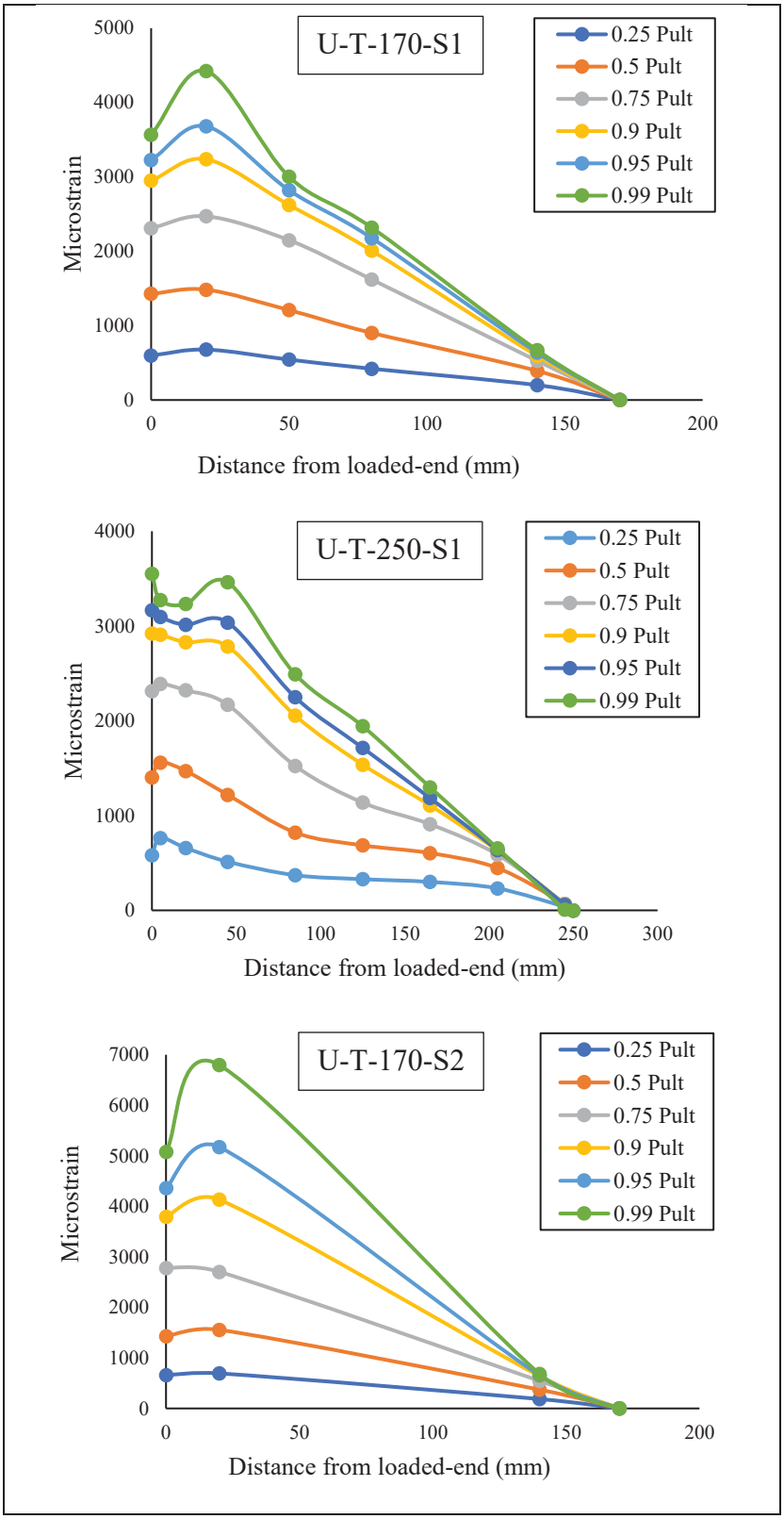

Figure 3.7 CFRP strain distributions for specimens

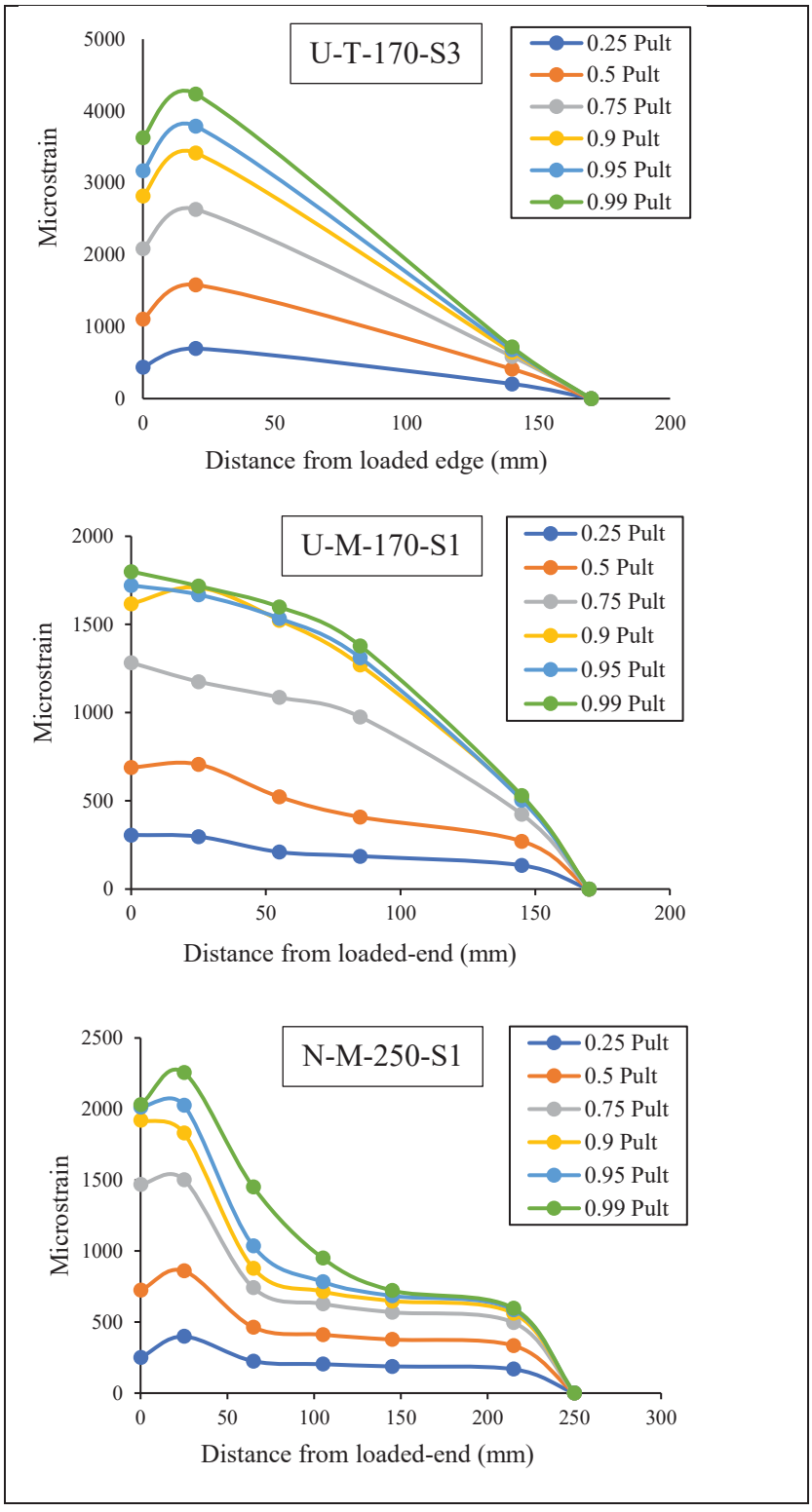

Figure 3.7 CFRP strain distributions for specimens (continued)

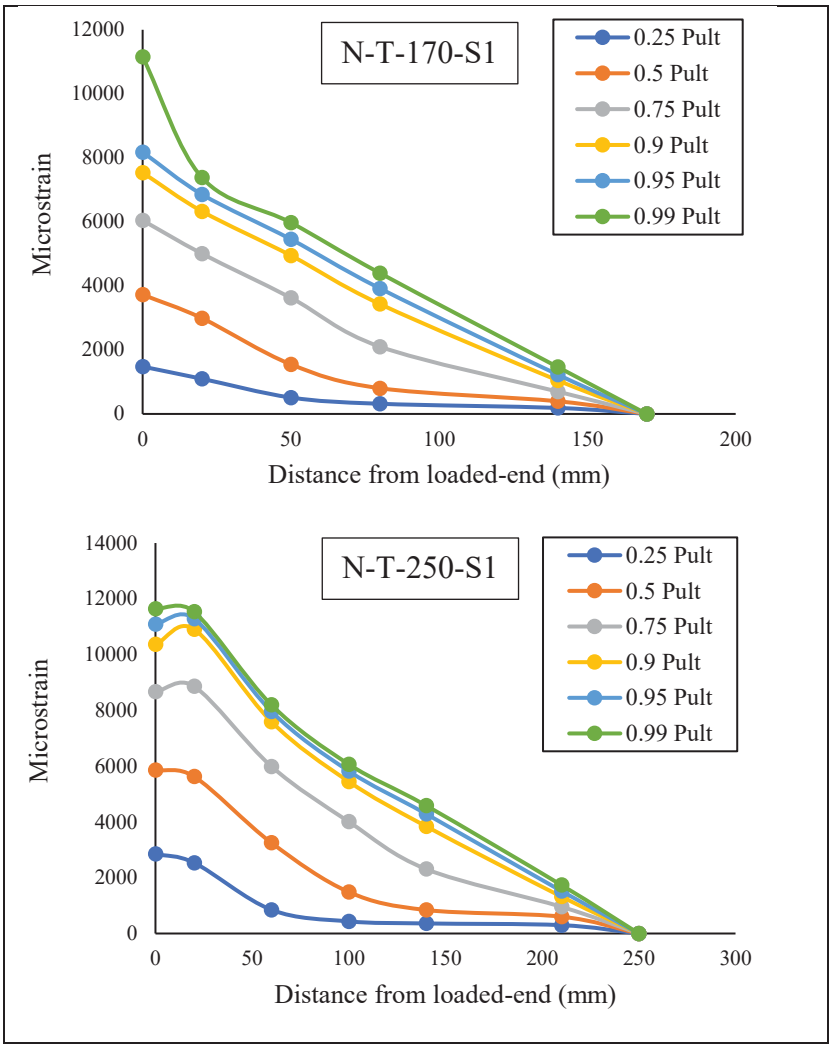

Figure 3.7 CFRP strain distributions for specimens (continued)

Regarding the effect of applied bond length, it can be observed that increasing the bond length resulted in higher maximum shear stresses recorded by the strain gauges. This suggests that bond shear resistance tends to increase in specimens with greater bond length, thereby yielding higher bond strength. However, the increase of bond strength only continues until the effective bond length is reached, beyond which the shear resistance tends to stabilize.

As for the surface preparation, the findings suggest that the maximum strains observed in specimens treated with sandblasting and sandpaper methods are roughly similar. However, the specimen treated with needle scaler shows higher strains close to loaded-end. The results also

reveal that UHM CFRPs bonded with nonlinear adhesive experience greater strains compared to those bonded with linear adhesive.

Comparing the strain distributions of NM versus UHM CFRP, it can be seen that the maximum strains reached by specimens with NM CFRP were significantly greater than those of specimens with UHM CFRP with similar bond lengths. This is attributed to the higher stiffness of UHM CFRP compared to NM CFRP, resulting in lower ductility but greater shear resistance for UHM CFRP.

3.5.3 Effective bond length

The bond strength of the CFRP/steel interface tends to increase at greater bond lengths. However, increasing the bond length beyond a certain value, known as effective bond length, does not result in a further increase in bond strength (Al-Zubaidy, Al-Mahaidi et al., 2012; Bocciarelli, Colombi et al., 2009; Chiew, Yu et al., 2011; Fawzia, Al-Mahaidi et al., 2006; Yang, Biscaia et al., 2017). Figure 3.8 presents bond strength versus bond length for the tested CFRP/steel joints. It can be seen that the bond strength of UHM CFRP/steel joints bonded with nonlinear adhesive increases when the bond length is between 40 mm to 170 mm. However, the bond strength reaches a plateau after a bond length of 170 mm, indicating that exceeding this bond length has no significant effect on the bond strength of the joints. Therefore, it can be concluded that the effective bond length for UHM CFRP bonded with nonlinear adhesive is around 170 mm.

For UHM CFRP/steel joints bonded with linear adhesive, it is observed that the bond strength increases as the bond length reaches 170 mm. However, the bond strength tends to stabilize beyond a bond length of 170 mm, excluding the specimens with a bond length of 210 mm. In this case, determining the exact rage of the effective bond length is not possible. However, it can be concluded that it is between 170 mm – 250 mm. Therefore, it can be inferred that the effective bond length for UHM CFRP bonded with linear adhesive is longer than its counterpart bonded with nonlinear adhesive. In contrast to previous study where the effective

bond length was found to be longer for specimens bonded with nonlinear adhesive (Araldite-420) compared to the specimens bonded with linear adhesive (Sikadur-30) (Wu, Zhao et al., 2012).

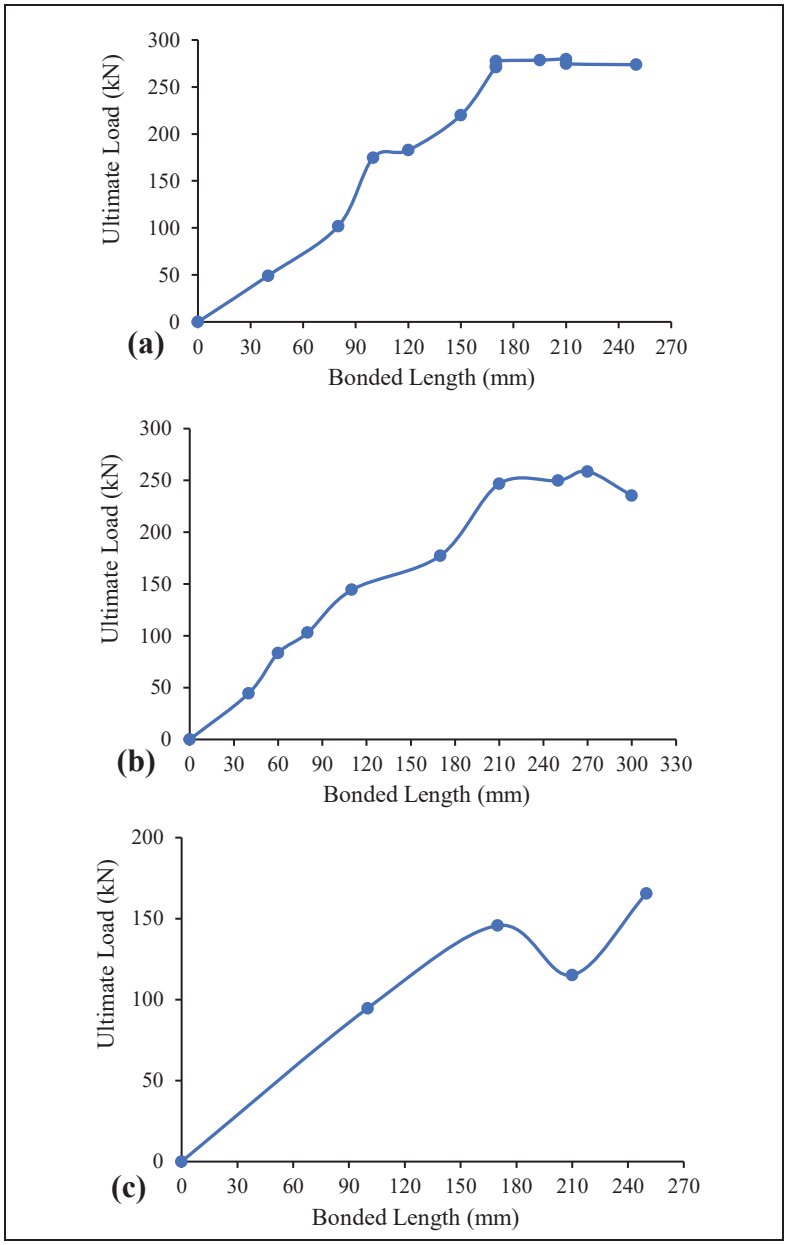

Figure 3.8 Bond strength versus bond length for; (a) UHM CFRP/steel joints bonded with nonlinear adhesive; (b) NM CFRP/steel joints bonded with nonlinear adhesive; (c) UHM CFRP/steel joints bonded with linear adhesive

Regarding the NM CFRP/steel joints bonded with nonlinear adhesive, the bond strength increases for bond lengths between 40 mm to 210 mm. However, the bond strength remains relatively unchanged for bond lengths in the range of 210 mm to 300 mm. As a result, the effective bond length of the NM CFRP/steel joints bonded with nonlinear adhesive is around 210 mm. The obtained results indicate that specimens with NM CFRP have a longer effective bond length compared to specimens with UHM CFRP, despite both types of CFRP having roughly equal tensile capacity. Accordingly, there is an inverse correlation between effective bond length and elastic modulus. However, this correlation is direct in the formulas presented in the literature for calculating effective bond length.

Table 3.3 shows the predicted effective bond length for the tested CFRP/steel joints. As observed, the predicted effective bond length obtained by the formula proposed by Xia and Teng (2005) is in good agreement with the tested specimens bonded with linear adhesives. It should be noted that this formula was developed only for linear adhesives. For UHM CFRP bonded with nonlinear adhesive, the obtained effective bond length is closer to Dehghani's (2012) formula. However, the proposed formulas underestimate the effective bond length for the NM CFRP/steel joints.

Table 3.3 Effective bond length formulas and predicted results for tested specimens

Ref.	Effective bond length	Remarks	Predicted le (mm) for specimens		
			(a)	(b)	(c)
Xia and Teng (2005)	$L_e = \frac{\pi}{2\sqrt{\tau_f / E_p t_p \delta_f}}$	-	223	NA	NA
Bocciarelli, Colombi et al. (2007)	$L_e = 2.77\sqrt{\frac{\beta}{\beta+1}} \times \frac{\sqrt{2G_f E_p t_p}}{\tau_f}$	$\beta = \frac{b_s t_s E_s}{2 b_p t_p E_p}$	138.26	223.02	98.65
Dehghani, Daneshjoo et al. (2012)	$L_e = 3.5\sqrt{\frac{E_p t_p t_a}{G_a}}$	-	101.47	163.80	72.46

(a) UHM bonded with MapeWrap
(b) UHM bonded with TYFO
(c) NM bonded with TYFO

3.5.4 Load displacement

Figure 3.9 shows the applied load versus displacement of the CFRP/steel joints. It is observed that the UHM CFRP joints bonded with nonlinear adhesive featured a larger area under the load-displacement curve, indicative of their superior energy absorption capacity. Conversely, the UHM CFRP joints bonded with linear adhesive failed to reach their maximum capacity due to premature debonding failure.

The results also reveal that the average ultimate load resisted by the UHM CFRP and NM CFRP bonded with nonlinear adhesive is around 275 kN and 248 kN, respectively. However, based on the product datasheets, the ultimate load that can be resisted by the UHM CFRP and NM CFRP is 330 kN (1500×2.2×50) and 336 kN (2800×1.2×50), respectively. According to the experimental results, the specimens bonded with UHM CFRP have a moderately better tensile capacity than those bonded with NM CFRP. It can also be inferred that there is a direct correlation between bond strength and the CFRP elastic modulus.

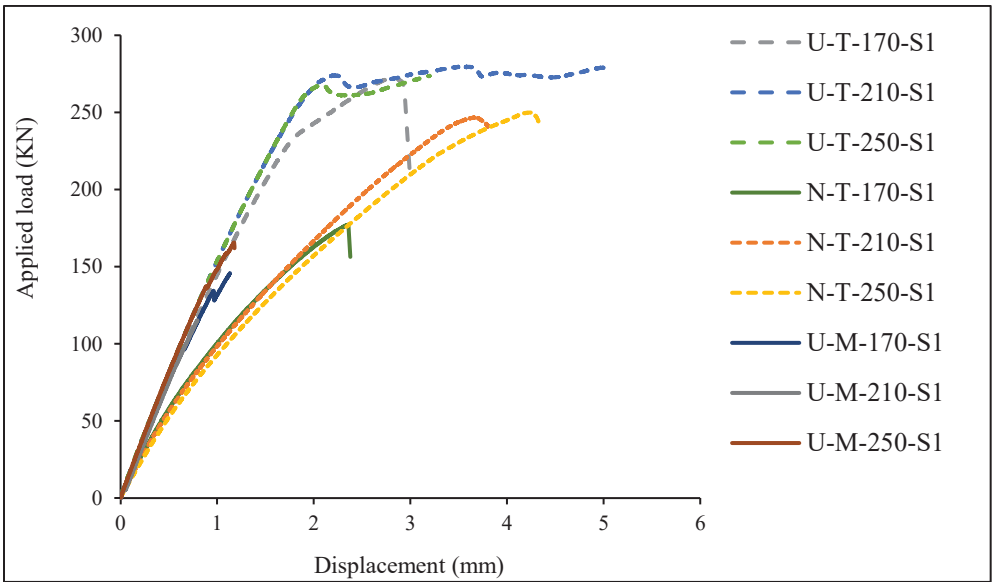

Figure 3.9 Applied load versus displacement of specimens

Table 3.4 presents the predicted ultimate load for the tested specimens. As observed, the prediction using the formula proposed by Wang and Wu (2018) is the closet to the experimental results obtained in this study. Nevertheless, all the formulas underestimate the ultimate load of NM CFRP/steel joints. Figure 3.10 also shows the bond strength for different bond lengths achieved by double strap joints. As demonstrated, UHM CFRP bonded with nonlinear adhesives outperforms the other specimens in terms of load-carrying capacity and reaches its maximum capacity at shorter bonded length.

Table 3.4 Ultimate load formulas presented in the literature and predicted results for tested specimens

Ref.	Ultimate load	Remarks	Predicted Pu (kN) for specimens		
			(a)	(b)	(c)
Xia and Teng (2005)	$P_u = b_p\sqrt{2G_f E_p t_p}$	-	263.48	NA	NA
Bocciarelli, Colombi et al. (2007)	$P_u = N\sqrt{\frac{\beta+1}{\beta}} \times b_p\sqrt{2G_f E_p t_p}$	$\beta = \frac{b_s t_s E_s}{2b_p t_p E_p}$	191.06	302.71	133.89
Wang and Wu (2018)	$P_u = b_p\sqrt{2G_f E_p t_p(1+\alpha)}$	$\alpha = \frac{b_p t_p E_p}{b_s t_s E_s}$	164.15	298.85	132.19

(a) UHM bonded with MapeWrap
(b) UHM bonded with TYFO
(c) NM bonded with TYFO

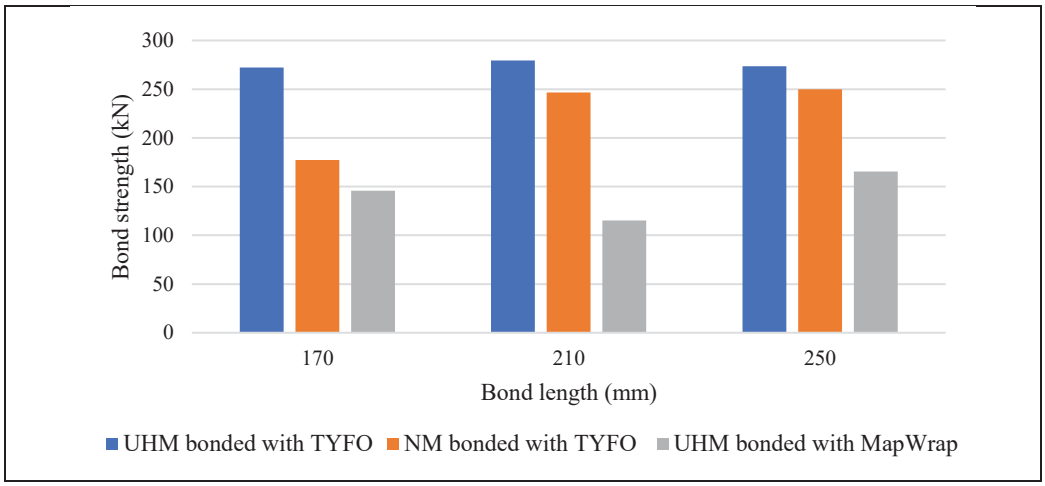

Figure 3.10 Bond strength obtained by specimens with different bond lengths

3.5.5 Bond-slip curves

The bond-slip curve presents the correlation between local shear stress and relative displacement between the CFRP and steel surface (Wang & Xian, 2021). The local shear stress and relative slip can be derived from the strains recorded by the gauges installed on the CFRP laminate as follows (Fernando, 2010; Guo, Liu et al., 2023; He & Xian, 2017; Zhou, Fernando et al., 2020):

$$\tau_{i+\frac{1}{2}} = E_f t_f \frac{\varepsilon_{i+1} - \varepsilon_i}{\Delta x_i} \tag{3.1}$$

$$\delta_{i+\frac{1}{2}} = \sum_{i}^{n} \frac{(\varepsilon_i + \varepsilon_{i+1})}{2} \Delta x_i \tag{3.2}$$

Where E_f and t_f are the elastic modulus and thickness of the CFRP, respectively; ε_i is the strain value recorded by the i^{th} strain gauge; Δx_i is the distance between two constitutive strain gauges. It may be noteworthy that the bond-slip curves should be presented for the specimens that underwent debonding failure (Fernando, 2010; Wu, Zhao et al., 2012).

Figure 3.11 presents the bond-slip curves of the specimens. As can be seen in the curves related to both UHM and NM CFRP bonded with nonlinear adhesive, the local bond-slip relationship of intervals close to the loaded-end can be approximated by trapezoidal shape. Thus, the bond-slip curves show a roughly linear ascending phase, followed by a plateau, and then a descending phase, as previously documented for the nonlinear adhesive in the literature (Fernando, 2010). In contrast, the bond-slip curves of intervals near the free-end (e.g., 2.5 mm) do not exhibit the same behavior. These intervals follow only a linear trend, likely due to the fact that the bond shear contribution is negligible at locations closer to the free end. Therefore, the nonlinear behavior is not reached in these regions of the bonded length. Consequently, it can be inferred that the local bond stress-slip relationship depends on the interval position along the bonded length. This observation was also reported in the literature for CFRP/concrete joints (Dai, Ueda et al., 2005; Nakaba, Kanakubo et al., 2001).

For UHM CFRP bonded with linear adhesive, the bond-slip curves close to loaded-end show a roughly linear ascending branch followed by a descending branch. In this case, the bond-slip can be approximated by bilinear curves characterized by both ascending and descending branches (Xia & Teng, 2005). It should be noted that the bond-slip of CFRP/concrete bonded joints always exhibit an approximately bilinear curve due to the brittle nature of the concrete (Yu, Fernando et al., 2012). However, depending on the type of adhesive, the bond-slip curves of CFRP/steel joints can have either a roughly bilinear or a trilinear shape. Linear adhesives tend to have an approximately triangle shape, whereas nonlinear adhesives tend to feature an approximately trapezoidal shape (Fernando, Yu et al., 2014).

The parameters defining a trapezoidal bond-slip curve are the maximum shear stress experienced by the interface (τ_{max}), the slip at which the plateau starts (δ_1), the slip at which the plateau ends (δ_2), and the slip at which failure occurs (δ_f) (Fernando, 2010). These parameters for bilinear bond-slip curves are the maximum shear stress experienced by the interface (τ_{max}), the relative slip corresponding to the peak interfacial shear stress (δ_1) and the maximum slip at which failure occurs (δ_f) (Pang, Wu et al., 2021a; Xia & Teng, 2005).

Several bond-slip models have been presented to characterize the interfacial behavior between CFRP and steel interfaces under static loading. Table 3.5 presents bond-slip models proposed for nonlinear and linear adhesives. To evaluate the accuracy of the existing bond-slip models, Figure 3.12 and Figure 3.13 present the bond-slip curves of the tested specimens for nonlinear and linear adhesive along with the curves obtained from the proposed models. It is worth noting that the bond-slip relationship of the interval nearest to the loaded-end is typically used to develop existing bond-slip models (Dai, Ueda et al., 2005). Consequently, only the bond-slip curves close to the load-ended are considered in those figures.

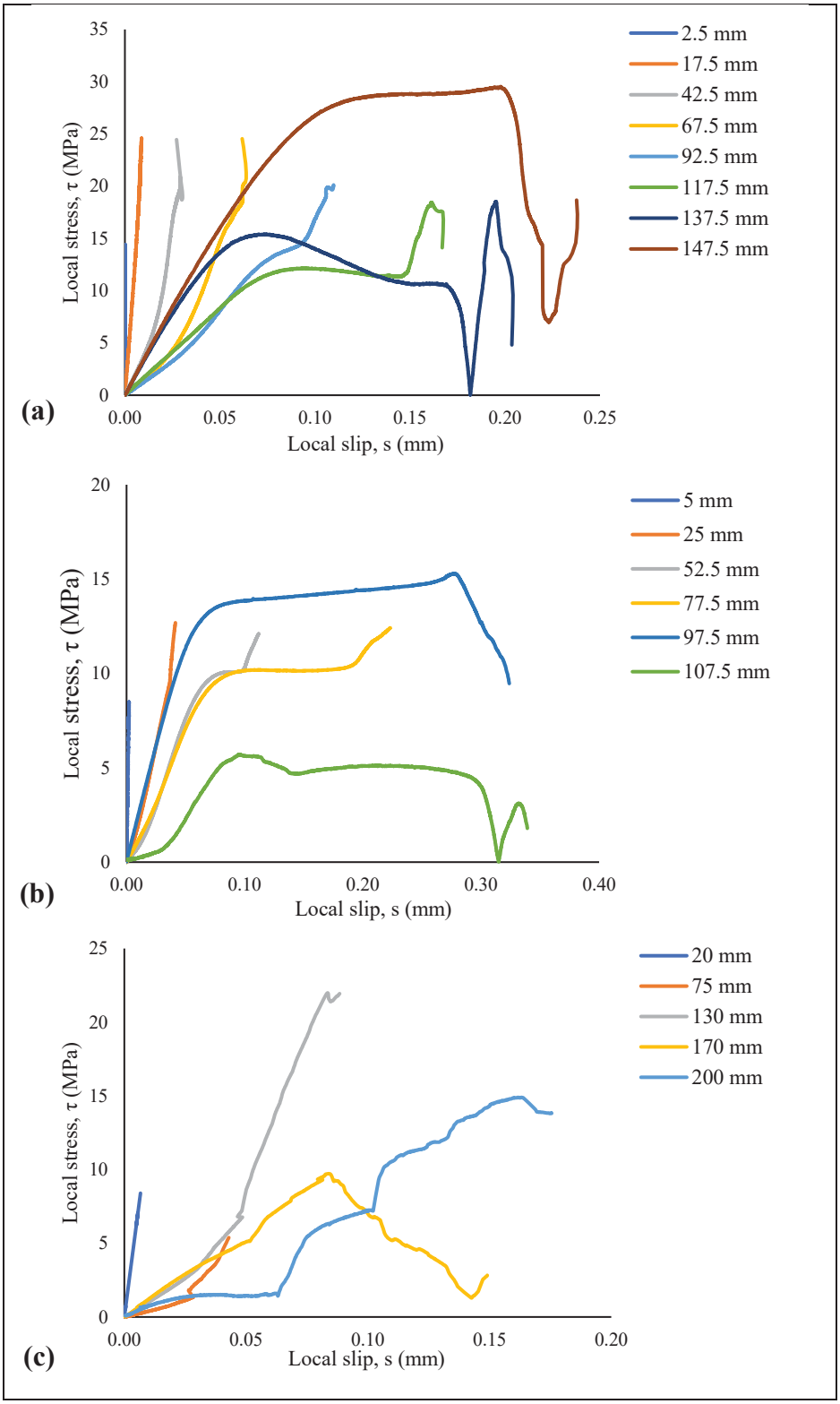

Figure 3.11 Local bond stress-slip curves of specimens: (a) U-T-150-S1; (b) N-T-110-S1; (c) U-M-210-S1

Table 3.5 Bond-slip models proposed in the literature for nonlinear and linear adhesives

Bond-slip model	Ref.	τ_f	δ_1	δ_2	δ_f	Remarks
Nonlinear Adhesive $\begin{cases} \tau = \tau_f \frac{\delta}{\delta_1} & \delta \le \delta_1 \\ \tau = \tau_f & \delta_1 < \delta \le \delta_2 \\ \tau = \tau_f \frac{\delta_f - \delta}{\delta_f - \delta_2} & \delta_2 < \delta \le \delta_f \\ \tau = 0 & \delta > \delta_f \end{cases}$	Wang and Wu (2018)	$0.9\, f_a$	$2.6 \frac{t_a^{0.34}}{G_a} f_a$	$180 \frac{t_a^{0.4} \mathrm{R}^{1.7}}{f_a} + 0.85 \frac{t_a^{0.34} f_a}{G_a}$	$\frac{2}{3}(\frac{2G_f}{\tau_f} + \delta_1)$	$G_f = 243\, t_a^{0.4} R^{1.7}$ $R = \frac{f_a^2}{2E_a}$
	He and Xian (2016)	$0.5\, f_a$	0.08 mm	$\frac{G_f}{\tau_f}$	$\delta_1 + \delta_2$	$G_f = 10.65\, t_a^{1.745} \mathrm{R}^{0.437}$ $R = \int \sigma(\varepsilon)\, d\varepsilon$
	Dehghani, Daneshjoo et al. (2012)	$0.8\, f_a$	$0.8 \frac{t_a}{G_a} f_a$	$\frac{\delta_f}{3}$	$\frac{3G_f}{2\tau_f} + \frac{3}{4}\delta_1$	-
Linear Adhesive $\begin{cases} \tau = \tau_f \frac{\delta}{\delta_1} & \delta \le \delta_1 \\ \tau = \tau_f \frac{\delta_f - \delta}{\delta_f - \delta_1} & \delta_1 < \delta \le \delta_f \\ \tau = 0 & \delta > \delta_f \end{cases}$	Wang and Wu (2018)	$0.9\, f_a$	$2.6 \frac{t_a^{0.34}}{G_a} f_a$	N/A	$540 \frac{t_a^{0.4} \mathrm{R}^{1.7}}{f_a}$	$G_f = 243\, t_a^{0.4} R^{1.7}$ $R = \frac{f_a^2}{2E_a}$
	Fawzia, Zhao et al. (2010)	f_a	$\frac{t_a}{10}$	N/A	$\begin{cases} \frac{t_a}{4} & if\ t_a = \mathrm{a} \\ 0.125 + \frac{t_a - 0.5}{10} & if\ t_a = \mathrm{b} \end{cases}$	-
	Xia and Teng (2005)	$0.8\, f_a$	$0.8 \frac{t_a}{G_a} f_a$	N/A	$\frac{2G_f}{\tau_f}$	-

a = 0.1 ~ 0.5 mm
b = 0.5 ~ 1 mm

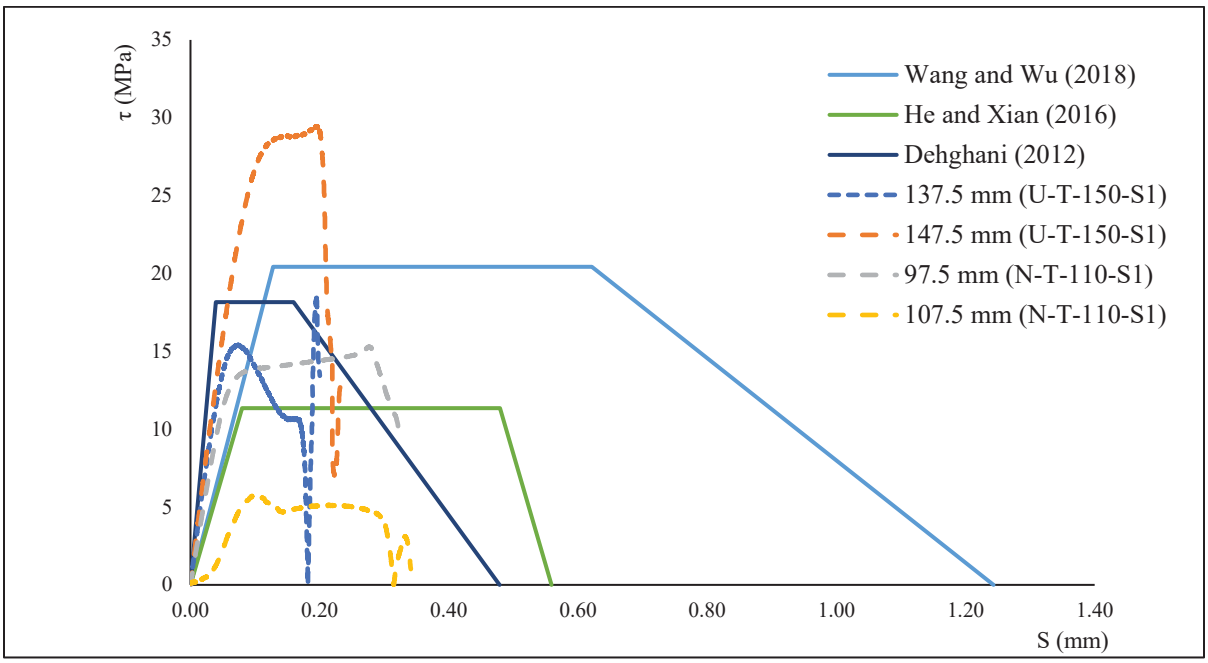

Figure 3.12 Local bond stress-slip models for nonlinear adhesive along with the bond slip curves of specimens: (a) U-T-150-S1; (b) (U-T-110-S1)

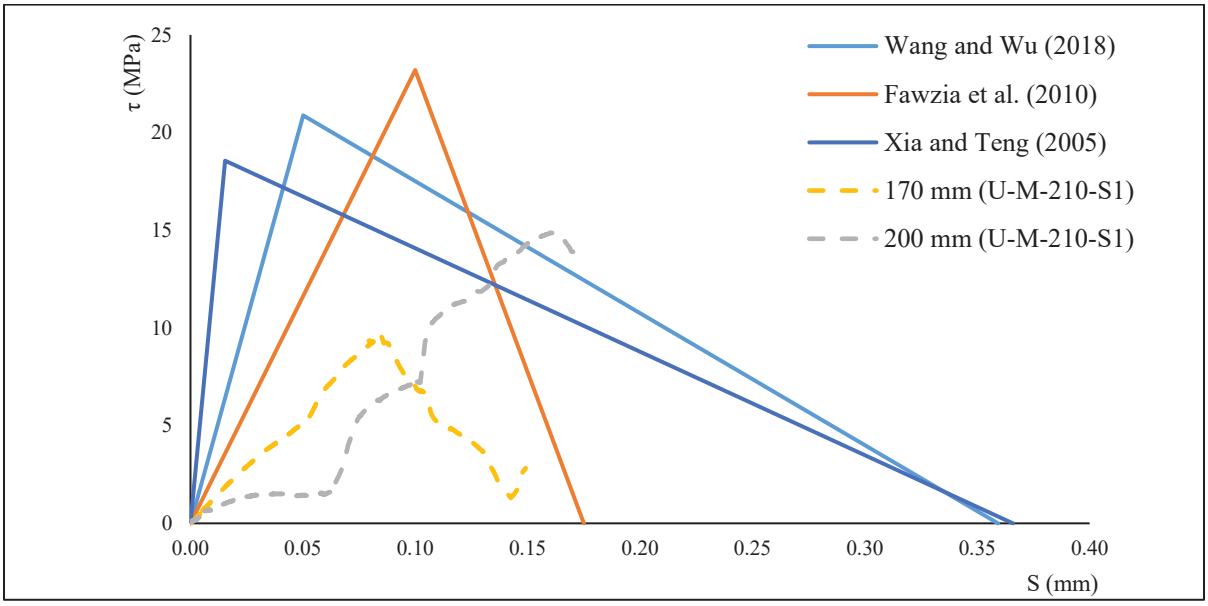

Figure 3.13 Local bond stress-slip models for linear adhesive along with the bond slip curves of specimens (U-M-210-S1)

As seen in Figure 3.12, the three proposed models overestimate the slip corresponding to failure. The peak bond shear stress captured in specimens bonded with nonlinear adhesive, except for the specimen bonded with UHM (@147.5 mm), appears to be lower compared to Wang and Wu (2018) as well as Dehghani's models (2012). However, it is underestimated by the model proposed by He and Xian (2016). Furthermore, it seems that the interfacial fracture energy (G_f), defined as the area enclosed by the stress-slip curve (He & Xian, 2016; Wang, Liu et al., 2021; Wang, Wu et al., 2024), is closest to the model proposed by Dehghani (2012). Consequently, the obtained bond-slip curves are in good agreement with Dehghani's model (2012) in comparison to the other models. Regarding the specimens bonded with a linear adhesive, as presented in Figure 3.13, all the three proposed models, overestimate the peak bond shear stress and the slip at which failure occurs.

3.6 Conclusions

In this study, the bond behavior between CFRP and steel substrate was investigated using double strap joints. The experimental program aimed to encompass the influential parameters on the bond behavior of the CFRP/steel joints, including adhesive type, CFRP elastic moduli, bond length, and surface preparation. Furthermore, the accuracy of the proposed formula for bond strength and effective bond length was evaluated. In addition, the accuracy of the existing bond-slip models was assessed. Based on the experimental results of this study, the following conclusions can be drawn:

- The failure mode of the UHM CFRP/steel joints bonded with nonlinear adhesive shifts from debonding to CFRP rupture after reaching the effective bond length. However, UHM CFRP bonded with linear adhesive failed by debonding. Furthermore, the failure mode for NM CFRP bonded with nonlinear adhesive changes from debonding to CFRP delamination with increasing bond length.

- Sandblasting, sandpaper machine, and needle scaler yield similar bond behavior results for UHM CFRP/steel joints bonded with nonlinear adhesive. However, sandblasting is often

considered the most effective method for achieving optimal surface roughness and cleanliness, leading to improved bonding strength.

- The effective bond length in CFRP/steel joint is inversely correlated to the elastic modulus; NM CFRP has a longer effective bond length than the UHM CFRP when both are bonded with nonlinear adhesive, despite having an equal tensile capacity. Moreover, the effective bond length for UHM CFRP bonded with linear adhesive is found to be longer than UHM CFRP bonded with nonlinear adhesive.

- The UHM CFRP/steel joints bonded with nonlinear adhesive achieved a moderately better tensile capacity compared to their counterparts.

- The intervals closer to the loaded-end carry the highest interfacial shear strains. Conversely, intervals closer to the free-end do not significantly contribute to bond shear resistance compared to regions near the loaded-end.

- Regarding the bond-slip behavior of specimens with respect to the existing trapezoidal models, it was observed that the models available in the literature do not adequately describe the bond-slip curves of CFRP bonded specimens in terms of peak bond stress and bond slip. This is attributed to the fact that a reliable bond-slip model for the CFRP/steel has yet to be developed.

3.7 Data availability statement

Some or all data, models, or code that support the findings of this study are available from the corresponding author on reasonable request.

3.8 Acknowledgments

The authors thank Fyfe FRP, Sika-Canada, and MAPEI-Canada for contributing to the cost of the materials. The efficient collaboration of Jonathan Auger (technician) at École de technologie supérieure in conducting the tests is also acknowledged.

CHAPTER 4

FLEXURAL BEHAVIOR OF RETROFITTED NOTCHED STEEL BEAMS USING CFRP: AN EXPERIMENTAL STUDY

M. Delzendeh [1], O. Chaallal [2]

[1,2] Department of Construction Engineering, École de Technologie Supérieure
1100 Notre-Dame St. West, Montreal, Quebec, Canada H3C 1K3

Article submitted to *Journal of Composites for Construction*, American Society of Civil Engineers (ASCE)

4.1 Abstract

In this study, the flexural behavior of notched steel beams retrofitted with CFRP is investigated. Two series of tests, including W200×22 and W14" wide flange notched beams rehabilitated with externally bonded (EB) CFRP are evaluated under static loading. The W200×22 beams were received directly from a factory, whereas the W14" wide flange beams were extracted from an ancient steel bridge after approximately 50 years of service. The parameters considered include the CFRP elastic modulus, CFRP configuration, notch depth, anchorage system, and adhesive type. The effect of CFRP elastic modulus on the rehabilitation technique is examined by using Normal Modulus (NM) and Ultra-High Modulus (UHM) CFRP with approximately the same tensile capacity. Failure modes, load-deflection behavior, strain distributions along the CFRPs, and Crack Mouth Opening Displacement (CMOD) are thoroughly discussed in this study. The results reveal that both UHM and NM CFRP significantly enhance the load-carrying capacity, although specimens bonded with UHM CFRP generally outperform in controlling crack mouth opening in retrofitted notched steel beams. Furthermore, the specimens rehabilitated with UHM exhibit brittle behavior compared to those rehabilitated with NM CFRP, which show more ductile behavior.

Keywords: Experimental study, Flexural behavior, Notched beams, CFRP rehabilitation technique, steel structures, old bridge elements

4.2 Introduction

The deterioration of steel structures, especially steel bridges, during their service life is an issue of significant concern. The strength and stiffness, and consequently the capacity of steel elements, decrease over time due to fatigue loadings and extreme weather conditions. The conventional method for retrofitting steel structures involves attaching steel plates to the structure using either welding or bolting techniques (Dexter & Ocel, 2013). However, these conventional techniques are associated with certain disadvantages, including residual stress imposed by welding and susceptibility to corrosion (Fisher, 1997; Schnerch, Dawood et al., 2007). In this context, externally bonded (EB) carbon fiber-reinforced polymers (CFRP) present a promising alternative due to their high strength-to-weight ratio, corrosion resistance and ease of application (Chataigner, Benzarti et al., 2018; Hu, Li et al., 2020; Oudah & El-Hacha, 2013; Wang, Liu et al., 2021). CFRP is also advantageous for structures where welding could increase the fire risk (Teng, Yu et al., 2012). CFRPs are classified based on their elastic modulus into Low Modulus (LM), Normal Modulus (NM) or Intermediate Modulus (IM), High Modulus (HM), and Ultra-High Modulus (UHM). There is no unanimous approach to define the range of the elastic modulus of each category. However, it can be expressed relative to the steel elastic modulus as presented in Table 4.1 (Ghafoori & Motavalli, 2015).

Table 4.1 CFRP laminate classification in terms of elastic modulus
Taken from Ghafoori and Motavalli (2015, p. 2)

Laminate Type	Laminate Modulus	Laminate Modulus Relative to Steel
Low Modulus (LM)	< 100 GPa	($E_{CFRP} < 0.5\ E_{steel}$)
Normal Modulus (NM)	100-200 GPa	($0.5\ E_{steel} \leq E_{CFRP} < E_{steel}$)
High Modulus (HM)	200-400 GPa	($E_{steel} \leq E_{CFRP} < 2\ E_{steel}$)
Ultra-High Modulus (UHM)	≥ 400 GPa	($E_{CFRP} \geq 2\ E_{steel}$)

Several studies have evaluated the application of CFRP in retrofitting steel elements. Sweedan et al. (2016) investigated the flexural performance of steel I-beams bonded with hybrid CFRP-GFRP laminates using an anchorage system. It was found that an increase in FRP thickness can considerably improve the flexural performance of the beams in terms of yield moment and ultimate load-carrying capacity. Furthermore, the specimens exhibited a ductile failure mode

when an adequate number of anchor bolts were provided. Yu and Wu (2018) investigated the fatigue behavior of cracked steel beams rehabilitated with HM CFRP laminates. Based on experimental results, it was recommended to use nonlinear adhesives (Araldite 420) for CFRP retrofitting of steel beams, as specimens bonded with linear adhesive (Sikadur-30) were more susceptible to interfacial debonding. Zeng et al. (2018) analyzed full-scale of H-section steel beams strengthened with NM CFRP. The results revealed that local buckling has a notable effect on the load capacity and interfacial shear stress distribution of the steel beams strengthened with CFRP. Selvaraj and Madhavan (2020) proposed design limit states for steel beams strengthened with LM CFRP to prevent debonding failure. Furthermore, through experimental studies, intermediate debonding was found to be a dominant failure mode due to the significant modulus difference between steel and LM CFRP. Bagale and Parvin (2021) investigated the behavior of retrofitted steel beams with FRP using nonlinear finite element analysis. In this study, a bilinear bond-slip model, presented for linear adhesives, was applied to define the bond properties. The results revealed that CFRP retrofitting technique can increase the flexural capacity of both undamaged and damaged steel beams. Kumaraguru and Alagusundaramoorthy (2021) studied the flexural behavior of steel beams strengthened with IM CFRP sheets using anchorage mechanisms. The results showed that CFRP sheets with proper anchorage systems are highly effective in increasing the flexural capacity of steel beams. Deng, Li et al. (2022) investigated the fatigue behavior of notched steel beams rehabilitated with prestressed NM CFRP plates subjected to wetting/drying cycles. The results indicated that prestressed NM CFRP can significantly enhance the fatigue life of the steel beams. However, wetting/drying cycles can reduce this improvement. Li et al. (2022) investigated the effect of prestressed NM CFRP system application on the rehabilitation of notched steel beams considering the effect of wetting/drying cycles. In this study, the fatigue loading was applied to the notch beams rehabilitated with prestressed NM CFRP. It was shown that the proposed CFRP strengthening system can decrease the interfacial stress at the notch location and thereby delay interfacial debonding. A mixed failure mode of CFRP fracture and CFRP extraction from the end anchorage was observed in the specimens subjected to fatigue damage, wetting/drying cycles, and the combined effects. Guo, Gao et al. (2023) investigated the impact of temperature variations on the performance of NM CFRP retrofitted steel beams.

It was found that debonding loads increase as the temperature rises from -20°C to 60°C. However, debonding loads decreases at 80°C due to adhesive softening.

Wang et al. (2023) investigated the effect of prestressing on NM CFRP performance. The results indicate that applying prestressed NM CFRP increases the efficiency of the strengthening method. Qiang, Chen et al. (2023) investigated the flexural performance of steel-concrete composite beams strengthened with prestressed NM CFRP plates using an unbonded retrofit system. The results revealed that the prestressed NM CFRP plates can significantly improve the yielding and ultimate load of the beams. Wang, Guo et al. (2023) studied the effect of bond-slip on the flexural performance of damaged steel beams rehabilitated with NM CFRP and its impact on intermediate debonding using finite element analysis. It was found that interfacial fracture energy is the critical parameter influencing flexural retrofitting efficiency compared to maximum bond stress, elastic, and plastic slips. In this regard, increasing the interfacial energy can delay debonding and improve both flexural capacity and ultimate deflection. Wang, Xian et al. (2023) examined the application of ductile adhesive in steel beams strengthened with NM CFRP, focusing on debonding failure. The results showed that using ductile adhesives is more effective in reducing normal stress at the plate end and improving stress distribution. Wang, Bian et al. (2023) investigated the flexural behavior of damaged steel beams rehabilitated with prestressed NM CFRP plates. It was found that prestressed NM CFRP plates can significantly improve the load capacity and stiffness of the beams. Moreover, the adhesive layer has a minor impact on the flexural strength and stiffness of the damaged beams rehabilitated with NM CFRP plates. However, it can contribute to the reliability of the retrofitting system by preventing sudden failures. Comprehensive reviews on the retrofitting of steel structures with CFRP can be found in the literature (Borrie, Al-Saadi et al., 2021; Delzendeh Moghadam, Fathi et al., 2024; Gholami, Sam et al., 2013; Teng, Yu et al., 2012; Zhao & Zhang, 2007).

Research studies on the flexural behavior of retrofitted steel beams with CFRP, particularly those involving UHM CFRP, are limited. Therefore, this study aims to fill this gap and provide insight into the design of CFRP retrofitting technique. This paper evaluates the flexural

behavior of CFRP rehabilitated notched steel beams, including elements extracted from an old bridge after experiencing more than 50 years of service, which were fabricated using older technology. These bridge elements have been subjected to prolonged periods of loading and unloading, coupled with exposure to harsh weather conditions, thereby adding a distinctive dimension to the research. Furthermore, CFRP elastic modulus, CFRP configuration, notch depth, anchorage system, and adhesive type are the parameters considered in this study. The effect of CFRP elastic modulus is examined by considering NM and UHM CFRP with roughly the same tensile capacity (1500 MPa × 2.2 mm × 100 mm versus 2800 MPa × 1.2 mm × 100 mm). The results are evaluated in terms of failure modes, load-deflection behavior, strain distributions along the CFRPs, and Crack Mouth Opening Displacement (CMOD).

4.3 Experimental program

4.3.1 Material properties

In this experimental study, two series of steel are considered. In the first series, W200×22 steel beams of G40.21 44W are used. The height and flange width of the beams are 206 mm and 102 mm, respectively. The thickness of the web and flanges are 6.2 mm and 8 mm, respectively. The total length of the specimens is 1600 mm, and the clear span is 1500 mm. These beams have a yield strength and a minimum tensile strength of 300 MPa and 400-600 MPa, respectively.

In the second series, W14" wide flange beams of G40.4, extracted from an old bridge in Montreal region, are used. The height and width of the beams section are 361 mm and 305 mm, respectively. The thickness of the web and flanges is 10.7 mm and 17.5 mm, respectively. The total length of the specimens is 2250 mm, and the clear span is 2100 mm. These beams have a yield strength and a minimum tensile strength of 230 MPa and 410-500 MPa, respectively.

To rehabilitate the notched steel beams, MAPEI® Carboplate UHM plate and Sika® CarboDur® S512 are applied, representing UHM CFRP and NM CFRP, respectively. The nominal width and thickness of the UHM CFRP plate are 100 mm and 2.2 mm, respectively. The UHM CFRP plate has an elastic modulus of 460 GPa, a tensile strength of 1500 MPa, and an elongation at break of 0.34%. The NM CFRP plate has a nominal width and thickness of 100 mm and 1.2 mm, respectively. The NM CFRP has an elastic modulus of 165 GPa, a tensile strength of 2800 MPa, and an elongation at break of 1.7%. It should be noted that UHM and NM CFRP used in this study have approximately the same tensile capacity (1500 MPa × 2.2 mm × 100 mm versus 2800 MPa × 1.2 mm × 100 mm). To enhance the effectiveness of the rehabilitation technique and prevent CFRP deboning failure, SikaWrap 1400C is used to anchor the CFRP ends. SikaWrap sheets have an elastic modulus of 116 GPa and a tensile strength of 1355 MPa.

To bond the CFRP plates to the steel beams, combined epoxies of Fyfe TYFO S (Saturant epoxy) and Fyfe TYFO TC (Tack Coat), which is a ductile adhesive, are used. TYFO S has a tensile strength of 72.4 MPa and a tensile modulus of 3.18 GPa. TYFO TC possesses a tensile strength of 22.7 MPa, a tensile modulus of 1.2 GPa, and a shear strength of 19.3 MPa. Additionally, MapeWrap12 epoxy, which exhibits linear behavior in terms of stress-strain relationship, is also used to bond CFRP for one specimen. Furthermore, Sikadur 300 with a tensile strength of 55 MPa and a tensile modulus of 1.7 GPa, is applied to saturate and bond SikaWrap sheets to the steel beams to anchor CFRP ends.

Table 4.2 presents the mechanical properties of the steel beams, CFRPs, and adhesives used to fabricate the specimens. To verify the mechanical properties of the materials provided in datasheets, four steel coupons extracted from each type of beam and five coupons of each adhesive type were tested under tensile tests in accordance with ASTM standards (ASTM-A370, 2020; ASTM-D638, 2014). The adhesive and steel coupons are shown in Figure 4.1 and Figure 4.2, while the stress-strain curves of these coupons are presented in Figure 4.3.

Table 4.2 Mechanical properties of materials

Material	Tensile Strength (MPa)	Tensile Modulus (GPa)	Yield Strength (MPa)
UHM CFRP (MAPEI)	1500	460	NA
NM CFRP (Sika)	2800	165	NA
SikaWrap 1400C	1355	116	NA
Tyfo S (FYFE)	72.4	3.18	-
Tyfo TC (FYFE)	22.7	1.2	-
MapeWrap12 (MAPEI)	23.2	-	NA
Sikadur-300	55	1.7	NA
Steel (G40.21 44W)	400-600	~ 200	300
Steel (G40.4)	410-500	~ 200	230

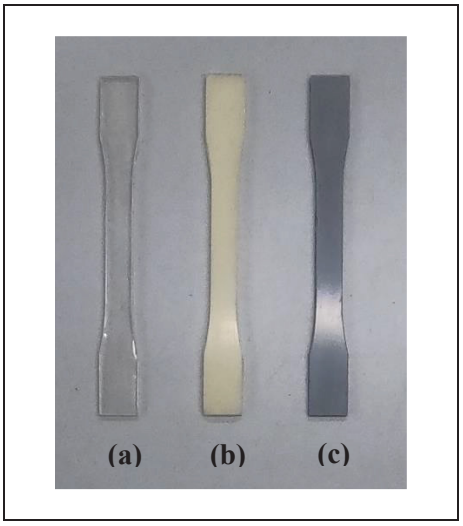

Figure 4.1 Adhesive coupons; (a) Sikadur 300, (b) Tyfo TC (FYFE), (c) MapeWrap12 (MAPEI)

Figure 4.2 Steel coupons extracted from the beams

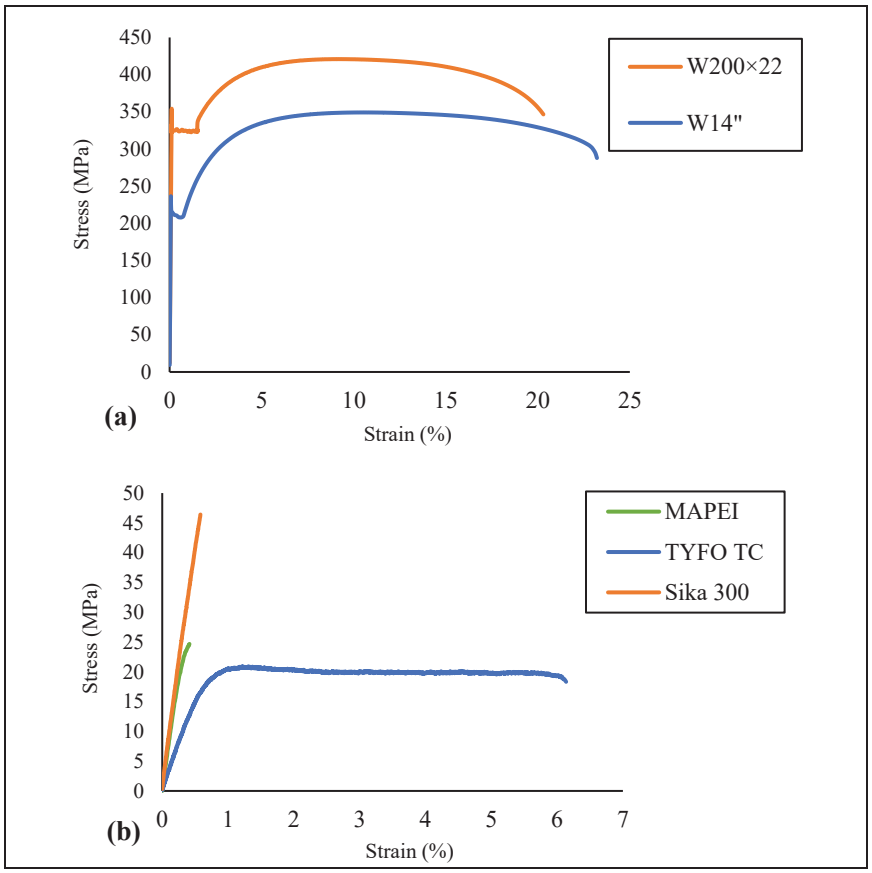

Figure 4.3 Tensile stress-strain curves of the steels and adhesives

4.3.2 Specimens preparation

Overall, 21 beams with different notch depths, CFRP elastic modulus, CFRP configurations, and adhesive types were prepared and tested. To avoid local buckling, eight stiffeners were welded on the web at the support and loading points, except for the specimens without anchorage systems. In addition, two different notch depths were applied to the beams. In the first case, the initial notch extends to the beam flange, while in the second case, it extends to the web of the beams.

Surface preparation has been found to be crucial and one of the influential parameters on the bond behavior between CFRP and the steel substrate (Fernando, Teng et al., 2013; Russian, Khan et al., 2021). Therefore, it is important to treat the steel surface to eliminate rust and contaminants and prevent thereby potential failure at the steel/adhesive interface. Following the guidelines of SSPC SP-10, the bond zones were treated using the sandblasting method. Prior to adhesive application, a thorough cleaning of both the steel surface and CFRP was conducted using acetone to improve mechanical interlocking.

The bonding procedure involves applying TYFO TC onto the steel surface using a specifically designed V notched trowel, ensuring a uniform thickness across all the bond zone. Subsequently, TYFO S was applied to the CFRP plate, which was then bonded to the beam. Once the laminate was in place, it was slightly adjusted to facilitate adhesive spreading and remove any trapped air. For the specimen using MapeWrap12 epoxy, the later was applied to both the steel and CFRP surfaces. The thickness of the adhesive material was approximately 1 mm –2 mm for all specimens (The Institution of Structural Engineers (ISE), 1999; Xia & Teng, 2005). After the bonding process, the specimens were cured at room temperature for approximately 14 days before testing (Wang, Wu et al., 2016a; Yang, Zhao et al., 2021; Yu, Fernando et al., 2012).

The test matrix and specimens labeling are presented in Table 4.3. As for specimens with anchorage mechanism, CFRP sheet (SikaWrap 1400C) were used to anchor the CFRP plate

ends, as shown in Figure 4.4, to increase the efficiency of the retrofitting technique. The schematic view of the CFRP configuration is given in Figure 4.5. Additionally, the details of each configuration are presented in Table 4.4.

To measure the strain distribution along the CFRP during the flexure test, a series of 20 mm and 30 mm strain gauges were installed on the outer surface of the CFRP plate. Strain gauges were also mounted on the beams to monitor the steel yielding. Displacements at the midspan were measured using linear variable differential transducers (LVDTs). In addition, crack gauges were installed to measure the crack mouth opening displacement (CMOD).

Table 4.3 Test matrix and labeling of specimens for flexure test

Series	No	Specimen	Beam section	CFRP type	Epoxy type	Anchorage	Notch depth (mm)	CFRP configuration
Series1	1	W200-REF	W200×22	-	-	-	-	-
	2	W200-N6-REF	W200×22	-	-	-	6	-
	3	W200-N58-REF	W200×22	-	-	-	58	-
	4	W200-N6-UHM-C1	W200×22	UHM	TYFO	-	6	Config. 1
	5	W200-N6-NM-C1	W200×22	NM	TYFO	-	6	Config. 1
	6	W200-N58-UHM-C2	W200×22	UHM	TYFO	-	58	Config. 2
	7	W200-N58-NM-C2	W200×22	NM	TYFO	-	58	Config. 2
	8	W200-N6-UHM-C3	W200×22	UHM	TYFO	Anchored	6	Config. 3
	9	W200-N6-NM-C3	W200×22	NM	TYFO	Anchored	6	Config. 3
	10	W200-N58-UHM-C4	W200×22	UHM	TYFO	Anchored	58	Config. 4
	11	W200-N58-NM-C4	W200×22	NM	TYFO	Anchored	58	Config. 4
	12	W200-N58-UHM-C5	W200×22	UHM	TYFO	Anchored	58	Config. 5
	13	W200-N6-UHM-C3-M	W200×22	UHM	MapeWrap12	Anchored	6	Config. 3
Series 2	14	W14-REF	W14" wide flange	-	-	-	-	-
	15	W14-N10-REF	W14" wide flange	-	-	-	10	-
	16	W14-N160-REF	W14" wide flange	-	-	-	160	-
	17	W14-N10-UHM-C1	W14" wide flange	UHM	TYFO	Anchored	10	Config. 1
	18	W14-N10-NM-C1	W14" wide flange	NM	TYFO	Anchored	10	Config. 1
	19	W14-N160-UHM-C2	W14" wide flange	UHM	TYFO	Anchored	160	Config. 2
	20	W14-N160-UHM-C3	W14" wide flange	UHM	TYFO	Anchored	160	Config. 3
	21	W14-N160-NM-C3	W14" wide flange	NM	TYFO	Anchored	160	Config. 3

Figure 4.4 Curing of the SikaWrap fabric

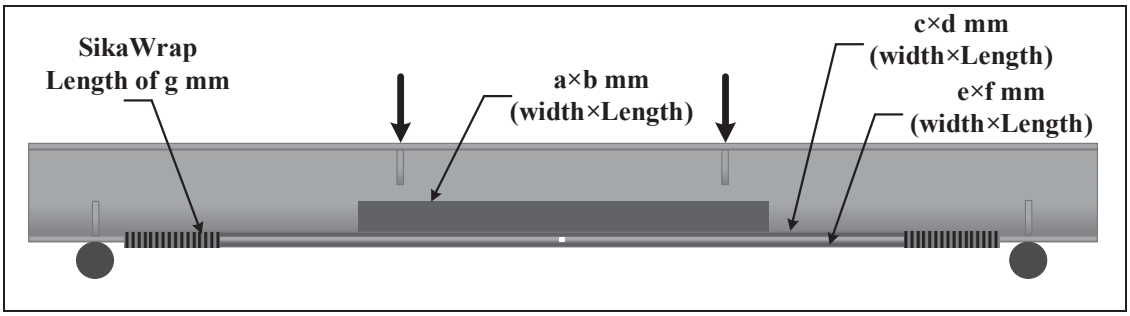

Figure 4.5 Schematic view of CFRP configuration

Table 4.4 Details of CFRP dimensions used in different configurations

Beam section	Configuration	CFRP dimensions (mm)						
		a	b	c	d	e	f	g
W200×22	Config. 1	-	-	-	-	100	800	-
	Config. 2	50	800	-	-	100	800	-
	Config. 3	-	-	-	-	100	1300	200
	Config. 4	80	1000	-	-	100	1300	200
	Config. 5	-	-	47	1300	100	1300	200
W14" wide flange	Config. 1	-	-	-	-	300	2000	300
	Config. 2	140	1000	-	-	300	2000	300
	Config. 3	-	-	135	2000	300	2000	300

4.3.3 Test setup

The beams were tested under four-point flexure using an MTS machine having a capacity of 1200 kN. The specimens were carefully placed between two supports, as shown in Figure 4.6, and the wires of the strain gauges, crack gauges, and LVDT were connected to the gauge reader of the machine. All specimens were loaded at a constant displacement rate of 1 mm/min up to failure. All experimental data, including measurements from the strain gauges, crack gauges, and LVDT, were automatically recorded using a data acquisition system.

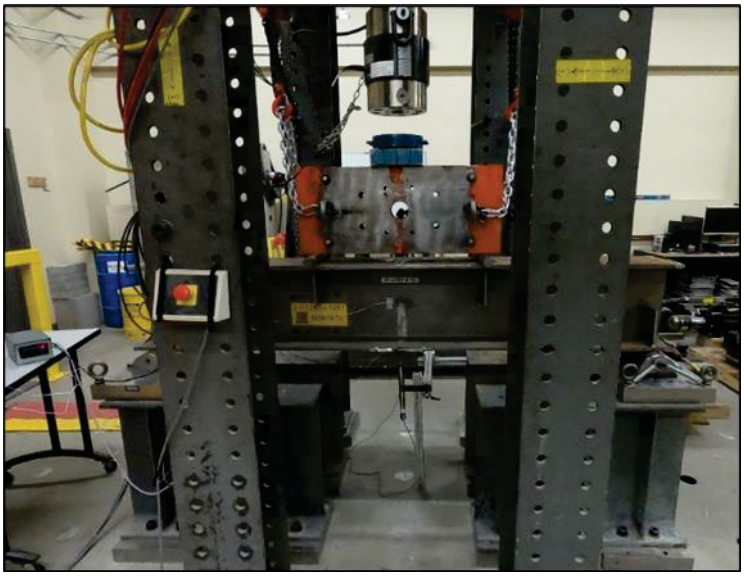

Figure 4.6 Test setup

4.4 Experimental results

4.4.1 Failure modes

The failure modes of the specimens retrofitted with CFRP are presented in Figure 4.7 and Figure 4.8. Observations from the tests indicated that cracking sounds were emitted, particularly at higher applied loads for rehabilitated beams. For W200×22 beams retrofitted with configurations 1 and 2, the failure mode was by debonding of the CFRP located on the bottom flange for both NM and UHM CFRP, indicating thereby that the CFRPs did not reach

their maximum load-carrying capacity. However, the UHM CFRP located on the web underwent rupture while delamination of NM CFRP was observed in configuration 2.

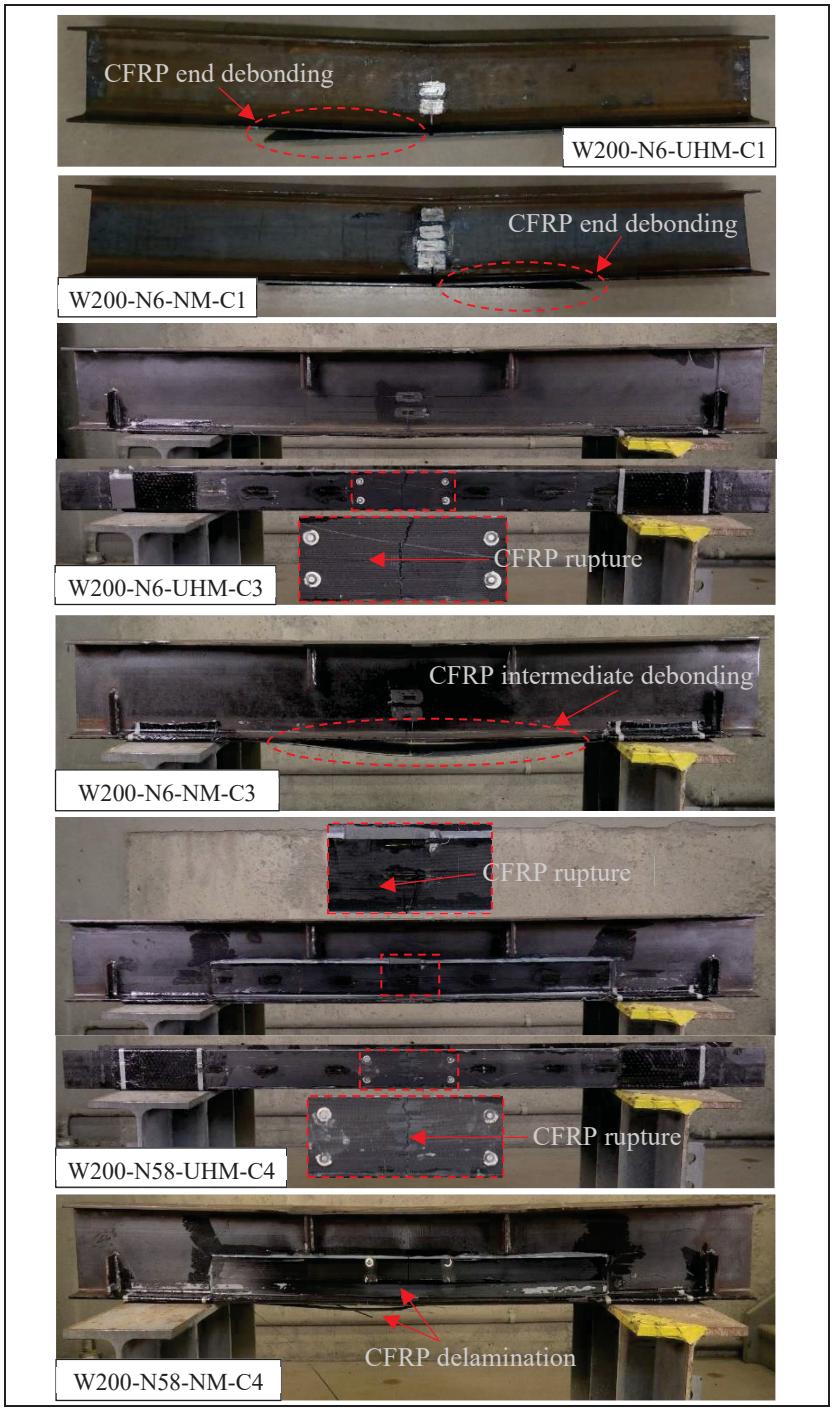

Figure 4.7 Failure modes of the W200×22 rehabilitated with CFRP

To enhance the effectiveness of the retrofitting system, several measures were implemented. Firstly, the bond length of the CFRP was increased, allowing for a larger area of contact and improved load transfer between the CFRP and the steel substrate. Additionally, the CFRP ends were anchored using CFRP sheets, preventing thereby premature debonding failure. The failure modes for the enhanced configurations were CFRP rupture for UHM and delamination for NM. However, it is worth mentioning that in specimen W200-N6-NM-C3, intermediate debonding occurred.

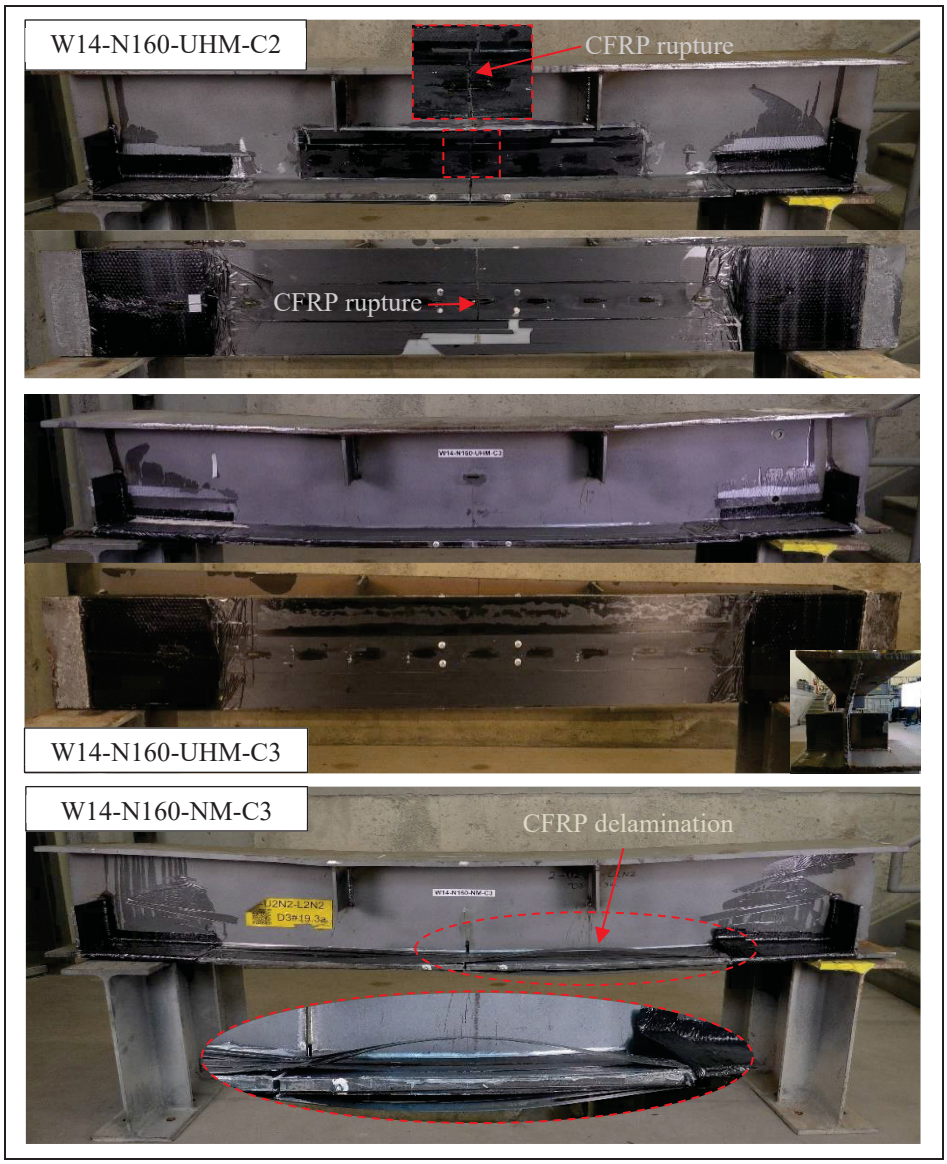

Figure 4.8 Failure modes of the W14" rehabilitated with CFRP

For configuration 5, it was observed that both UHM CFRPs located on the top and bottom sides of the bottom flange ruptured. As for the specimen with MapeWrap12 epoxy, the failure mode was CFRP rupture. This result indicates that the type of adhesive does not influence the failure modes when an effective anchorage system is employed. Furthermore, it was observed that only UHM CFRP experienced rupture as a failure mode, while NM CFRP underwent delamination despite reaching its maximum capacity.

Regarding the W14" beams with an initial crack extending to the beam's flange and with CFRP configuration 1, for both NM and UHM CFRP, the failure mode was identified as flange local buckling on the compression side. This result indicates that the CFRP did not reach its maximum load-carrying capacity, and the steel failed before the CFRP laminate. For W14-N160-UHM-C2, both UHM CFRPs on the web and the bottom flange experienced CFRP rupture. However, in W14-N160-UHM-C3, the steel beams failed due to lateral-torsional buckling. It should be noted that the failure in the CFRP rupture case was sudden, whereas specimens with steel failure experienced a more gradual failure process. As for W14-N160-UHM-C3, specimen exhibited CFRP delamination failure between the midspan and the support.

4.4.2 Load-deflection behavior

The load-deflection curves of the specimens are shown in Figure 4.9. Specimens W200-N6-UHM-C1 and W200-N6-NM-C1, where the initial crack extends to the beam's flange, exhibit load deflection behaviors similar to REF-6. These results indicate that the CFRP configuration does not contribute to restoring the capacity of the beams. Similarly, in specimens W200-N58-UHM-C2 and W200-N58-NM-C2, the CFRP located on the flange does not effectively restore the flexural capacity. However, a comparison between W200-N6-REF and these specimens reveals that the CFRP applied to the web successfully compensates for the steel loss in the web. In the case of specimens W200-N6-UHM-C3 and W200-N6-NM-C3, featuring an enhanced configuration, the CFRP effectively restores the capacity of the beams. However,

both specimens exhibit brittle behavior, which can be attributed to the lower rupture strain of UHM CFRP.

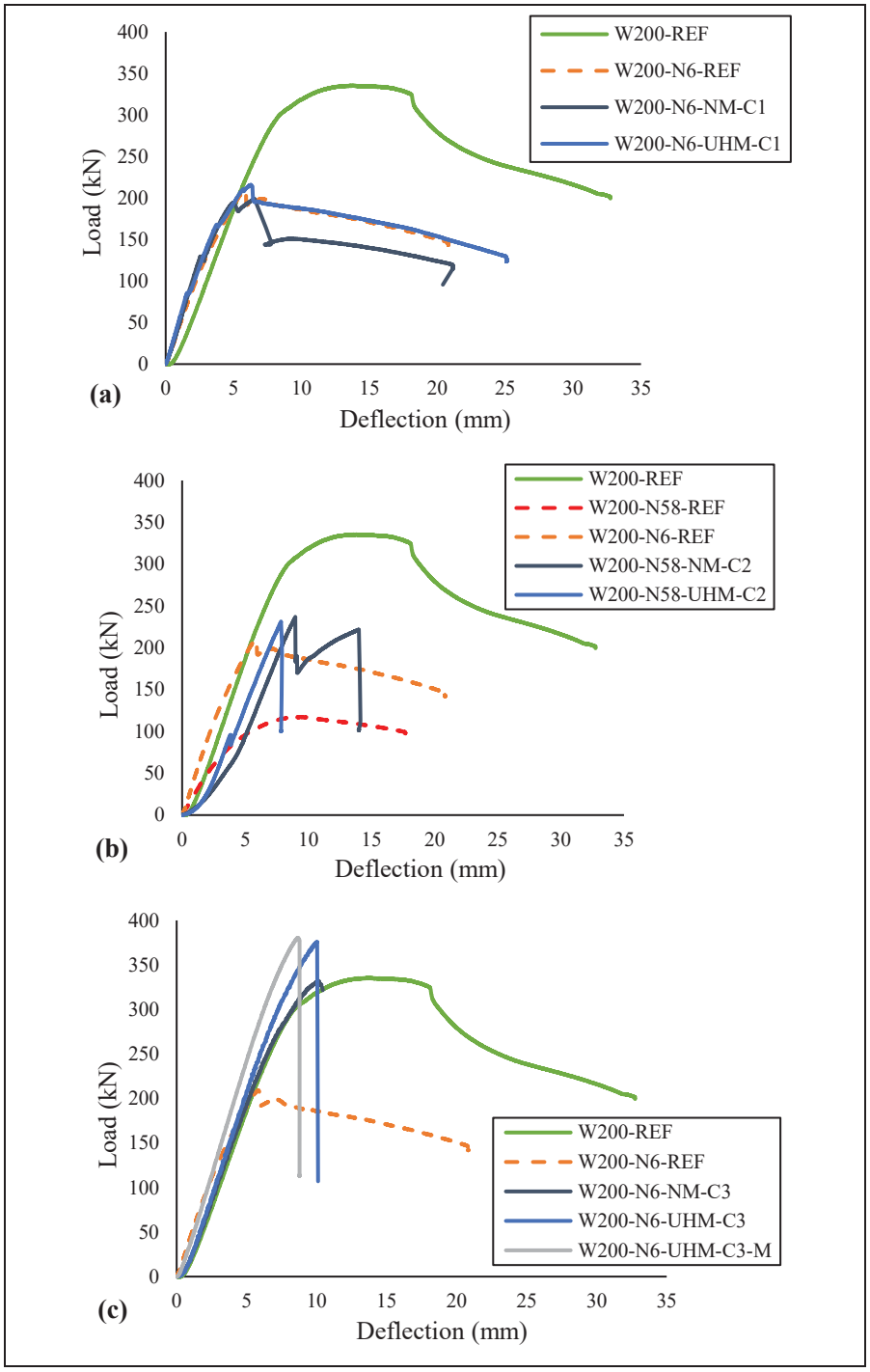

Figure 4.9 Load-deflection curves: Reference vs. rehabilitated beams

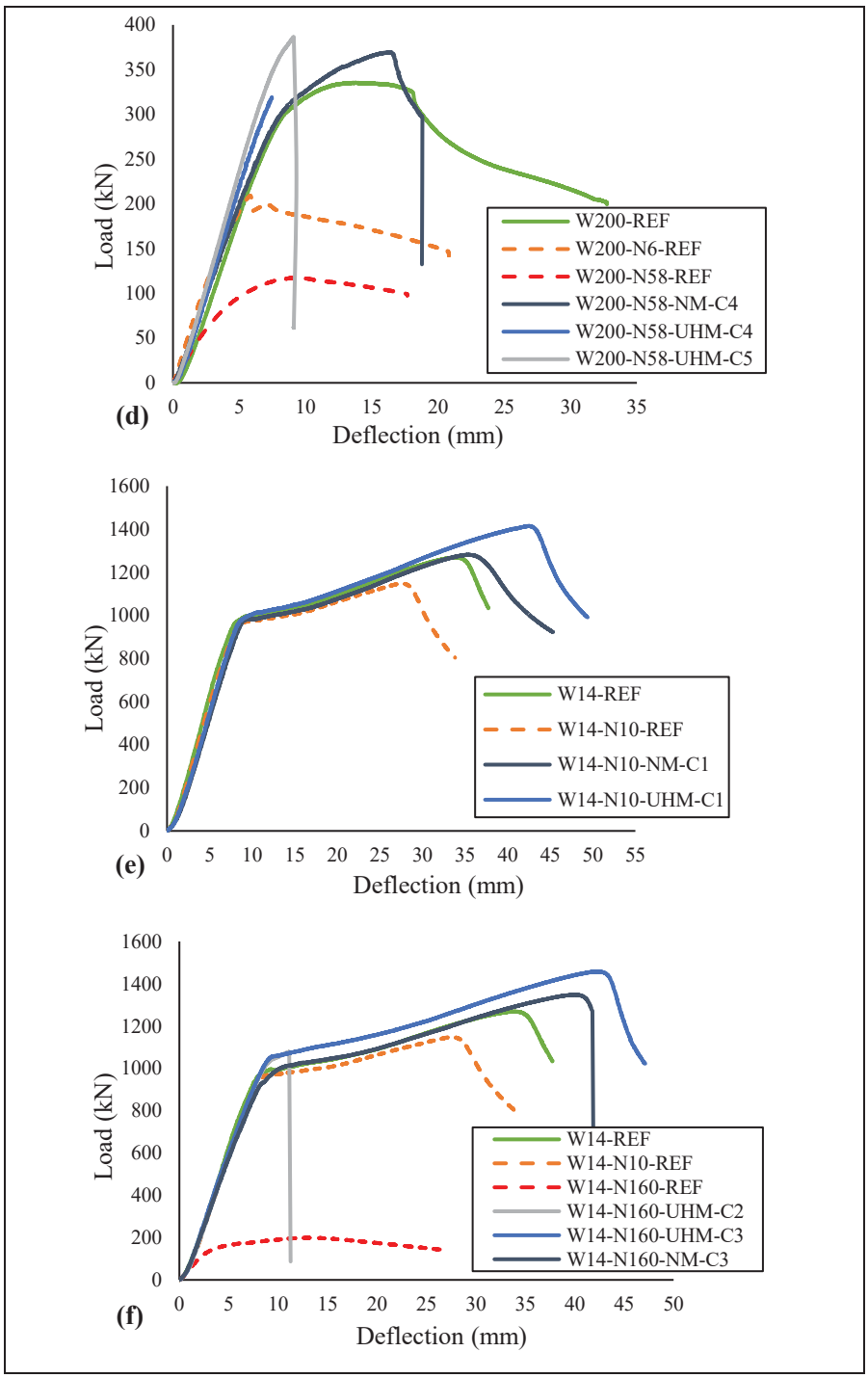

Figure 4.9 Load-deflection curves: Reference vs. rehabilitated beams (continued)

Conversely, the brittle behavior in NM CFRP specimens is due to intermediate debonding. Moving on to specimens W200-N58-UHM-C4 and W200-N58-NM-C4, these demonstrate the successful restoration of the capacity of the beams using the new CFRP configuration. The W200-N58-UHM-C4 specimen exhibits brittle behavior due to the aforementioned reason, while the W200-N58-NM-C4 beam displays a ductile behavior. Furthermore, it was observed that the UHM CFRP rehabilitated specimen bonded with linear epoxy exhibited similar behavior compared to the specimen bonded with nonlinear adhesives (specimens W200-N6-UHM-C3 vs. W200-N6-UHM-C3-M).

Regarding the rehabilitation of the steel bridge elements, specimens W14-N10-NM-C1 and W14-N10-UHM-C1, where the initial notch extends to the beam's flange, exhibit load-deflection behaviors similar to W14-REF. This indicates that both types of NM and UHM CFRP effectively contributed to restoring the capacity of the beams. Notably, the beam rehabilitated with UHM CFRP achieved a higher maximum load compared to its counterpart rehabilitated with NM CFRP. Similarly, specimens W14-N160-UHM-C2 and W14-N160-UHM-C3, where the initial notch extends to the beam's web, successfully restored the flexural capacity. Furthermore, a comparison between these two specimens reveals that the specimens with configuration 2 exhibit brittle behavior and experience a sudden failure after yielding. In contrast, the specimen with configuration 3 features a gradual failure and achieves a higher load-carrying capacity. This discrepancy can be attributed to the location of the CFRP. In configuration 2, the CFRP is bonded to the lower part of the web, whereas in configuration 3, the CFRP is attached to the upper side of the bottom flange. Consequently, bonding CFRP farther from the neutral axis can increase the flexural capacity of the specimens. Moreover, this arrangement can contribute to reducing the interfacial shear stress of the adhesive between the bottom CFRP plate and the steel by shifting the neutral axis to a lower level (Al-Saidy, 2001). It should be noted that CFRP configuration 3 could restore 84% of the load-carrying capacity by compensating for steel loss. The maximum loads achieved by retrofitted W200×22 and W14" wide flange beams are shown in Figure 4.10 and Figure 4.11. As can be seen, the specimens with an anchoring system can successfully restore the capacity of the notched steel beams. Furthermore, the specimens rehabilitated with UHM CFRP generally outperform those

rehabilitated with NM in terms of load-carrying capacity, despite the fact that both CFRPs have a similar tensile capacity.

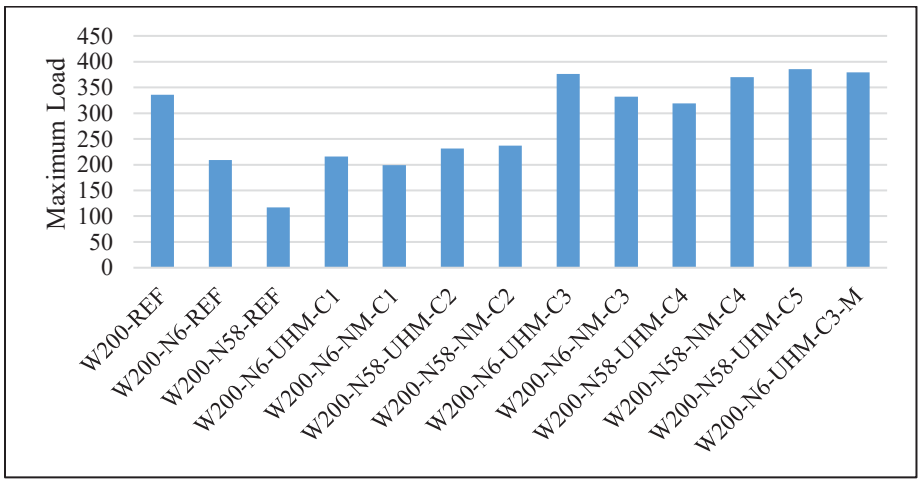

Figure 4.10 Maximum attained load for reference and rehabilitated W200×22 beams

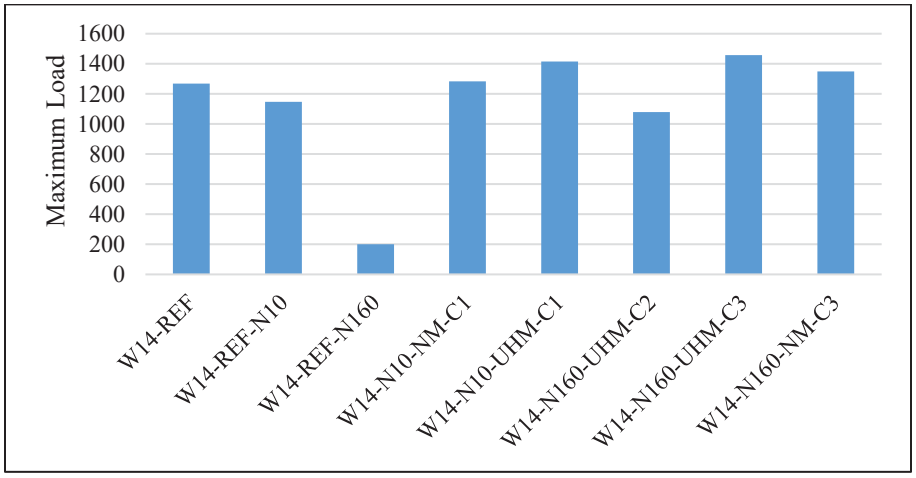

Figure 4.11 Maximum attained load for reference and rehabilitated W14" wide flange beams

4.4.3 Distributions of CFRP strains in beams rehabilitated with CFRP

Figure 4.12 presents the strain distributions of the CFRP for the rehabilitated beams with an anchorage system. In specimens without an anchorage system, debonding was observed at lower load levels, resulting in lower strain experienced by the CFRP compared to the specimens with an anchorage system. Analysis of the strain distributions along the bonded length reveals that locations closer to the midspan of the beams exhibited higher strain values compared to those near the supports.

This observation clearly demonstrates that, under monotonic loading, the major part of bond shear resistance takes place in the bonded length section near the midspan, while the shear contribution of intervals closer to the supports is relatively lower. This phenomenon is particularly prominent at load levels approaching the ultimate load capacity of the beams (0.9 P_{ult} - 0.99 P_{ult}). However, the strain distributions along the bonded length of W14-N10-UHM-C1 specimen shows that locations closer to the loading area exhibited higher strain values compared to those near the supports and the midspan of the beams. Comparing the strain distributions of the two CFRPs, NM and UHM, it is observed that the maximum strains reached by specimens with NM CFRP were significantly higher than those with UHM CFRP. This is attributed to the higher stiffness of UHM CFRP compared to NM CFRP, which results in lower ductility of UHM CFRP.

Regarding the effect of adhesive type, the results show that using linear and nonlinear adhesives yields similar results when an anchorage system is applied. As can be seen, the strain distribution for both specimens, W200-N6-UHM-C3 and W200-N6-UHM-C3-M, are roughly identical, despite the former being bonded with nonlinear epoxy and the latter with linear epoxy.

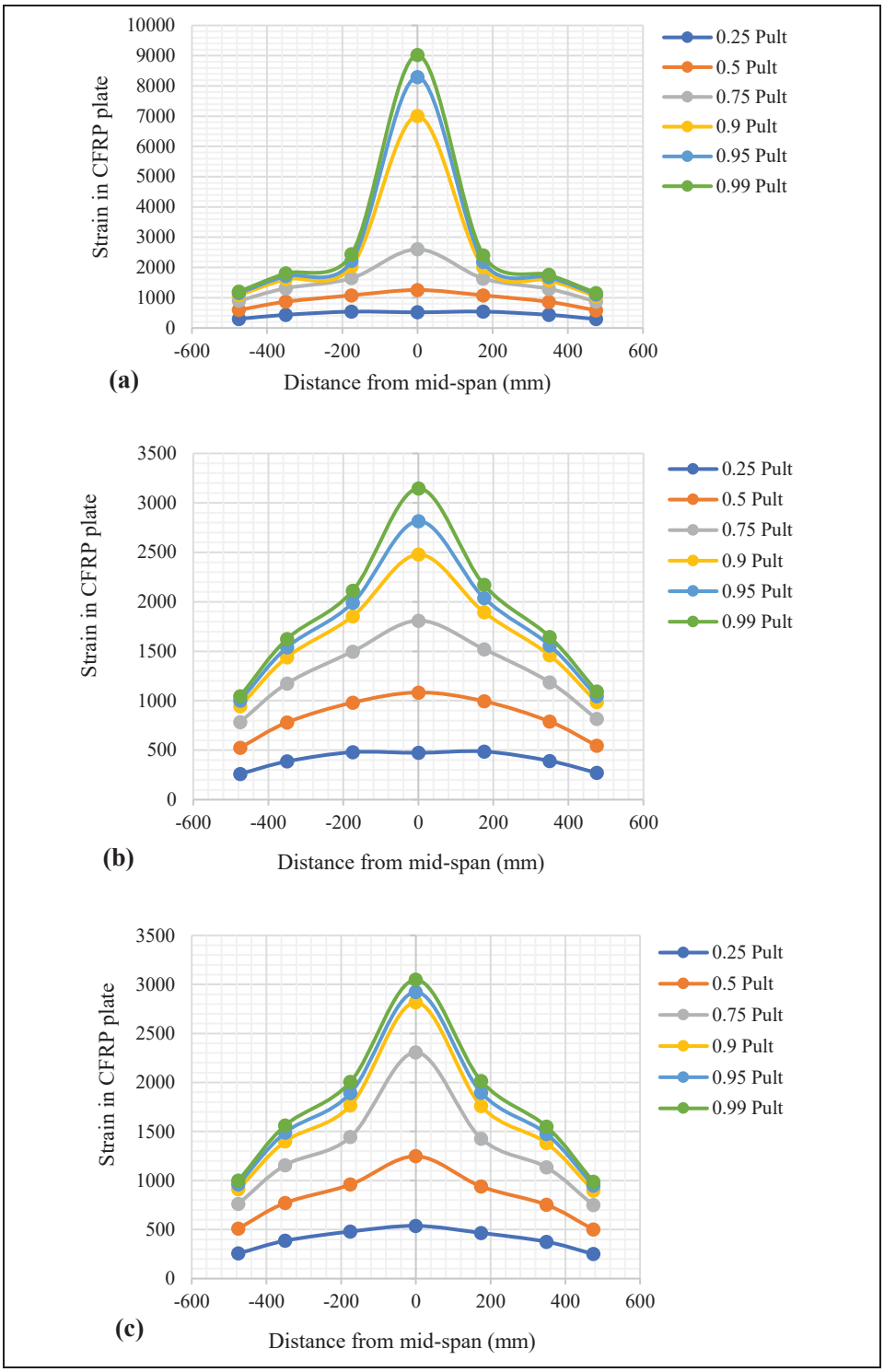

Figure 4.12 Strain distributions of CFRP located on flange of specimens; (a) W200-N6-NM-C3; (b) W200-N6-UHM-C3; (c) W200-N6-UHM-C3-M; (d) W14-N10-UHM-C1;(e) W14-N160-UHM-C2 ;(f) W14-N160-NM-C3

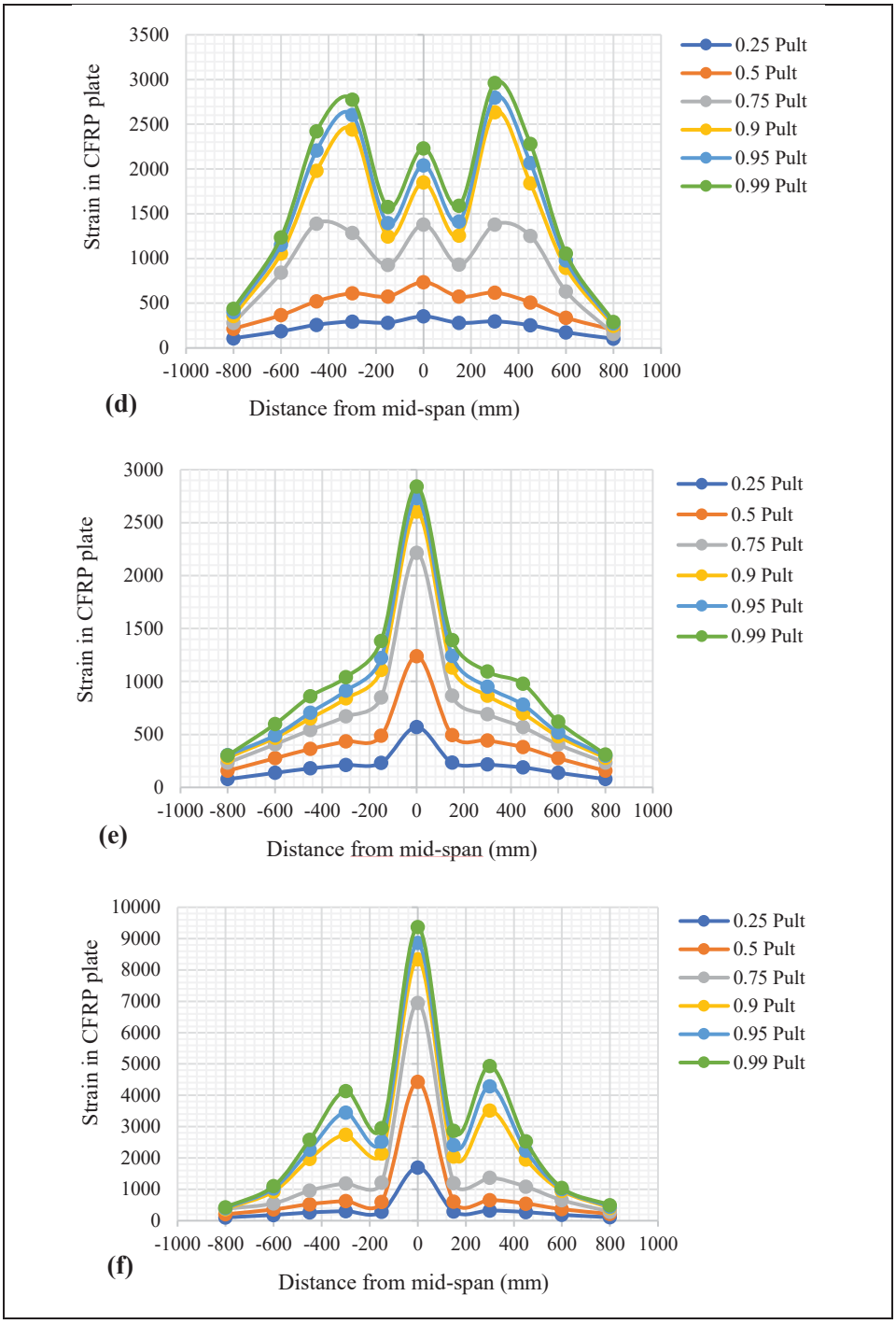

Figure 4.12 Strain distributions of CFRP located on flange of specimens; (a) W200-N6-NM-C3; (b) W200-N6-UHM-C3; (c) W200-N6-UHM-C3-M; (d) W14-N10-UHM-C1;(e) W14-N160-UHM-C2 ;(f) W14-N160-NM-C3 (continued)

4.4.4 Crack Mouth Opening Displacement (CMOD)

Figure 4.13 shows the load-crack mouth opening displacement (CMOD) for W200×22 rehabilitated beams with an anchorage system. The results indicate that the CFRP rehabilitation technique can effectively control the crack mouth opening. As can be seen, the CMOD increased linearly with load until failure of the specimens for UHM CFRP rehabilitated beams. Regarding the effect of adhesive type on the rehabilitation system, both W200-N6-UHM-C3 and W200-N6-UHM-C3-M reached approximately the same peak load and CMOD. This result indicates that, with an effective anchorage system, the type of adhesive does not significantly affect the flexural behavior of the rehabilitated notched beams. The results also show that the specimens rehabilitated with NM CFRP exhibit greater CMOD compared to those with UHM CFRP. The behavior of the W200-N58-NM-C4 specimen shows a significant load drop while the CMOD remains relatively unchanged, indicating a potential sudden fracture or rapid crack propagation. In this case, the specimen shows significant deformation and energy absorption before failure.

Figure 4.14 presents the CMOD for the W14" wide flange rehabilitated beams. A comparison between specimens W14-N10-NM-C1 and W14-N10-UHM-C1 indicates that the specimen rehabilitated with UHM CFRP exhibits a lower CMOD than its NM CFRP counterpart. This result can be attributed to the higher stiffness of the UHM CFRP which contributes to more efficient control of crack opening. Regarding specimens W14-N160-UHM-C2 and W14-N160-UHM-C3, where the initial notch extends to the beam's web, the results show that configuration 3 is more efficient in terms of load-carrying capacity and mitigating crack opening.

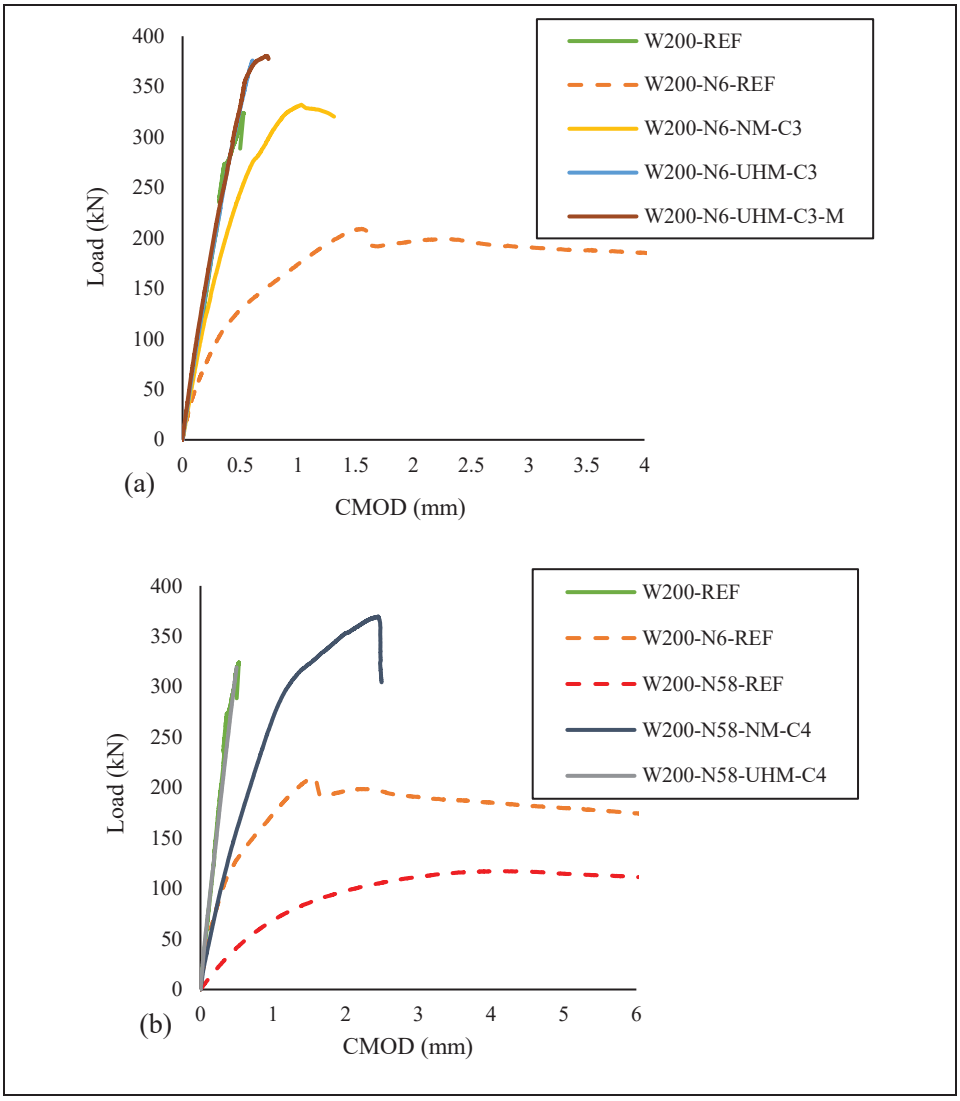

Figure 4.13 Load-crack mouth opening displacement: Reference vs. W200×22 rehabilitated beams

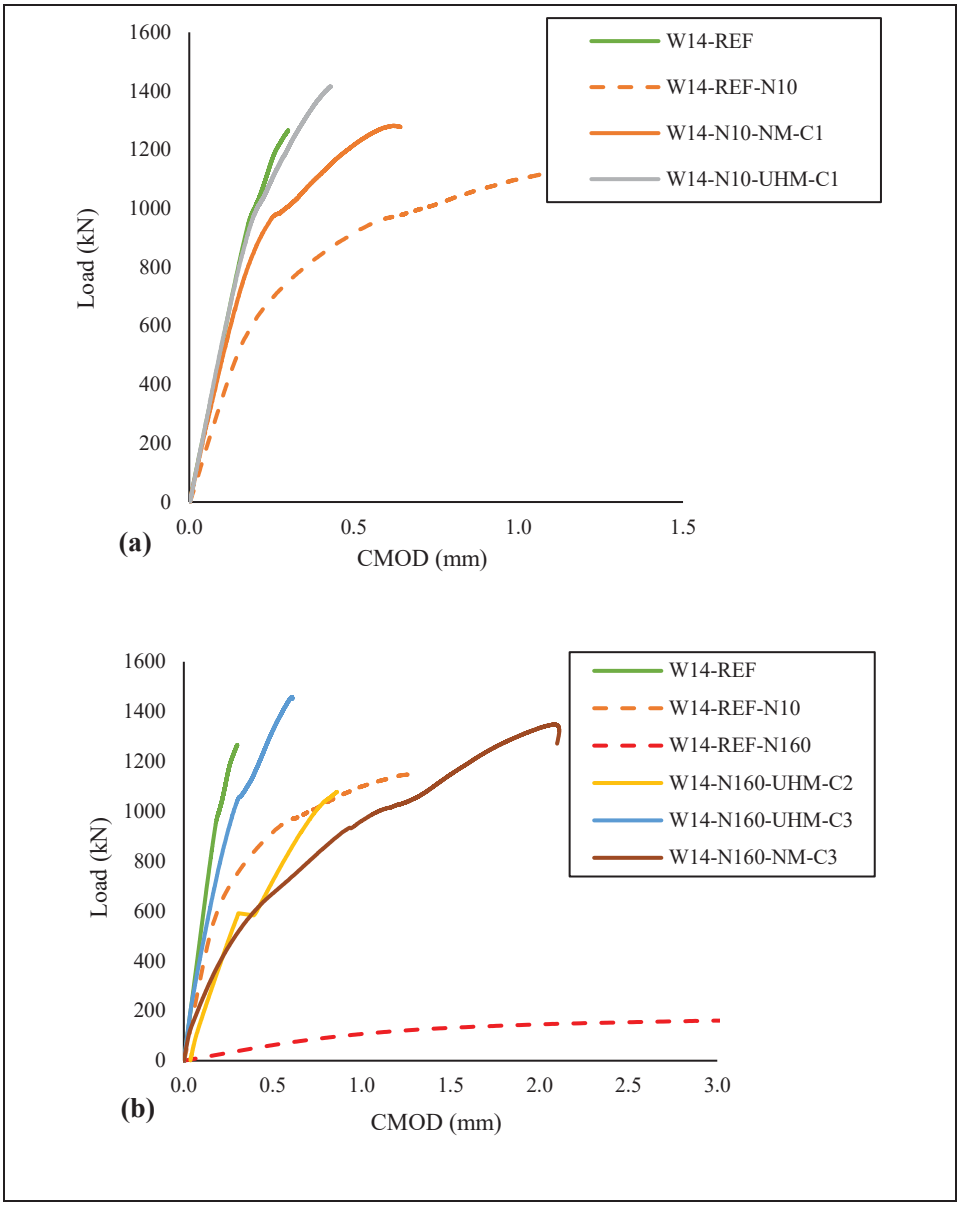

Figure 4.14 Load-crack mouth opening displacement: Reference vs. W14" rehabilitated beams

4.5 Conclusions

In this study, the flexural behavior of notched steel beams rehabilitated with CFRP was evaluated. In the experimental program various parameters, including the CFRP elastic modulus, anchorage system, adhesive type, and notch depth were considered. Based on the experimental results, the following conclusions can be drawn:

- Specimens bonded with UHM CFRP or NM CFRP without an anchorage system failed by debonding. However, using CFRP sheets as an anchorage system changes the failure mode to steel failure or CFRP delamination and rupture for NM CFRP and UHM CFRP, respectively. This result indicates that the anchorage system at the CFRP ends successfully prevents premature failure, allowing the CFRP rehabilitation technique to effectively restore the capacity of the notched beams. It is noteworthy to highlight that the anchorage system introduced in this study is notably simpler in terms of application compared to the solutions suggested in existing literature.

- Specimens rehabilitated with EB UHM CFRP exhibit brittle behavior, while those rehabilitated with EB NM CFRP feature ductile behavior. This difference is attributed to the lower rupture strain of UHM CFRP compared to NM CFRP. Furthermore, a comparison of the failure modes reveals that specimens with UHM CFRP undergo CFRP rupture, whereas those with NM CFRP experience delamination with CFRP breaking longitudinally.

- Both UHM CFRP-rehabilitated specimens bonded with linear and nonlinear adhesives show similar performance in terms of load-carrying capacity, CMOD, strain distribution along the CFRP, and failure mode. This result suggests that the type of adhesive does not significantly alter the flexural behavior of the retrofitted beams when an effective anchorage system is used.

- The findings indicate that the CFRP rehabilitation technique effectively control crack opening, especially in specimens rehabilitated with UHM CFRP, due to its superior stiffness. Furthermore, UHM CFRP outperformed NM CFRP in terms of load-carrying capacity, despite that both have approximately the same tensile capacity.

- The results suggest that installing CFRP on both the upper and lower sides of the bottom flange is more efficient when the notch extends into the web. This configuration increases the flexural capacity of the specimens by bonding CFRP farther from the neutral axis. However, in real-life situations, covering the crack on the web of the damaged beam is inevitable to guarantee the serviceability of the structure.

4.6 Data availability statement

Some or all data, models, or code that support the findings of this study are available from the corresponding author on reasonable request.

4.7 Acknowledgments

The authors thank Fyfe FRP, Sika-Canada, and MAPEI-Canada for contributing to the cost of the materials. The efficient collaboration of Jonathan Auger (technician) at École de technologie supérieure in conducting the tests is also acknowledged.

CONCLUSIONS

In this section, the key findings of the current research are highlighted. The present experimental study can be divided into the following two parts:

Part 1. In this part, the bond behavior between CFRP and the steel interface is studied. A total of 25 CFRP/steel bonded joints were prepared and tested under static loading. The different parameters considered include CFRP elastic modulus, adhesive type, surface preparation, and CFRP bond length. Furthermore, the accuracy of the proposed formulas for bond strength and effective bond length is examined. The accuracy of the existing bond-slip models is also assessed. The following conclusions can be drawn from this part:

- The failure mode of the UHM CFRP/steel joints bonded with linear adhesive is debonding. However, UHM CFRP bonded with nonlinear adhesive showed CFRP rupture for the specimens with a bond length greater than effective bond length. For the NM CFRP/steel joints bonded with nonlinear adhesive, the failure mode shifted from debonding to CFRP delamination with increasing bond length.

- The three surface treatment methods considered in this study resulted in similar bond behavior for UHM CFRP joints bonded with nonlinear adhesive. However, sandblasting method is reported as the most effective method in the literature for achieving optimal surface roughness and cleanliness (Wang, Wu et al., 2016a).

- The effective bond length for specimens bonded with NM CFRP is longer than those bonded with UHM CFRP using nonlinear adhesive, despite the fact that, both CFRPs have approximately the same tensile capacity. Furthermore, the effective bond length for the UHM CFRP joints bonded with linear adhesive is longer than those bonded with nonlinear adhesive.

- The UHM CFRP/steel joints bonded with nonlinear adhesive achieved moderately better tensile capacity compared to those bonded with NM CFRP using nonlinear adhesive.

- The intervals closer to the loaded-end carry the highest interfacial shear strains. Conversely, intervals closer to the free-end do not significantly contribute to bond shear resistance compared to regions near the loaded-end.

- The models available in the literature do not accurately capture the bond-slip curves of CFRP bonded specimens in terms of peak bond stress and bond slip.

Part 2. In the second part, the flexural performance of the retrofitted steel notched beams is evaluated. A total of 21 beams, including reference and rehabilitated beams, were tested under static loading. Two types of beams were considered: W200×22 beams received directly from a factory and W14" wide flange beams extracted from the old Champlain bridge after approximately 50 years of service. The parameters considered include CFRP elastic modulus, CFRP configuration, notch depth, anchorage system, and adhesive type. The following conclusions can be drawn from the experimental research study:

- The results show that the anchorage system at the CFRP ends successfully prevents premature failure, allowing the CFRP rehabilitation technique to effectively restore the capacity of the notched beams. It should be noted that the proposed anchorage system in this study is significantly easier to apply compared to those suggested in the existing literature.

- The findings reveal that notch beams rehabilitated with EB NM CFRP exhibit a ductile behavior, while those rehabilitated with EB UHM CFRP show brittle behavior due to the lower rupture strain of UHM CFRP compared to NM CFRP. Moreover, specimens with UHM CFRP undergo CFRP rupture, whereas those with NM CFRP experience delamination with CFRP breaking longitudinally.

- It is found that the effect of adhesive type (linear vs. nonlinear) is negligible in terms of influencing the load-carrying capacity, crack mouth opening displacement (CMOD), strain distribution along the CFRP, and the failure mode of the retrofitted beams with an anchorage mechanism.

- The findings indicate that the CFRP rehabilitation technique effectively control crack opening, particularly in specimens rehabilitated with UHM CFRP owing to its superior stiffness. Furthermore, UHM CFRP outperformed NM CFRP in terms of load-carrying capacity, despite that both have approximately the same tensile capacity.

- The findings indicate that installing CFRP to both the upper and lower sides of the bottom flange is more effective when the notch extends into the web. This configuration enhances the flexural capacity of the specimens by positioning the CFRP farther from the neutral axis. Nevertheless, in practical applications, it is essential to cover the crack on the web of the damaged beam to ensure the structure's serviceability.

RECOMMENDATIONS

The following recommendations for further research on the application of CFRP in retrofitting steel structures are suggested:

- As the proposed specimens are not sufficient to fully investigate the design parameters, finite element models should be developed to fill this gap. In this regard, a parametric study can be carried out to identify the influential parameters on the bond and flexural behavior of the CFRP retrofitted specimens. These parameters include: a) CFRP thickness; b) Adhesive thickness; c) Notch location; d) CFRP bond length; f) Loading frequency, and amplitude.

- Further research should be conducted to investigate the effect of interrelated parameters on the bond behavior of the CFRP/steel interface to propose an optimal retrofitting system. Moreover, the effect of some parameters such as CFRP to steel width ratio on the bond behavior and the effective bond length is needed to be studied.

- Further analytical research is required to develop a reliable bond–slip model at the CFRP/steel interface under static loading by considering the influencing variables that are representative of conditions in practice.

- More investigation is needed to develop adhesives with enhanced mechanical properties to improve bond strength and durability, as the weakest link in the CFRP/steel bond is the adhesive layer.

- More research is needed to investigate the effect of fatigue loading on the CFRP retrofitted specimens and the effective bond length. Also, the effect of shear combined with flexure on the bond length needs to be clarified. In this regard, a reliable effective bond length relationship may be developed.

- More research could be conducted to investigate the effect of galvanic corrosion, especially in the CFRP retrofitting method utilizing a steel anchorage system. The long-term effect of galvanic corrosion has not been properly investigated in this case. In addition, the fatigue performance of the anchorage mechanisms for EB CFRP should be investigated.

LIST OF BIBLIOGRAPHICAL REFERENCES

Afifi, M. Z., Mohamed, H. M., Chaallal, O., & Benmokrane, B. (2015). Confinement model for concrete columns internally confined with carbon FRP spirals and hoops. *Journal of structural engineering, 141*(9), 04014219.

Al-Mosawe, A., & Al-Mahaidi, R. (2019). Performance of CFRP-steel joints enhanced with bi-directional CFRP fabric. *Construction and Building Materials, 197*, 72-82. doi:10.1016/j.conbuildmat.2018.11.235

Al-Mosawe, A., Al-Mahaidi, R., & Zhao, X.-L. (2016). Bond behaviour between CFRP laminates and steel members under different loading rates. *Composite Structures, 148*, 236-251. doi:10.1016/j.compstruct.2016.04.002

Al-Saidy, A. H. (2001). Structural behavior of composite steel beams strengthened/repaired with carbon fiber reinforced polymer plates.

Al-Zubaidy, H., Al-Mahaidi, R., & Zhao, X.-L. (2012). Experimental investigation of bond characteristics between CFRP fabrics and steel plate joints under impact tensile loads. *Composite Structures, 94*(2), 510-518. doi:10.1016/j.compstruct.2011.08.018

Al-Zubaidy, H., Al-Mahaidi, R., & Zhao, X.-L. (2013). Finite element modelling of CFRP/steel double strap joints subjected to dynamic tensile loadings. *Composite Structures, 99*, 48-61. doi:10.1016/j.compstruct.2012.12.003

Al-Zubaidy, H. A., Zhao, X.-L., & Al-Mahaidi, R. (2012). Dynamic bond strength between CFRP sheet and steel. *Composite Structures, 94*(11), 3258-3270. doi:10.1016/j.compstruct.2012.04.025

Al-Zubaidy, H. A., Zhao, X.-L., & Al-Mahaidi, R. (2013). Experimental evaluation of the dynamic bond strength between CFRP sheets and steel under direct tensile loads. *International Journal of Adhesion and Adhesives, 40*, 89-102. doi:10.1016/j.ijadhadh.2012.08.001

Aljabar, N. J., Zhao, X. L., Al-Mahaidi, R., Ghafoori, E., Motavalli, M., & Koay, Y. C. (2017). Fatigue tests on UHM-CFRP strengthened steel plates with central inclined cracks under different damage levels. *Composite Structures, 160*, 995-1006. doi:10.1016/j.compstruct.2016.10.122

Aljabar, N. J., Zhao, X. L., Al-Mahaidi, R., Ghafoori, E., Motavalli, M., & Powers, N. (2016). Effect of crack orientation on fatigue behavior of CFRP-strengthened steel plates. *Composite Structures, 152*, 295-305. doi:10.1016/j.compstruct.2016.05.033

ASTM-A370. (2020). Standard Test Methods and Definitions for Mechanical Testing of Steel Products. In. ASTM International Designation.

ASTM-D638. (2014). Standard Test Method for Tensile Properties of Plastics. In: ASTM International Designation.

Bagale, B. R., & Parvin, A. (2021). Fiber-Reinforced Polymer Strengthening of Steel Beams under Static and Fatigue Loadings. *Practice Periodical on Structural Design and Construction, 26*(1). doi:10.1061/(asce)sc.1943-5576.0000534

Baldan, A. (2004). Adhesively-bonded joints and repairs in metallic alloys, polymers and composite materials: Adhesives, adhesion theories and surface pretreatment. *Journal of materials science, 39*(1), 1-49.

Bocciarelli, M., Colombi, P., Fava, G., & Poggi, C. (2007). Interaction of interface delamination and plasticity in tensile steel members reinforced by CFRP plates. *International Journal of Fracture, 146*(1-2), 79-92. doi:10.1007/s10704-007-9144-8

Bocciarelli, M., Colombi, P., Fava, G., & Poggi, C. (2009). Prediction of debonding strength of tensile steel/CFRP joints using fracture mechanics and stress based criteria. *Engineering Fracture Mechanics, 76*(2), 299-313. doi:10.1016/j.engfracmech.2008.10.005

Borrie, D., Al-Saadi, S., Zhao, X. L., Raman, R. K. S., & Bai, Y. (2021). Bonded CFRP/Steel Systems, Remedies of Bond Degradation and Behaviour of CFRP Repaired Steel: An Overview. *Polymers (Basel), 13*(9). doi:10.3390/polym13091533

Buyukozturk, O., Gunes, O., & Karaca, E. (2004). Progress on understanding debonding problems in reinforced concrete and steel members strengthened using FRP composites. *Construction and Building Materials, 18*(1), 9-19.

CBC-News-Staff. (2011). Mercier Bridge inspections reveal alarming decay. Retrieved from https://www.cbc.ca/news/canada/montreal/mercier-bridge-inspections-reveal-alarming-decay-1.1083694

CBC-News-Staff. (2021). Urgent 911 calls after major crack found in Interstate 40 bridge linking Arkansas and Tennessee. Retrieved from https://www.cbsnews.com/news/i-40-bridge-major-crack-tennessee-arkansas/

Chaallal, O., Mofidi, A., Benmokrane, B., & Neale, K. (2011). Embedded through-section FRP rod method for shear strengthening of RC beams: Performance and comparison with existing techniques. *Journal of Composites for Construction, 15*(3), 374-383.

Chataigner, S., Benzarti, K., Foret, G., Caron, J. F., Gemignani, G., Brugiolo, M., . . . Lehmann, F. (2018). Design and testing of an adhesively bonded CFRP strengthening system for

steel structures. *Engineering Structures, 177*, 556-565. doi:10.1016/j.engstruct.2018.10.004

Cheng, J., Qiu, J., Xu, X., Ji, H., Takagi, T., & Uchimoto, T. (2016). Research advances in eddy current testing for maintenance of carbon fiber reinforced plastic composites. *International Journal of Applied Electromagnetics and Mechanics, 51*(3), 261-284.

Chiew, S. P., Yu, Y., & Lee, C. K. (2011). Bond failure of steel beams strengthened with FRP laminates – Part 1: Model development. *Composites Part B: Engineering, 42*(5), 1114-1121. doi:10.1016/j.compositesb.2011.02.015

Colombi, P., & Fava, G. (2015). Experimental study on the fatigue behaviour of cracked steel beams repaired with CFRP plates. *Engineering Fracture Mechanics, 145*, 128-142.

Colombi, P., & Fava, G. (2016). Fatigue crack growth in steel beams strengthened by CFRP strips. *Theoretical and Applied Fracture Mechanics, 85*, 173-182. doi:10.1016/j.tafmec.2016.01.007

Colombi, P., & Poggi, C. (2006a). An experimental, analytical and numerical study of the static behavior of steel beams reinforced by pultruded CFRP strips. *Composites Part B: Engineering, 37*(1), 64-73. doi:10.1016/j.compositesb.2005.03.002

Colombi, P., & Poggi, C. (2006b). Strengthening of tensile steel members and bolted joints using adhesively bonded CFRP plates. *Construction and Building Materials, 20*(1-2), 22-33. doi:10.1016/j.conbuildmat.2005.06.042

Dai, J., Ueda, T., & Sato, Y. (2005). Development of the Nonlinear Bond Stress–Slip Model of Fiber Reinforced Plastics Sheet–Concrete Interfaces with a Simple Method. *Journal of Composites for Construction, 9*(1), 52-62. doi:10.1061/(asce)1090-0268(2005)9:1(52)

Daud, R. A., Cunningham, L. S., & Wang, Y. C. (2015). Static and fatigue behaviour of the bond interface between concrete and externally bonded CFRP in single shear. *Engineering Structures, 97*, 54-67. doi:10.1016/j.engstruct.2015.03.068

Dawood, M., Rizkalla, S., & Sumner, E. (2007). Fatigue and overloading behavior of steel–concrete composite flexural members strengthened with high modulus CFRP materials. *Journal of Composites for Construction, 11*(6), 659-669.

Dehghani, E., Daneshjoo, F., Aghakouchak, A. A., & Khaji, N. (2012). A new bond-slip model for adhesive in CFRP–steel composite systems. *Engineering Structures, 34*, 447-454. doi:10.1016/j.engstruct.2011.08.037

Delzendeh Moghadam, M., Fathi, A., & Chaallal, O. (2024). Retrofitting of Steel Structures with CFRP: Literature Review and Research Needs. *Applied Sciences, 14*(13). doi:10.3390/app14135958

Deng, J., & Lee, M. M. K. (2007). Behaviour under static loading of metallic beams reinforced with a bonded CFRP plate. *Composite Structures, 78*(2), 232-242. doi:10.1016/j.compstruct.2005.09.004

Deng, J., Li, J., Wang, Y., & Xie, W. (2018). Numerical study on notched steel beams strengthened by CFRP plates. *Construction and Building Materials, 163*, 622-633. doi:10.1016/j.conbuildmat.2017.12.110

Deng, J., Li, J., & Zhu, M. (2022). Fatigue behavior of notched steel beams strengthened by a prestressed CFRP plate subjected to wetting/drying cycles. *Composites Part B: Engineering, 230*. doi:10.1016/j.compositesb.2021.109491

Dexter, R. J., & Ocel, J. M. (2013). *Manual for repair and retrofit of fatigue cracks in steel bridges*. Retrieved from

Duncan, B. (2010). Developments in testing adhesive joints. In *Advances in structural adhesive bonding* (pp. 389-436): Elsevier.

Ebnesajjad, S., & Ebnesajjad, C. (2013). *Surface treatment of materials for adhesive bonding*: William Andrew.

Ebnesajjad, S., & Landrock, A. H. (2014). *Adhesives technology handbook*: William Andrew.

El-Saikaly, G., & Chaallal, O. (2015). Extending the fatigue life of reinforced concrete T-beams strengthened in shear with externally bonded FRP: Upgrading versus repairing. *Journal of Composites for Construction, 19*(1), 04014027.

Elkhabeery, O. H., Safar, S. S., & Mourad, S. A. (2018). Flexural strength of steel I-beams reinforced with CFRP sheets at tension flange. *Journal of Constructional Steel Research, 148*, 572-588. doi:10.1016/j.jcsr.2018.05.038

Emdad, R., & Al-Mahaidi, R. (2015). Effect of prestressed CFRP patches on crack growth of centre-notched steel plates. *Composite Structures, 123*, 109-122. doi:10.1016/j.compstruct.2014.12.007

Fam, A., MacDougall, C., & Shaat, A. (2009). Upgrading steel–concrete composite girders and repair of damaged steel beams using bonded CFRP laminates. *Thin-Walled Structures, 47*(10), 1122-1135. doi:10.1016/j.tws.2008.10.014

Fathi, A., El-Saikaly, G., & Chaallal, O. (2023). Fatigue Behavior in the Carbon-Fiber-Reinforced Polymer-to-Concrete Bond by Cyclic Pull-Out Test: Experimental and

Analytical Study. *Journal of Composites for Construction, 27*(4). doi:10.1061/jccof2.Cceng-4222

Fawzia, S. (2007). *Bond characteristics between steel and carbon fibre reinforced polymer (CFRP) composites.* Monash University,

Fawzia, S. (2013). Evaluation of shear stress and slip relationship of composite lap joints. *Composite Structures, 100*, 548-553. doi:10.1016/j.compstruct.2012.12.027

Fawzia, S., Al-Mahaidi, R., & Zhao, X.-L. (2006). Experimental and finite element analysis of a double strap joint between steel plates and normal modulus CFRP. *Composite Structures, 75*(1-4), 156-162. doi:10.1016/j.compstruct.2006.04.038

Fawzia, S., Zhao, X.-L., & Al-Mahaidi, R. (2010). Bond–slip models for double strap joints strengthened by CFRP. *Composite Structures, 92*(9), 2137-2145. doi:10.1016/j.compstruct.2009.09.042

Fawzia, S., Zhao, X., Al-Mahaidi, R., & Rizkalla, S. (2005). Bond characteristics between CFRP and steel plates in double strap joints. *Advanced Steel Construction, 1*(2), 17-27.

Fernando, D., Teng, J.-G., Yu, T., & Zhao, X.-L. (2013). Preparation and characterization of steel surfaces for adhesive bonding. *Journal of Composites for Construction, 17*(6), 04013012.

Fernando, D., Yu, T., & Teng, J. G. (2014). Behavior of CFRP Laminates Bonded to a Steel Substrate Using a Ductile Adhesive. *Journal of Composites for Construction, 18*(2). doi:10.1061/(asce)cc.1943-5614.0000439

Fernando, N. D. (2010). Bond behaviour and debonding failures in CFRP-strengthened steel members.

Ferreira, F. V., Brito, F. S., Franceschi, W., Simonetti, E. A. N., Cividanes, L. S., Chipara, M., & Lozano, K. (2018). Functionalized graphene oxide as reinforcement in epoxy based nanocomposites. *Surfaces and Interfaces, 10*, 100-109. doi:10.1016/j.surfin.2017.12.004

Fisher, J. W. (1997). Evolution of fatigue-resistant steel bridges. *Transportation research record, 1594*(1), 5-17.

Ghafoori, E. (2015). *Fatigue strengthening of metallic members using un-bonded and bonded CFRP laminates.* ETH Zurich,

Ghafoori, E., & Motavalli, M. (2015). Normal, high and ultra-high modulus carbon fiber-reinforced polymer laminates for bonded and un-bonded strengthening of steel beams. *Materials & Design, 67*, 232-243. doi:10.1016/j.matdes.2014.11.031

Ghafoori, E., Motavalli, M., Nussbaumer, A., Herwig, A., Prinz, G. S., & Fontana, M. (2015). Determination of minimum CFRP pre-stress levels for fatigue crack prevention in retrofitted metallic beams. *Engineering Structures, 84*, 29-41. doi:10.1016/j.engstruct.2014.11.017

Gholami, M., Sam, A. R. M., Yatim, J. M., & Tahir, M. M. (2013). A review on steel/CFRP strengthening systems focusing environmental performance. *Construction and Building Materials, 47*, 301-310. doi:10.1016/j.conbuildmat.2013.04.049

Godat, A., Chaallal, O., & Neale, K. W. (2013). Nonlinear finite element models for the embedded through-section FRP shear-strengthening method. *Computers & Structures, 119*, 12-22.

Godat, A., Hammad, F., & Chaallal, O. (2020). State-of-the-art review of anchored FRP shear-strengthened RC beams: A study of influencing factors. *Composite Structures, 254*, 112767.

Guo, D., Gao, W.-Y., Liu, Y.-L., & Dai, J.-G. (2023). Intermediate crack-induced debonding in CFRP-retrofitted notched steel beams at different service temperatures: Experimental test and finite element modeling. *Composite Structures, 304*. doi:10.1016/j.compstruct.2022.116388

Guo, D., Liu, Y.-L., Gao, W.-Y., & Dai, J.-G. (2023). Bond behavior of CFRP-to-steel bonded joints at different service temperatures: Experimental study and FE modeling. *Construction and Building Materials, 362*. doi:10.1016/j.conbuildmat.2022.129836

Guo, X., Wu, Z., Yang, Y., Bai, J., & Zhou, Q. (2022). A Study on the Bond-Slip Relationship of the CFRP-Steel Interface of CFRP Strengthened Steel. *Materials (Basel), 15*(12). doi:10.3390/ma15124187

Hao, S. (2010). I-35W bridge collapse. *Journal of bridge engineering, 15*(5), 608-614.

He, J., & Xian, G. (2016). Debonding of CFRP-to-steel joints with CFRP delamination. *Composite Structures, 153*, 12-20. doi:10.1016/j.compstruct.2016.05.100

He, J., & Xian, G. (2017). Bond-slip behavior of fiber reinforced polymer strips-steel interface. *Construction and Building Materials, 155*, 250-258. doi:10.1016/j.conbuildmat.2017.08.062

He, J., Xian, G., & Zhang, Y. X. (2020). Effect of moderately elevated temperatures on bond behaviour of CFRP-to-steel bonded joints using different adhesives. *Construction and Building Materials, 241*. doi:10.1016/j.conbuildmat.2020.118057

Heshmati, M., Haghani, R., Al-Emrani, M., & André, A. (2018). On the strength prediction of adhesively bonded FRP-steel joints using cohesive zone modelling. *Theoretical and Applied Fracture Mechanics, 93*, 64-78. doi:10.1016/j.tafmec.2017.06.022

Hmidan, A., Kim, Y. J., & Yazdani, S. (2011). CFRP Repair of Steel Beams with Various Initial Crack Configurations. *Journal of Composites for Construction, 15*(6), 952-962. doi:10.1061/(asce)cc.1943-5614.0000223

Hollaway, L. C., & Cadei, J. (2002). Progress in the technique of upgrading metallic structures with advanced polymer composites. *Progress in Structural Engineering and Materials, 4*(2), 131-148. doi:10.1002/pse.112

Honarparast, S., & Chaallal, O. (2022). Seismic performance of coupled shear walls designed according to old and new codes and retrofitted with Eb-CFRP composites. *Journal of Earthquake Engineering, 26*(4), 1875-1898.

Hu, B., Li, Y., Jiang, Y.-T., & Tang, H.-Z. (2020). Bond behavior of hybrid FRP-to-steel joints. *Composite Structures, 237*. doi:10.1016/j.compstruct.2020.111936

Hu, L. L., Zhao, X. L., & Feng, P. (2016). Fatigue Behavior of Cracked High-Strength Steel Plates Strengthened by CFRP Sheets. *Journal of Composites for Construction, 20*(6). doi:10.1061/(asce)cc.1943-5614.0000698

Huo, J., Liu, J., Dai, X., Yang, J., Lu, Y., Xiao, Y., & Monti, G. (2016). Experimental study on dynamic behavior of CFRP-to-concrete interface. *Journal of Composites for Construction, 20*(5), 04016026.

Huo, J., Zhang, X., Yang, J., & Xiao, Y. (2019). Experimental study on dynamic behavior of CFRP-to-steel interface. *Structures, 20*, 465-475. doi:10.1016/j.istruc.2019.05.007

Islam, M. S., Tong, L., & Falzon, P. J. (2014). Influence of metal surface preparation on its surface profile, contact angle, surface energy and adhesion with glass fibre prepreg. *International Journal of Adhesion and Adhesives, 51*, 32-41. doi:10.1016/j.ijadhadh.2014.02.006

Jagtap, P., Pore, S., & Prakash, V. (2015). Necessity of strengthening of steel structures with FRP composites: a review. *International Journal of Latest Trends in Engineering and Technology (IJLTET), 5*(4), 390-394.

Jiao, H., & Zhao, X.-L. (2004). CFRP strengthened butt-welded very high strength (VHS) circular steel tubes. *Thin-Walled Structures, 42*(7), 963-978.

Kamruzzaman, M., Jumaat, M. Z., Sulong, N. H., & Islam, A. B. (2014). A review on strengthening steel beams using FRP under fatigue. *ScientificWorldJournal, 2014*, 702537. doi:10.1155/2014/702537

Karam, E. C. (2015). *Retrofitting of Composite Steel Beams Pre-Damaged in Flexure using Fiber Reinforced Polymers.*

Ke, L., Li, C., He, J., Shen, Q., Liu, Y., & Jiao, Y. (2020). Enhancing fatigue performance of damaged metallic structures by bonded CFRP patches considering temperature effects. *Materials & Design, 192*. doi:10.1016/j.matdes.2020.108731

Korayem, A. H., Li, C. Y., Zhang, Q. H., Zhao, X. L., & Duan, W. H. (2015). Effect of carbon nanotube modified epoxy adhesive on CFRP-to-steel interface. *Composites Part B: Engineering, 79*, 95-104. doi:10.1016/j.compositesb.2015.03.063

Kumaraguru, S., & Alagusundaramoorthy, P. (2021). Flexural strengthening of steel beams using pultruded CFRP composite sheets with anchorage mechanisms. *Structures, 33*, 1414-1427. doi:10.1016/j.istruc.2021.05.024

Lenwari, A., Thepchatri, T., & Albrecht, P. (2006). Debonding strength of steel beams strengthened with CFRP plates. *Journal of Composites for Construction, 10*(1), 69-78.

Li, C., Ke, L., He, J., Chen, Z., & Jiao, Y. (2019). Effects of mechanical properties of adhesive and CFRP on the bond behavior in CFRP-strengthened steel structures. *Composite Structures, 211*, 163-174. doi:10.1016/j.compstruct.2018.12.020

Li, J., Zhu, M., & Deng, J. (2022). Flexural behaviour of notched steel beams strengthened with a prestressed CFRP plate subjected to fatigue damage and wetting/drying cycles. *Engineering Structures, 250*. doi:10.1016/j.engstruct.2021.113430

Li, Y., Li, C., He, J., Gao, Y., & Hu, Z. (2020). Effect of functionalized nano-SiO2 addition on bond behavior of adhesively bonded CFRP-steel double-lap joint. *Construction and Building Materials, 244*. doi:10.1016/j.conbuildmat.2020.118400

Linghoff, D., & Al-Emrani, M. (2010). Performance of steel beams strengthened with CFRP laminate – Part 2: FE analyses. *Composites Part B: Engineering, 41*(7), 516-522. doi:10.1016/j.compositesb.2009.07.002

Linghoff, D., Al-Emrani, M., & Kliger, R. (2010). Performance of steel beams strengthened with CFRP laminate – Part 1: Laboratory tests. *Composites Part B: Engineering, 41*(7), 509-515. doi:10.1016/j.compositesb.2009.05.008

Liu, X. (2003). *Rehabilitation of steel bridge members with FRP composite materials*: University of Missouri-Rolla.

Lorenzo, M. A. (1997). *Experimental methods for evaluating epoxy coating adhesion to steel reinforcement.* University of Texas at Austin,

Lu, X. Z., Teng, J. G., Ye, L. P., & Jiang, J. J. (2005). Bond–slip models for FRP sheets/plates bonded to concrete. *Engineering Structures, 27*(6), 920-937. doi:10.1016/j.engstruct.2005.01.014

MinnPost-staff. (2007). An image of the I-35W bridge collapse site as seen from a U.S. military helicopter in Minneapolis on August 4, 2007/ Credit: REUTERS/Larry Downing. In. http://www.minnpost.com/glean/2022/08/bridge-safety-15-years-after-the-i-35w-bridge-collapse/: Minnpost.com.

Mofidi, A., & Chaallal, O. (2011). Shear strengthening of RC beams with EB FRP: Influencing factors and conceptual debonding model. *Journal of Composites for Construction, 15*(1), 62-74.

Mofidi, A., & Chaallal, O. (2014). Tests and design provisions for reinforced-concrete beams strengthened in shear using FRP sheets and strips. *International Journal of Concrete Structures and Materials, 8*, 117-128.

Mohabeddine, A., Malik, G., Correia, J., Silva, F., De Jesus, A., Fantuzzi, N., & Castro, J. M. (2023). Experimental parametric investigation on the behavior of adhesively bonded CFRP/steel joints. *Composite Structures, 307*. doi:10.1016/j.compstruct.2022.116598

Monti, G., Renzelli, M., & Luciani, P. (2003). FRP adhesion in uncracked and cracked concrete zones. In *Fibre-Reinforced Polymer Reinforcement for Concrete Structures: (In 2 Volumes)* (pp. 183-192): World Scientific.

Nakaba, K., Kanakubo, T., Furuta, T., & Yoshizawa, H. (2001). Bond behavior between fiber-reinforced polymer laminates and concrete. *Structural Journal, 98*(3), 359-367.

Narmashiri, K., Jumaat, M. Z., & Sulong, N. R. (2012). Strengthening of steel I-beams using CFRP strips: an investigation on CFRP bond length. *Advances in Structural Engineering, 15*(12), 2191-2204.

Narmashiri, K., Ramli Sulong, N. H., & Jumaat, M. Z. (2012). Failure analysis and structural behaviour of CFRP strengthened steel I-beams. *Construction and Building Materials, 30*, 1-9. doi:10.1016/j.conbuildmat.2011.11.009

Nguyen, T.-C., Bai, Y., Zhao, X.-L., & Al-Mahaidi, R. (2013). Curing effects on steel/CFRP double strap joints under combined mechanical load, temperature and humidity. *Construction and Building Materials, 40*, 899-907. doi:10.1016/j.conbuildmat.2012.11.035

Nozaka, K., Shield, C. K., & Hajjar, J. F. (2005). Effective bond length of carbon-fiber-reinforced polymer strips bonded to fatigued steel bridge I-girders. *Journal of bridge engineering, 10*(2), 195-205.

Oudah, F., & El-Hacha, R. (2013). Research progress on the fatigue performance of RC beams strengthened in flexure using Fiber Reinforced Polymers. *Composites Part B: Engineering, 47*, 82-95.

Pang, Y.-Y., Wu, G., Wang, H.-T., Su, Z.-L., & He, X.-Y. (2019). Experimental study on the bond behavior of the CFRP-steel interface under the freeze–thaw cycles. *Journal of Composite Materials, 54*(1), 13-29. doi:10.1177/0021998319851191

Pang, Y., Wu, G., Wang, H., Gao, D., & Zhang, P. (2021a). Bond-slip model of the CFRP-steel interface with the CFRP delamination failure. *Composite Structures, 256*. doi:10.1016/j.compstruct.2020.113015

Pang, Y., Wu, G., Wang, H., Gao, D., & Zhang, P. (2021b). Experimental study on the bond behavior of the CFRP-steel interface under rapid loading. *Thin-Walled Structures, 159*. doi:10.1016/j.tws.2020.107233

Peiris, A., & Harik, I. (2018). FRP-steel bond study of IM and UHM CFRP strips. *Construction and Building Materials, 185*, 628-637. doi:10.1016/j.conbuildmat.2018.07.109

Peiris, A., & Harik, I. (2021). Steel beam strengthening with UHM CFRP strip panels. *Engineering Structures, 226*. doi:10.1016/j.engstruct.2020.111395

Peiris, N. A. (2011). Steel beams strengthened with ultra high modulus CFRP laminates.

Pellegrino, C., Tinazzi, D., & Modena, C. (2008). Experimental study on bond behavior between concrete and FRP reinforcement. *Journal of Composites for Construction, 12*(2), 180-189.

Phares, B. M., Wipf, T. J., Klaiber, F. W., Abu-Hawash, A., & Lee, Y.-S. (2003). *Strengthening of steel girder bridges using FRP.* Paper presented at the Proceedings of the 2003 Mid-Continent Transportation Research Symposium, Ames, Iowa.

Photiou, N. K. (2005). *Rehabilitation of steel members utilising hybrid FRP composite material systems*: University of Surrey (United Kingdom).

Qiang, X., Chen, L., & Jiang, X. (2023). Experimental and theoretical study on flexural behavior of steel–concrete composite beams strengthened by CFRP plates with unbonded retrofit systems. *Composite Structures, 309*. doi:10.1016/j.compstruct.2023.116763

Razavi, S. M. J., Ayatollahi, M. R., Nemati Giv, A., & Khoramishad, H. (2018). Single lap joints bonded with structural adhesives reinforced with a mixture of silica nanoparticles and multi walled carbon nanotubes. *International Journal of Adhesion and Adhesives, 80*, 76-86. doi:10.1016/j.ijadhadh.2017.10.007

Reddy, J. N. (2003). *Mechanics of laminated composite plates and shells: theory and analysis*: CRC press.

Russian, O., Khan, S., Belarbi, A., & Dawood, M. (2021). Effect of surface preparation technique on bond behavior of CFRP-steel double-lap joints: Experimental and numerical studies. *Composite Structures, 255*. doi:10.1016/j.compstruct.2020.113048

Sallam, H., Ahmad, S., Badawy, A., & Mamdouh, W. (2006). Evaluation of steel I-beams strengthened by various plating methods. *Advances in Structural Engineering, 9*(4), 535-544.

Saraç, İ., Adin, H., & Temiz, Ş. (2018). Experimental determination of the static and fatigue strength of the adhesive joints bonded by epoxy adhesive including different particles. *Composites Part B: Engineering, 155*, 92-103. doi:10.1016/j.compositesb.2018.08.006

Schnerch, D., Dawood, M., Rizkalla, S., & Sumner, E. (2007). Proposed design guidelines for strengthening of steel bridges with FRP materials. *Construction and Building Materials, 21*(5), 1001-1010. doi:10.1016/j.conbuildmat.2006.03.003

Schnerch, D., Dawood, M., Rizkalla, S., Sumner, E., & Stanford, K. (2006). Bond behavior of CFRP strengthened steel structures. *Advances in Structural Engineering, 9*(6), 805-817.

Schnerch, D., & Rizkalla, S. (2008). Flexural strengthening of steel bridges with high modulus CFRP strips. *Journal of bridge engineering, 13*(2), 192-201.

Schnerch, D. A. (2005). *Strengthening of steel structures with high modulus carbon fiber reinforced polymer (CFRP) materials*: North Carolina State University.

Selvaraj, S., & Madhavan, M. (2020). Design of Steel Beams Strengthened with Low-Modulus CFRP Laminates. *Journal of Composites for Construction, 24*(1). doi:10.1061/(asce)cc.1943-5614.0000983

Shaat, A., & Fam, A. (2008). Repair of cracked steel girders connected to concrete slabs using carbon-fiber-reinforced polymer sheets. *Journal of Composites for Construction, 12*(6), 650-659.

Shaat, A., Schnerch, D., Fam, A., & Rizkalla, S. (2004). *Retrofit of steel structures using fiber-reinforced polymers (FRP): State-of-the-art.* Paper presented at the Transportation research board (TRB) annual meeting.

Siddika, A., Mamun, M. A. A., Ferdous, W., & Alyousef, R. (2020). Performances, challenges and opportunities in strengthening reinforced concrete structures by using FRPs – A state-of-the-art review. *Engineering Failure Analysis, 111*. doi:10.1016/j.engfailanal.2020.104480

Sousa, J. M., Correia, J. R., & Cabral-Fonseca, S. (2018). Durability of an epoxy adhesive used in civil structural applications. *Construction and Building Materials, 161*, 618-633. doi:10.1016/j.conbuildmat.2017.11.168

Stanford, K. A. (2009). Strengthening of Steel Structures with High Modulus Carbon Fiber Reinforced Polymers (CRRP) Materials: Bond and Development Length Study.

Sweedan, A. M. I., Alhadid, M. M. A., & El-Sawy, K. M. (2016). Experimental study of the flexural response of steel beams strengthened with anchored hybrid composites. *Thin-Walled Structures, 99*, 1-11. doi:10.1016/j.tws.2015.10.026

Tabrizi, S., Kazem, H., Rizkalla, S., & Kobayashi, A. (2015). New small-diameter CFRP material for flexural strengthening of steel bridge girders. *Construction and Building Materials, 95*, 748-756. doi:10.1016/j.conbuildmat.2015.07.109

Tafsirojjaman, T., Fawzia, S., Thambiratnam, D. P., & Zhao, X.-L. (2021). FRP strengthened SHS beam-column connection under monotonic and large-deformation cyclic loading. *Thin-Walled Structures, 161*. doi:10.1016/j.tws.2021.107518

Tavakkolizadeh, M., & Saadatmanesh, H. (2003). Fatigue strength of steel girders strengthened with carbon fiber reinforced polymer patch. *Journal of structural engineering, 129*(2), 186-196.

Teng, J. G., Fernando, D., & Yu, T. (2015). Finite element modelling of debonding failures in steel beams flexurally strengthened with CFRP laminates. *Engineering Structures, 86*, 213-224. doi:10.1016/j.engstruct.2015.01.003

Teng, J. G., Yu, T., & Fernando, D. (2012). Strengthening of steel structures with fiber-reinforced polymer composites. *Journal of Constructional Steel Research, 78*, 131-143. doi:10.1016/j.jcsr.2012.06.011

The Institution of Structural Engineers (ISE), L., UK. (1999). The structural use of adhesives. In.

Tong, L., Xu, G., Zhao, X.-L., & Yan, Y. (2021). Fatigue tests and design of CFRP-strengthened CHS gap K-joints. *Thin-Walled Structures, 163*. doi:10.1016/j.tws.2021.107694

Vatandoost, F. (2010). *Fatigue behaviour of steel girders strengthened with prestressed CFRP strips.* University of Waterloo,

Wan, Y.-J., Gong, L.-X., Tang, L.-C., Wu, L.-B., & Jiang, J.-X. (2014). Mechanical properties of epoxy composites filled with silane-functionalized graphene oxide. *Composites Part*

A: Applied Science and Manufacturing, 64, 79-89. doi:10.1016/j.compositesa.2014.04.023

Wang, H.-T., Bian, Z.-N., Chen, M.-S., Hu, L., & Wu, Q. (2023). Flexural strengthening of damaged steel beams with prestressed CFRP plates using a novel prestressing system. *Engineering Structures, 284*. doi:10.1016/j.engstruct.2023.115953

Wang, H.-T., Guo, C.-C., Liu, Q.-L., & Wu, Q. (2023). Influences of the bond-slip on the flexural performance of CFRP plate-strengthened damaged steel beams with intermediate debonding: A numerical study. *Structures, 58*. doi:10.1016/j.istruc.2023.105661

Wang, H.-T., Liu, S.-S., Liu, Q.-L., Pang, Y.-Y., & Shi, J.-W. (2021). Influences of the joint and epoxy adhesive type on the CFRP-steel interfacial behavior. *Journal of Building Engineering, 43*. doi:10.1016/j.jobe.2021.103167

Wang, H.-T., & Wu, G. (2018). Bond-slip models for CFRP plates externally bonded to steel substrates. *Composite Structures, 184*, 1204-1214. doi:10.1016/j.compstruct.2017.10.033

Wang, H.-T., Wu, G., Dai, Y.-T., & He, X.-Y. (2016a). Determination of the bond–slip behavior of CFRP-to-steel bonded interfaces using digital image correlation. *Journal of Reinforced Plastics and Composites, 35*(18), 1353-1367. doi:10.1177/0731684416651342

Wang, H.-T., Wu, G., Dai, Y.-T., & He, X.-Y. (2016b). Experimental Study on Bond Behavior between CFRP Plates and Steel Substrates Using Digital Image Correlation. *Journal of Composites for Construction, 20*(6). doi:10.1061/(asce)cc.1943-5614.0000701

Wang, H.-T., Wu, G., Pang, Y.-Y., Shi, J.-W., & Zakari, H. M. (2019). Experimental study on the bond behavior between CFRP plates and steel substrates under fatigue loading. *Composites Part B: Engineering, 176*. doi:10.1016/j.compositesb.2019.107266

Wang, H.-T., Wu, Q., Li, L., Wei, F.-F., Zhu, D.-C., & Yu, X.-P. (2024). Mechanical behaviors of steel-CFRP plate bonded joints after freezing-thawing cycles. *Construction and Building Materials, 412*. doi:10.1016/j.conbuildmat.2024.134876

Wang, Z., & Xian, G. (2021). Effects of thermal expansion coefficients discrepancy on the CFRP and steel bonding. *Construction and Building Materials, 269*. doi:10.1016/j.conbuildmat.2020.121356

Wang, Z., Xian, G., & Yue, Q. (2023). Finite element modeling of debonding failure in CFRP-strengthened steel beam using a ductile adhesive. *Composite Structures, 311*. doi:10.1016/j.compstruct.2023.116818

Wu, C., Yu, Y.-Z., Tam, L.-h., & He, L. (2023). Effects of bondline defects on the bond behaviour of CFRP-steel double strap joints. *Composite Structures, 308*. doi:10.1016/j.compstruct.2023.116682

Wu, C., Yu, Y.-Z., Tam, L.-h., Orr, J., & He, L. (2021). Effect of glass fiber sheet in adhesive on the bond and galvanic corrosion behaviours of CFRP-Steel bonded system. *Composite Structures, 259*. doi:10.1016/j.compstruct.2020.113218

Wu, C., Zhao, X., Hui Duan, W., & Al-Mahaidi, R. (2012). Bond characteristics between ultra high modulus CFRP laminates and steel. *Thin-Walled Structures, 51*, 147-157. doi:10.1016/j.tws.2011.10.010

Wu, C., Zhao, X. L., Chiu, W. K., Al-Mahaidi, R., & Duan, W. H. (2013). Effect of fatigue loading on the bond behaviour between UHM CFRP plates and steel plates. *Composites Part B: Engineering, 50*, 344-353. doi:10.1016/j.compositesb.2013.02.040

Wu, G., Wang, H.-T., Wu, Z.-S., Liu, H.-Y., & Ren, Y. (2012). Experimental study on the fatigue behavior of steel beams strengthened with different fiber-reinforced composite plates. *Journal of Composites for Construction, 16*(2), 127-137.

Xia, S., & Teng, J. (2005). *Behaviour of FRP-to-steel bonded joints.* Paper presented at the International Symposium on Bond Behaviour of FRP in Structures, BBFS 2005.

Xie, G.-h., You, Y., Tao, Z.-a., & Li, S.-q. (2023). Experimental and theoretical study on mechanical behaviors of CFRP–steel interface. *Thin-Walled Structures, 182*. doi:10.1016/j.tws.2022.110208

Yang, Y., Biscaia, H., Chastre, C., & Silva, M. A. G. (2017). Bond characteristics of CFRP-to-steel joints. *Journal of Constructional Steel Research, 138*, 401-419. doi:10.1016/j.jcsr.2017.08.001

Yang, Y., Zhao, J., Zhang, S., Chastre, C., & Biscaia, H. (2021). Effect of mechanical anchorage on the bond performance of double overlapped CFRP-to-steel joints. *Composite Structures, 267*. doi:10.1016/j.compstruct.2021.113902

Yu, Q.-Q., & Wu, Y.-F. (2017a). Fatigue behaviour of cracked steel beams retrofitted with carbon fibre–reinforced polymer laminates. *Advances in Structural Engineering, 21*(8), 1148-1161. doi:10.1177/1369433217729518

Yu, Q.-Q., & Wu, Y.-F. (2017b). Fatigue durability of cracked steel beams retrofitted with high-strength materials. *Construction and Building Materials, 155*, 1188-1197. doi:10.1016/j.conbuildmat.2017.09.051

Yu, Q.-Q., & Wu, Y.-F. (2018). Fatigue retrofitting of cracked steel beams with CFRP laminates. *Composite Structures, 192*, 232-244. doi:10.1016/j.compstruct.2018.02.090

Yu, T., Fernando, D., Teng, J. G., & Zhao, X. L. (2012). Experimental study on CFRP-to-steel bonded interfaces. *Composites Part B: Engineering, 43*(5), 2279-2289. doi:10.1016/j.compositesb.2012.01.024

Yuan, C., Chen, W., Pham, T. M., & Hao, H. (2019). Bond behaviour between hybrid fiber reinforced polymer sheets and concrete. *Construction and Building Materials, 210*, 93-110. doi:10.1016/j.conbuildmat.2019.03.082

Zeng, J.-J., Gao, W.-Y., & Liu, F. (2018). Interfacial behavior and debonding failures of full-scale CFRP-strengthened H-section steel beams. *Composite Structures, 201*, 540-552. doi:10.1016/j.compstruct.2018.06.045

Zhao, J., Liu, G., Yang, Y., Zhang, S., & Biscaia, H. (2024). experimental study on the mixed mode debonding by using a modified CFRP-to-steel double strap joint. *Structures, 60*. doi:10.1016/j.istruc.2024.105874

Zhao, X.-L., & Zhang, L. (2007). State-of-the-art review on FRP strengthened steel structures. *Engineering Structures, 29*(8), 1808-1823. doi:10.1016/j.engstruct.2006.10.006

Zhou, H., Fernando, D., Thuan Nguyen, V., & Dai, J.-G. (2021). The bond behaviour of CFRP-to-concrete bonded joints under fatigue cyclic loading: An experimental study. *Construction and Building Materials, 273*. doi:10.1016/j.conbuildmat.2020.121674

Zhou, H., Fernando, D., Torero, J. L., Torres, J. P., Maluk, C., & Emberley, R. (2020). Bond Behavior of CFRP-to-Steel Bonded Joints at Mild Temperatures: Experimental Study. *Journal of Composites for Construction, 24*(6). doi:10.1061/(asce)cc.1943-5614.0001073

Zhou, H., Liu, H.-Y., Zhou, H., Zhang, Y., Gao, X., & Mai, Y.-W. (2016). On adhesive properties of nano-silica/epoxy bonded single-lap joints. *Materials & Design, 95*, 212-218. doi:10.1016/j.matdes.2016.01.055